SLAC – 290
UC – 34D
(E)

MEASUREMENT OF THE CHARGED AND NEUTRAL D MESON LIFETIMES*

John Mark Butler

Stanford Linear Accelerator Center
Stanford University
Stanford, California 94305

February 1986

Prepared for the Department of Energy
under contract number DE-AC03-76SF00515

Printed in the United States of America. Available from the National Technical Information Service, U.S. Department of Commerce, 5285 Port Royal Road, Springfield, Virginia 22161. Price: Printed Copy A07, Microfiche A01.

* Ph.D. Dissertation.

Abstract

In an exposure of the SLAC Hybrid Facility (SHF) to a backward scattered laser beam, 136 charm events produced in γp interactions at 20 GeV have been observed. The SHF 1 m bubble chamber was equipped with a High Resolution Optics camera in order to detect directly the production and decay of charm particles. After imposing rigorous cuts, 48 charged, 50 neutral, and 2 topologically ambiguous decays remain. Using a novel method for estimating the momentum of unconstrained decays, the D meson lifetimes from this sample are measured to be $\tau_{D^\pm} = (8.6 \pm 1.3^{+0.8}_{-0.3}) \times 10^{-13}$ sec and $\tau_{D^0} = (6.1 \pm 0.9 \pm 0.3) \times 10^{-13}$ sec with a ratio of $R = \tau_{D^\pm}/\tau_{D^0} = (1.4 \pm 0.3^{+0.2}_{-0.1})$. This value of R indicates the Spectator Model charm particle decay mechanism is the dominate piece in the $D^\pm$ and D^0 decay rates. Limits are placed on additional contributions to the D decay rates from other processes including W-Exchange, Final State Interactions, and Pauli Principle Interference.

Acknowledgments

A bubble chamber experiment where millions of pictures are taken and scanned to find a hundred very special events is only possible through the hard work of a large number of people. It is a pleasure to acknowledge the efforts and to have been a part of the SLAC Hybrid Facility Photon Collaboration. The diligence of the SHF bubble chamber crew, the SLAC scanners and film processors is greatly appreciated. Thanks go to the members of SLAC Group BC, in particular to Ken Moffeit for advice and leadership, and to Clive Field for making the HRO camera system a great success. I would like to thank my advisor, Joe Ballam, for guidance and prodding. I am grateful to Fred Gilman for instructive discussions on charm decay theory. Finally, thanks go to my fellow graduate students (particularly the infamous lunch bunch at SLAC) for making my Stanford experience so enjoyable, to my mother and sisters for enthusiastic support in spite of not knowing just what I was up to, and to Sara for love and patience.

Table of Contents

Chapter 1: Introduction

1.1 OVERVIEW

The goal of elementary particle physics is to identify and understand the fundamental constituents of matter and the forces through which they interact. In our current understanding, the fundamental constituents are point-like spin 1/2 quarks and leptons listed in Table 1.1 which interact through four forces mediated by the exchange of gauge bosons listed in Table 1.2. The ideal in particle physics is to find an underlying structure that would allow the unification of these forces resulting in a more fundamental theory. A part of this unification has been successfully achieved in combining electromagnetism and the weak force into a unified electro-weak theory described below.

Table 1.1

Fermions	Leptons		Quarks	
Charge	0	-1	$2/3$	$-1/3$
Flavor	ν_e	e^-	u up	d down
	ν_μ	μ^-	c charm	s strange
	ν_τ	τ^-	t top	b bottom

Table 1.2	
Interaction	Gauge Boson
Gravitation	graviton
Electromagnetic	γ photon
Weak	$W^{\pm}, Z^0$ bosons
Strong	g gluon

While both quarks and leptons undergo gravitational, electromagnetic and weak interactions only quarks experience the strong force. In fact this is what distinguishes quarks from leptons. This is because quarks carry an additional quantum number "color charge" to which only the gluons couple. The current candidate for a theory of the strong interaction is Quantum Chromodynamics (QCD). Unlike all other fundamental interactions, the color force in QCD has the property that it increases in magnitude with the separation of the interacting quarks. The consequence is that at short distances (or high q^2) quarks behave as if they were free particles, the phenomena known as "asymptotic freedom", and at large distances (or low q^2) quarks are "confined" in color singlet bound states called hadrons. The hadrons are of two types: (1) mesons – quark anti-quark states and (2) baryons – three quark states. Charm hadrons contain at least one charm quark, those relevant for this thesis are listed in Table 1.3.

Table 1.3	
Charm Particle	Quark Content
D^+	$c\bar{d}$
D^0	$c\bar{u}$
F^+	$c\bar{s}$
Λ_c^+	cud

The lifetimes of charm particles provide an excellent laboratory for the study of several aspects of elementary particles and their interactions [1]. Charm particle decays are characterized by a subtle interplay of the weak and strong interactions because of the specific properties of the charm quark. The weak decay of particles containing sufficiently heavy quarks can be described in a simple spectator model which treats the heavy quark as essentially a free particle. In the case of particles containing light quarks, the decay involves complicated strong interaction bound state effects which are difficult, if not impossible, to calculate. Thus the quark mass is a primary factor in determining the way in which the particle decays. The mass of a quark is, however, difficult to define because quarks do not exist as free particles and the mass is a function of the energy of the probe used to measure it. To set a rough scale of quark masses, Table 1.4 lists the so-called "constituent masses" [2]. As seen in the Table 1.4, the charm quark could be described as "medium - heavy" and thus a complete picture of its decay, and hence the lifetimes of charm particles, must incorporate both the weak and strong interactions.

Table 1.4	
Quark	Mass (GeV)
u	0.34
d	0.34
s	0.51
c	1.5
b	4.9
t	> 30

1.2 THE WEAK INTERACTION

In the standard Glashow-Weinberg-Salam unified electro-weak theory [3] based on the $SU(2)_L \otimes U(1)$ group, the quarks and leptons form left handed doublets of the weak isospin of $SU(2)$ while the right handed components are kept as singlets. The doublets are arranged as follows: the leptons are grouped in three "generations" as

$$\begin{pmatrix} \nu_e \\ e^- \end{pmatrix}; \begin{pmatrix} \nu_\mu \\ \mu^- \end{pmatrix}; \begin{pmatrix} \nu_\tau \\ \tau^- \end{pmatrix}$$

and in a very similar fashion the quarks are grouped as

$$\begin{pmatrix} u \\ d' \end{pmatrix}; \begin{pmatrix} c \\ s' \end{pmatrix}; \begin{pmatrix} t \\ b' \end{pmatrix}$$

The d', s', b' weak eigenstates are related to the mass eigenstates through the transformation

$$\begin{pmatrix} d' \\ s' \\ b' \end{pmatrix} = V \begin{pmatrix} d \\ s \\ b \end{pmatrix}$$

where V is a 3×3 unitary matrix. In general, the rotation can be described by three angles and one (CP violating) phase. The commonly used Kobayashi-Maskawa parameterization [4] is given by

$$V = \begin{pmatrix} c_1 & s_1 c_3 & s_1 s_3 \\ -s_1 c_2 & c_1 c_2 c_3 - s_2 s_3 e^{i\delta} & c_1 c_2 s_3 + s_2 c_3 e^{i\delta} \\ -s_1 s_2 & c_1 s_2 c_3 + c_2 s_3 e^{i\delta} & c_1 s_2 s_3 - c_2 c_3 e^{i\delta} \end{pmatrix}$$

where $c_i \equiv \cos\theta_i$, $s_i \equiv \sin\theta_i$ $(i = 1, 2, 3)$.

Since the center of mass energy of this experiment is well below bottom or top threshold, a 4 flavor approximation will be used to describe the mixing where

$$\begin{pmatrix} d' \\ s' \end{pmatrix} = \begin{pmatrix} \cos\theta_c & \sin\theta_c \\ -\sin\theta_c & \cos\theta_c \end{pmatrix} \begin{pmatrix} d \\ s \end{pmatrix}$$

and θ_c is just the familiar Cabibbo angle.

The flavor changing weak decays proceed exclusively via the charged current interaction; that is, by the radiation or exchange of a $W^{\pm}$ boson. The charged current is given by

$$J^{\mu}_{\pm} = J^{\mu}_{\ell\pm} + J^{\mu}_{H\pm}$$

where the leptonic current piece is

$$J^{\mu}_{\ell\pm} = \sum_{i=1}^{2} \bar{\ell}_i \gamma^{\mu}(1 - \gamma_5)\tau_{\pm}\ell_i$$

$$\ell_1 = \begin{pmatrix} \nu_e \\ e^- \end{pmatrix}, \quad \ell_2 = \begin{pmatrix} \nu_\mu \\ \mu^- \end{pmatrix}$$

and the hadronic current piece is

$$J^{\mu}_{H\pm} = \sum_{i=1}^{2} \bar{q}_i \gamma^{\mu}(1 - \gamma_5)\tau_{\pm} q_i$$

$$q_1 = \begin{pmatrix} u \\ d' \end{pmatrix}, \quad q_2 = \begin{pmatrix} c \\ s' \end{pmatrix}$$

and $\tau_{\pm}$ are the usual isospin raising and lowering operators.

An effective weak Hamiltonian (in the limit $m_W \to \infty$; that is, m_W much larger than the relevant quark masses) can be written down for the weak decay process

$$H_W = \frac{G_F}{\sqrt{2}}(J_+^\mu(0)J_{-\mu}(0) + h.c.).$$

In principle, all the tools necessary for calculating the decay rate (and hence the lifetime) of charm particles are at hand. However, to calculate the rate for the process $D \to X$, where X is any final state, one must evaluate the matrix element $\langle X|H_W|D\rangle$ and the initial and final state wave functions involve hadronic bound state effects that are not yet calculable within the theory.

1.3 The Naïve Spectator Model

Although the decay rate can not be calculated from first principles the problem can be simplified by making the following approximation. It is observed that the momentum transfer in weak decays of heavy, that is, charm and bottom, hadrons is on the order of the heavy quark mass. Therefore it is not unreasonable to expect that the decay of heavy flavors reflects the dynamics at short distances. If the short distance behavior dominates, then the heavy quark can be treated as essentially a free particle (this being a consequence of "asymptotic freedom" in QCD). Thus the decay of charm mesons is described by the decay of the charm quarks with the light constituents of the mesons acting as passive "spectators". In this spectator model [5] picture, the decay of a charm meson proceeds as shown is Figure 1.1.

Explicitly, the simplifying assumptions of the spectator model are the following

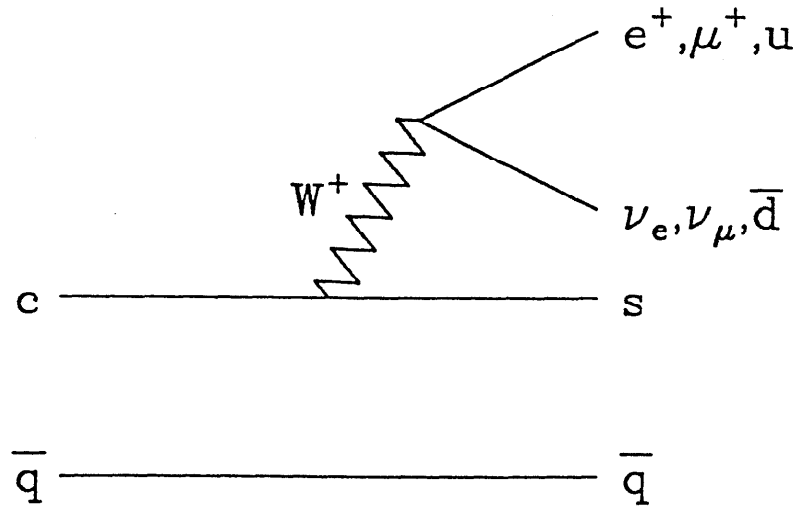

Figure 1.1: The Spectator Diagram.

(i) The charm meson is represented by its valence quark configuration, *i.e.* a charm quark and a light anti-quark only. All complex bound state fluctuations are disregarded.

(ii) Soft gluon emission is neglected.

(iii) The sum of all possible hadronic final states is replaced with final states of "free" quarks emitted in the decay.

Using these assumptions, the charm meson lifetime is readily calculated. The matrix element for either D meson to decay as in Figure 1.1 into an arbitrary non-leptonic (NL) hadronic final state X_H is given by

$$\mathcal{M} = \langle X_H \mid (\bar{u}d)(\bar{s}c) \mid D \rangle$$

where the convenient notation $(\bar{q}_1 q_2) = \bar{q}_{1i}\gamma^\mu(1-\gamma_5)q_{2i}$, i being a color index, has been used. Assumption (iii) reduces this to

$$\mathcal{M} = \langle \bar{q}su\bar{d} \mid (\bar{u}d)(\bar{s}c) \mid D \rangle$$

Now using assumption (i) gives

$$\begin{aligned}\mathcal{M} &\cong \langle su\bar{d} \mid (\bar{u}d)(\bar{s}c) \mid c \rangle \\ &= (\bar{u}_u\gamma^\mu(1-\gamma_5)v_{\bar{d}})(\bar{u}_s\gamma_\mu(1-\gamma_5)u_c)\end{aligned}$$

where u,v are the usual Dirac spinors. This last expression is formally identical to the matrix element for μ decay [6]. Thus the decay rate can be written down straight away

$$\begin{aligned}\Gamma_{NL}(D \to X_H) &\cong \Gamma_{NL}(c \to su\bar{d}) \\ &= 3\left(\frac{m_c}{m_\mu}\right)^5 \Gamma(\mu \to e\bar{\nu}_e\nu_\mu) = 3\frac{G_F^2 m_c^5}{192\pi^3}\end{aligned}$$

where the factor of 3 arises from the 3 color combinations of the final state $u\bar{d}$ pair. In analogous fashion, the semi-leptonic (SL) rate for a given final state lepton $\ell = e, \mu$ is

$$\Gamma_{SL}(D \to \ell^+ \nu_\ell X) \cong \Gamma_{SL}(c \to \ell^+ \nu_\ell s) = \frac{G_F^2 m_c^5}{192\pi^3}$$

The D meson lifetime is then

$$\tau_D \cong \frac{1}{\Gamma_{NL} + 2\Gamma_{SL}} = \frac{1}{5}\left(\frac{m_\mu}{m_c}\right)^5 \tau_\mu \approx 3 \times 10^{-13}\text{sec.}$$

where $m_c = 1.8$ GeV has been used for the numerical evaluation. This value of τ_D should be taken as a very rough estimate since varying m_c by 20% changes τ_D by a factor of 3 and the relevant value of m_c is not well determined.

As is clear from the above calculation, an important prediction of the spectator model is that since the charm quark decay is independent of the light quarks in the charm hadron then all charm particles will have the same lifetime. That is

$$\tau_{D^+} = \tau_{D^0} = \tau_{F^+} = \tau_{\Lambda_c^+} = \ldots = \tau_c$$

Deviations from this relation require contributions from other processes or modification of the naïve Spectator Model picture. Both possibilities will be discussed in a later sections.

Inspection of Figure 1.1 reveals another prediction of the spectator model, namely that all charm particles have the same semi-leptonic branching ratio

$$BR_\ell(D^+) = BR_\ell(D^0) = BR_\ell(F^+) = BR_\ell(\Lambda_c^+) = \ldots = BR_\ell(c)$$

where $\ell = e, \mu$. Semi-leptonic branching ratios are relevant to charm lifetime studies because a number of experiments which can not measure the charm meson

lifetimes directly are nonetheless able to measure the *ratio* of lifetimes with good precision. Explicitly

$$\frac{BR_\ell(D^+)}{BR_\ell(D^0)} = \frac{\Gamma(D^0 \to X)}{\Gamma(D^+ \to X)} \cdot \frac{\Gamma(D^+ \to \ell X)}{\Gamma(D^0 \to \ell X)}$$
$$= \tau_{D^\pm}/\tau_{D^0}$$

where $\Gamma(D^+ \to \ell X) = \Gamma(D^0 \to \ell X)$ is assumed and is a rather good approximation.

Given the number of diagrams implied by Figure 1.1, it is clear that

$$BR_\ell(c) = \frac{1}{5} = 20\%$$

Deviations from this prediction again require contributions from other processes or modification of the naïve Spectator Model; both options are described in the following sections.

1.4 The QCD Corrected Spectator Model

Although the naïve spectator model is aesthetically pleasing in its simplicity it is perhaps unreasonable to expect the model to provide a complete description of charm particle decay. Possible strong interaction contributions to the basic picture are discussed in this section.

Strong interaction corrections are of two kinds: (1) soft gluon radiation corrections and (2) hard gluon exchange corrections to the effective weak hamiltonian. Strong interaction corrections to the naïve spectator model are *a priori* expected to be necessary. This is because a real meson in nature is a complicated superposition of short lived quark and gluon configurations, where the valence quark configuration used in the spectator model is merely the simplest. Since the weak interaction time ($\sim 1/m_W$) is considerably shorter than the typical lifetime of a

given configuration it is not unlikely to have one (or more) gluons in the meson's wavefunction during heavy flavor decay and so influence the lifetime. This fact will be important for non-spectator processes as well.

The effect of lowest order soft gluon radiation is easily calculated [7] because the calculation is formally identical to the usual electromagnetic (EM) radiative correction to μ decay with the substitution of the EM coupling constant α by the strong coupling constant α_s which has been averaged and summed over initial and final color states

$$\frac{\alpha}{\pi} \to \frac{1}{3}\mathrm{Tr}\left(\frac{\lambda^a}{2}\cdot\frac{\lambda^a}{2}\right)\frac{\alpha_s}{\pi} = \frac{4\alpha_s}{3\pi}$$

where

$$\alpha_s(\mu^2) = \frac{4\pi}{(11-\frac{2}{3}N_f)\ln\left(\frac{\mu^2}{\Lambda^2}\right)},$$

μ is the mass scale where α_s is evaluated, N_f is the number of available flavors and Λ is the QCD scale parameter. For charm decay, $\mu = m_c$, $N_f = 4$ and $\Lambda \sim 0.1 - 0.5$ GeV.

For simplicity, consider only the corrected semi-leptonic width

$$\frac{\Gamma_{SL}^{corr}}{\Gamma_{SL}} = g(\epsilon)\left[1 - \frac{2}{3}\frac{\alpha_s(m_c^2)}{\pi}f(\epsilon)\right]$$

where as before

$$\Gamma_{SL} = \frac{G_F^2 m_c^5}{192\pi^3}$$

is the uncorrected width, $g(\epsilon)$ is a mass correction for finite strange quark mass

$$g(\epsilon) = 1 - 8\epsilon^2 - 24\epsilon^4\ln\epsilon + 8\epsilon^6 - \epsilon^8$$

$$\epsilon = m_s/m_c,$$

and $f(\epsilon)$ is a smoothly decreasing function of ϵ bounded by

$$f(0) = \pi^2 - \frac{25}{4}\ ;\quad f(1) = \frac{3}{2}.$$

$f(0)$ corresponds to the μ decay result. The value of $\Gamma_{SL}^{corr}/\Gamma_{SL}$ for $\epsilon \sim 0$ is on the order of 0.50. The semi-leptonic branching ratio is not largely affected however because a large part of the correction to Γ_{SL}^{corr} exactly cancels the effect in the hadronic channel. The overall effect on the spectator model predictions is to raise the lifetime by a factor of ~ 3 and lower $BR_\ell(c)$ by $\sim 30\%$.

The non-leptonic piece of the spectator model Hamiltonian for the process $c \to su\bar{d}$ can be written

$$H_{NL} = \frac{G_F}{\sqrt{2}} \cos^2\theta_c (\bar{s}c)(\bar{u}d).$$

Since the W boson does not carry color, the s quark has the same color as the c quark and the $u\bar{d}$ pair can be produced in any of 3 color states. The color configuration can be altered by allowing gluon exchange across the weak interaction vertex as shown if Figure 1.2. Changing the color flow in this way renormalizes the weak coupling and creates more non-leptonic diagrams. After the calculation of the QCD enhancement, the Hamiltonian is written

$$H_{NL} = \frac{G_F}{\sqrt{2}} \cos^2\theta_c \left[\frac{c_+ + c_-}{2}(\bar{s}c)(\bar{u}d) + \frac{c_+ - c_-}{2}(\bar{s}d)(\bar{u}c)\right]$$

where the first term retains the previous color structure, *i.e.* the s quark has the same color as the c quark, and in the second piece the color flow is modified so that the u quark has the same color as the c quark. The QCD enhancement coefficients c_+ and c_- are given by

$$c_- = {c_+}^{-2} = \left[\frac{\alpha_s(m_c^2)}{\alpha_s(m_W^2)}\right]^{[12/(33-2N_f)]}.$$

When $c_+ = c_- = 1$ there is no enhancement, and H_{NL} reduces to what we had before. Rückl [1] has calculated the coefficients including quark mass effects and gets

$$c_+ = 0.74\ ,\quad c_- = 1.8;$$

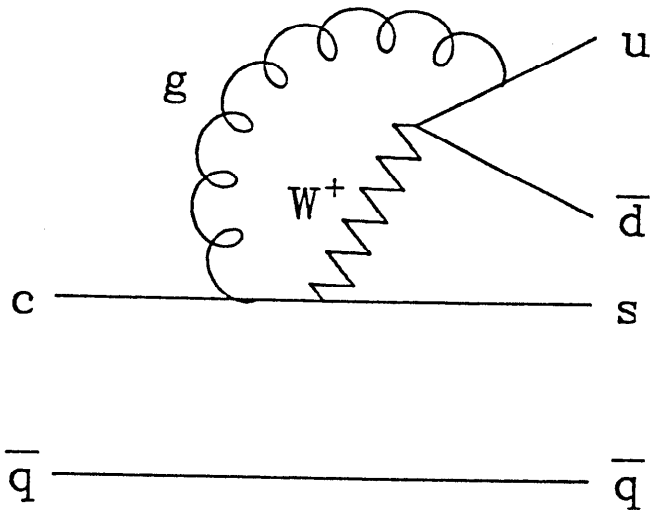

Figure 1.2: Lowest order hard gluon correction to the weak interaction vertex.

depending on parameters, $c_\pm$ can easily vary by $\pm \sim 10\%$. These numbers lead to a non-leptonic enhancement of $2c_+^2 + c_-^2 = 4.34$ compared to the previous factor of 3. The effect of the enhancement on the lifetime is unfortunately totally washed out by the uncertainty in m_c; but the enhancement does show up in lowering the semi-leptonic branching ratio

$$BR_\ell(c) \to \frac{1}{2 + 2c_+^2 + c_-^2} \approx 16\%$$

where the naïve spectator model prediction was 20%. Combining the short distance enhancement and gluon radiation, $BR_\ell(c)$ is lowered to $\sim 10\%$, although putting in finite quark mass corrections raises $BR_\ell(c)$ back up to $\sim (13 - 20)\%$.

1.5 OTHER PROCESSES

It should be stressed that the strong interaction corrections are refinements of the naïve spectator model and do not produce *differences* in D meson lifetimes or semi-leptonic branching ratios. In order to produce differences, other processes must be introduced. This section will present three leading candidates for mechanisms outside the naïve spectator model which are expected to make sizeable contributions to the D decay rate: non-spectator diagrams, final state interactions and identical quark interference.

W-Exchange and W-Annihilation The non-spectator diagrams for D decay are shown in Figure 1.3. Figure 1.3 (a) is referred to as "W-exchange" and Figure 1.3 (b) as "W-annihilation". Two things should be noted: (1) W-exchange is a totally non-leptonic process and thus produces a non-leptonic enhancement in the D^0 rate and (2) W-annihilation is Cabibbo suppressed and so the contribution to the D^+ rate is believed to be negligible. Originally these non-spectator diagrams

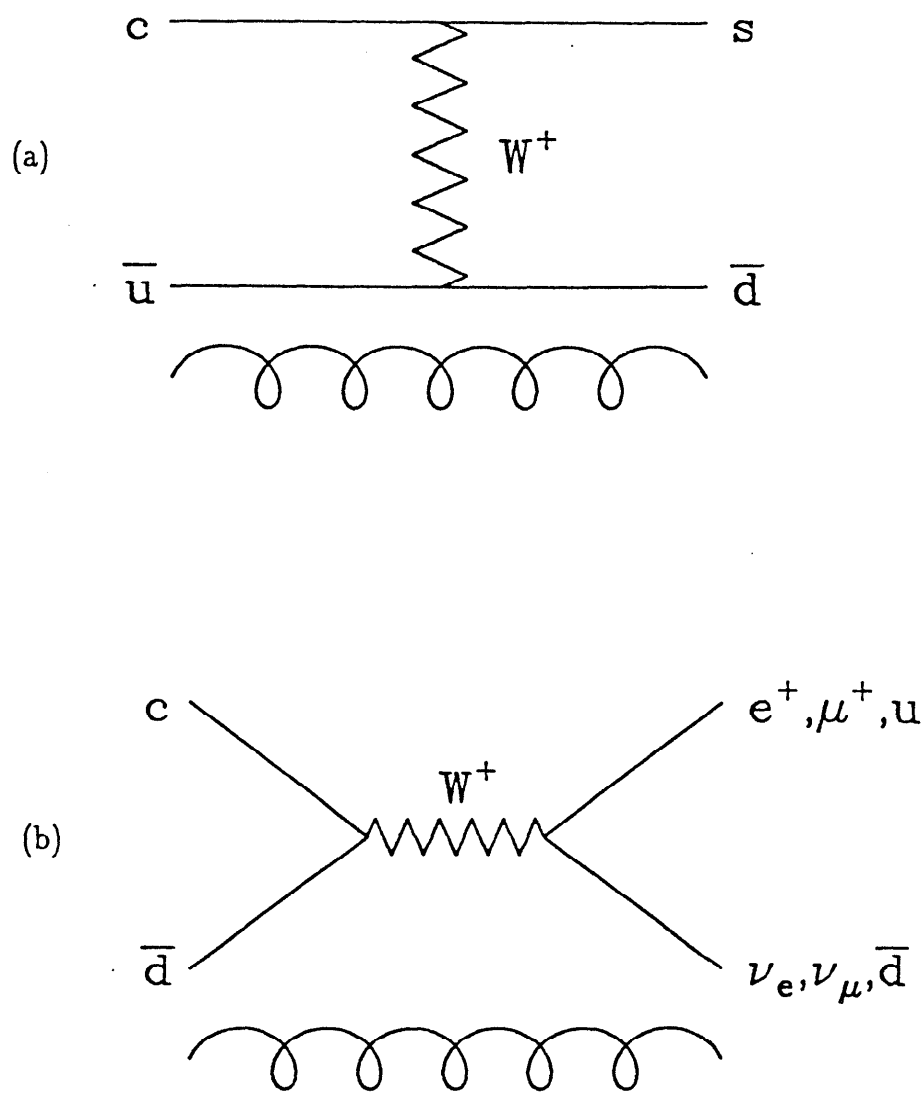

Figure 1.3: Non-spectator diagrams for D decay: (a) W-exchange which contributes only to D^0 decay and (b) W-annihilation which contributes only to $D^{\pm}$ decay.

were thought to be highly suppressed relative to c-quark decay because of helicity suppression which arises since a pseudo-scalar state can not decay into a massless fermion anti-fermion pair. This effect is well known in π decay where $\pi \to e\bar{\nu}_e$ is highly suppressed relative to $\pi \to \mu\bar{\nu}_\mu$ despite a favorable phase space factor. This suppression can be overcome by having one of the initial state quarks radiate a gluon or by having a gluon in the D wave function. As was argued previously, it is reasonable to expect to have one (or more) gluons in the wave function during the decay some considerable fraction of the time. Various authors [8] have estimated the non-spectator contribution to the non-leptonic D^0 rate is about the same size or even larger than the spectator rate. The calculations are not very precise because they contain bound state effects that involve large model uncertainties.

Regardless of theoretical uncertainties, evidence for W-exchange can be observed experimentally by looking for decay modes which occur only through W-exchange and not the spectator graph, for example $D^0 \to \phi\bar{K}^0$. The strength of non-spectator diagrams relative to the spectator graph will be determined by such measurements and to some extent by the measurement of $\tau_{D^\pm}/\tau_{D^0}$.

Final State Interactions Final state interactions (FSI) are expected to make significant contributions to D decay rates because there are strangeness 1 resonances in the nearby 1.4–1.5 GeV region [9]. A complete theoretical analysis of FSI in D decays is complicated by the fact that most final states are highly inelastic. An example that will illustrate the importance of FSI is the $K\pi$ final state in D^0 decay. This analysis is fairly reliable since s-wave $K\pi$ scattering appears to be elastic up to about 1.4 GeV and can be extrapolated smoothly up to the D mass. In the naïve spectator model where color suppression factors are taken seriously, the $\bar{K}^0\pi^0$ decay mode is suppressed relative to $K^-\pi^+$ so that

$\Gamma(D^0 \to \bar{K}^0\pi^0) \approx \frac{1}{18}\Gamma(D^0 \to K^-\pi^+)$. Adding QCD corrections further suppresses the $\bar{K}^0\pi^0$ rate so that it is about $\frac{1}{45}$ of $\Gamma(D^0 \to K^-\pi^+)$ whereas experimentally it is found that [10]

$$\frac{\Gamma(D^0 \to \bar{K}^0\pi^0)}{\Gamma(D^0 \to K^-\pi^+)} = 0.35 \pm 0.07 \pm 0.07.$$

Note that the two rates can be written as linear combinations of isospin states. The suppression of $\bar{K}^0\pi^0$ implies a cancellation of the isospin amplitudes. This cancellation can be removed by FSI which introduce phase shifts between the amplitudes. The following exercise demonstrates this.

Assuming $K\pi$ scattering in the 0^+ state is elastic up to the D mass, the FSI are parameterized by elastic scattering phases δ_1 and δ_3. The D^0 decay amplitudes can then be written as

$$A(D^0 \to \bar{K}^0\pi^0) = \frac{1}{\sqrt{3}}\left(\sqrt{2}A_3 e^{i\delta_3} + A_1 e^{i\delta_1}\right)$$
$$A(D^0 \to K^-\pi^+) = \frac{1}{\sqrt{3}}\left(A_3 e^{i\delta_3} - \sqrt{2}A_1 e^{i\delta_1}\right)$$

where A_1 and A_3 are the $I = \frac{1}{2}$ and $I = \frac{3}{2}$ amplitudes without FSI, respectively. If the $\bar{K}^0\pi^0$ is suppressed in the absence of FSI, then $A_1 = -\sqrt{2}A_3$ and

$$\frac{\Gamma(D^0 \to \bar{K}^0\pi^0)}{\Gamma(D^0 \to K^-\pi^+)} = \frac{8}{9\cot^2\left[\frac{1}{2}(\delta_3 - \delta_1)\right] + 1}.$$

With FSI, however, the $\bar{K}^0\pi^0$ rate is suppressed only if $\delta_3 \approx \delta_1$. Note now that the $I = \frac{3}{2}$ channel is exotic and has no resonances while the $I = \frac{1}{2}$ channel contains many resonances, in particular the $\kappa(1350)$ 0^+ state. Therefore at 1.4 GeV $\delta_1 = 90°$ and δ_3 is known to be about $-25°$ to $-30°$, leading to a value for $(\delta_3 - \delta_1)$ of 120° to 180° at the D mass. This yields the remarkable result that

$$\frac{\Gamma(D^0 \to \bar{K}^0\pi^0)}{\Gamma(D^0 \to K^-\pi^+)} \gtrsim 1$$

which is in complete disagreement with spectator model expectations.

The conclusion is that FSI can introduce strong interaction effects which completely dominate the underlying weak interaction processes. A consequence of this is that lifetime difference for charged and neutral D's can be generated within the spectator model framework. The reason is the non-leptonic $D^{\pm}$ decays are purely $I = \frac{3}{2}$ whereas non-leptonic D^0 decays, as shown above, contain both $I = \frac{3}{2}$ and $I = \frac{1}{2}$ contributions and are thus susceptible to FSI. Unfortunately, the magnitude of lifetime difference produced by FSI can not be predicted accurately and the role of FSI will be ascertained only by precise measurement and comparison of two body D decays (see Kamal, ref. [9]).

Pauli Principle Interference Another mechanism exists which can produce D lifetime differences, namely interference in the final state of $D^{\pm}$ decay [11]. Figure 1.4 shows the quark configurations and final states for the Spectator Model decays of the D^0 and D^+ resulting from the two terms in the QCD corrected H_{NL}. For D^0 decays the final states are distinct, while for the D^+ they are identical since there are two $\bar{d}$ quarks in the final state. Therefore the two D^+ decay amplitudes can interfere. The interference is destructive, in accordance with the Pauli Principle where the reassignment of identical fermions, namely the $\bar{d}$ quarks, between the two diagrams introduces a relative minus sign between the amplitudes. Note that if color suppression of diagram (d) in Figure 1.4 is lifted (the case of so-called $\underline{6}$ dominance where $c_- \gg c_+$ [11]) the cancellation of the D^+ amplitudes is complete. This interference serves to suppress the $D^{\pm}$ non-leptonic rate, thus increasing $\tau_{D^{\pm}}$ and the $D^{\pm}$ semi-leptonic branching ratios.

The magnitude of the interference effect on the total $D^{\pm}$ rate clearly depends on the overlap of the quark wave functions, and therefore is not calculable exactly

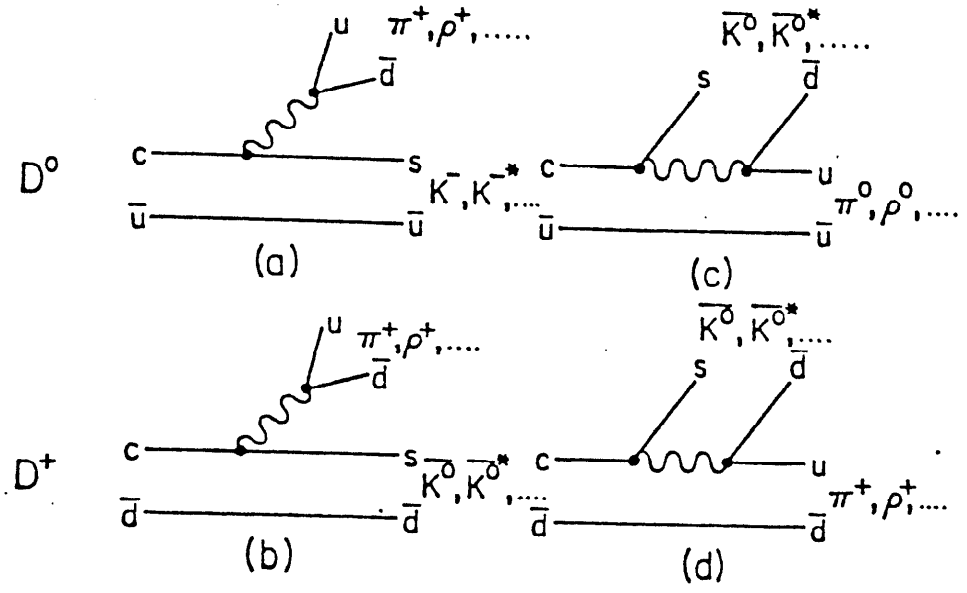

Figure 1.4: Spectator Model diagrams for non-leptonic D^0 and D^+ decays. Diagrams (a) and (b) have amplitudes proportional to $(c_- + c_+)$, (c) and (d) are proportional to $(c_- - c_+)$.

and must be estimated in some model. Following Ref. [1], the contribution Γ_I of interference to the $D^{\pm}$ decay rate is

$$\Gamma_I = -\left(c_-^2 - 2c_+^2\right)\frac{G_F^2}{\pi} m_D^2 \left|\psi(0)\right|^2 .$$

The wave function at the origin $\psi(0)$ can be evaluated in bag models, by using QCD sum rules, or alternatively by its relation to the D decay constant

$$f_D^2 = 12\,\frac{\left|\psi(0)\right|^2}{m_D}.$$

The ratio of the interference rate to the $D^{\pm}$ non-leptonic rate is then

$$\frac{\Gamma_I}{\Gamma_{NL}} = \frac{\left(c_-^2 - 2c_+^2\right)}{\left(2c_+^2 + c_-^2\right)}\left(\frac{4\pi f_D}{m_D}\right)^2 .$$

To demonstrate the uncertainty in the calculations consider that, with $f_D =$ 200 MeV [1] and c_+,c_- as found previously in this chapter, the above expression yields $\Gamma_I/\Gamma_{NL} \sim 90\%$ while relativistic quark model calculations suggest $\Gamma_I/\Gamma_{NL} \sim$ 20% [11]. In any case, the interference effect can be observed experimentally, for example, by comparing the Cabibbo suppressed modes $D^+ \to \pi^0\pi^+$ and $D^+ \to \bar{K}^0K^+$, where interference is expected for the former mode but not the latter. Data on these modes will be discussed in Chapter 5.

1.6 SUMMARY

The theoretical predictions for D meson lifetimes are

$$\tau_D \sim (1-10)\times 10^{-13}\text{sec.}$$

$$1 \lesssim \tau_{D^\pm}/\tau_{D^0} \lesssim 10$$

The current state of the theory is clearly malleable enough to accommodate a wide range of experimental results. The uncertainties in the predictions arise because

charm quarks are not free particles but come in complicated bound states. It is therefore up to experiment to give the theory the guidance necessary to decide the relative importance of the many and varied contributions to the charm meson lifetimes.

In this thesis, I will describe the results of two experiments, BC72/73 and BC75, performed at the Stanford Linear Accelerator Center (SLAC) using the SLAC Hybrid Facility (SHF). Charm particles were produced in γp interactions with 20 GeV photons incident on a hydrogen filled bubble chamber. Both experiments used essentially the same apparatus, although BC75 incorporated many improvements, and so the data will be combined for the final results. Throughout this work BC73/75 will refer to the combined experiments. The SHF apparatus and improvements will be detailed in Chapter 2, the charm event sample will be extracted in Chapter 3 and used in Chapter 4 for the D lifetime analysis. Discussion and conclusions about what the lifetime results can say about the theoretical situation outlined above will be the subject of Chapter 5.

Chapter 2: Experimental Details

The experiments BC72/73 and BC75 were performed at the SHF with essentially the same apparatus shown in Figure 2.1. Briefly, the experiments consisted of a photon beam incident on a liquid hydrogen filled bubble chamber (BC) followed by a downstream hybrid system made up of four sets of proportional wire chambers, two threshold Cherenkov counters and finally a wall of lead glass blocks. This chapter will describe the beam, the SHF and the trigger.

2.1 Backscattered Photon Beam

The unique feature of BC73/75 is the 20 GeV photon beam shown in Figure 2.2. The beam is essentially monochromatic and has a quite different spectrum from other high energy photon beams which are produced by bremsstrahlung. The beam is produced by scattering 4.68 eV photons from a frequency quadrupled Nd:YAG laser off the 30 GeV electrons delivered from the SLAC linear accelerator. The laser was pulsed at 10–12 Hz matching the bubble chamber expansion rate. The ultra-relativistic Compton scattering kinematics give the following relation for E_γ, the scattered photon beam energy

$$E_\gamma = \frac{\omega_i(1-\beta\cos\theta_1)}{1-\beta\cos\theta_2+(\omega_i/E_i)(1-\cos\theta)}$$

where

ω_i = incident photon energy

E_i = incident electron energy

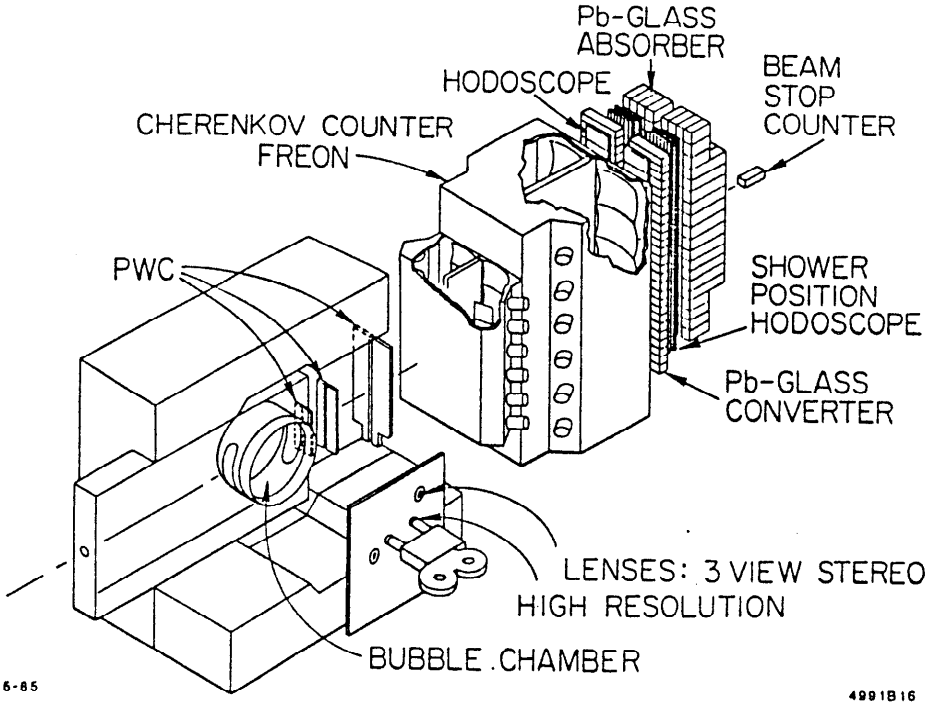

Figure 2.1: The SLAC Hybrid Facility.

θ_1 = angle between incident photon and incident electron

θ_2 = angle between scattered photon and incident electron

θ = angle between incident and scattered photon

β = velocity of incident electron

The maximum E_γ is achieved by making the collision head on, *i.e.* $\theta_1 = \pi$, $\theta_2 = 0$ and $\theta = \pi$. After a little manipulation, the expression for E_γ reduces to

$$E_\gamma^{max} = \frac{4\omega_i E_i}{m_e^2 + 4\omega_i E_i} E_i$$

Plugging in $\omega_i = 4.68$ eV and $E_i = 30$ GeV gives $E_\gamma^{max} = 20.5$ GeV. The beam in reality is not exactly monochromatic primarily because the backscattered photons have a finite angular acceptance.

The photon beam was monitored by a drift chamber pair spectrometer located just upstream of the bubble chamber, see Figure 2.2. A thin copper foil converted about 1% of the beam photons into e^+e^- pairs which were subsequently analyzed by the spectrometer, details of the pair spectrometer and an excellent discussion of the entire beam line are found in [12]. The E_γ spectrum obtained from the pair spectrometer is displayed in Figure 2.3 and shows that the beam is nearly monochromatic with an average energy of 19.5 GeV with a FWHM of about 2 GeV.

The beam intensity was typically 20–30 γ/pulse. The photon flux was made as large as possible to maximize statistics but was restricted in order to maintain good conditions for photographing charm events. If the flux is too high there are two detrimental effects: (1) the number of e^+e^- conversion pairs per photograph becomes so large that it becomes difficult to scan the film for the hadronic events of interest, and (2) these same e^+e^- pairs, due to their $\sim 0^\circ$ opening angle, deposit much of their ionization loss energy along the beam path which, after a number

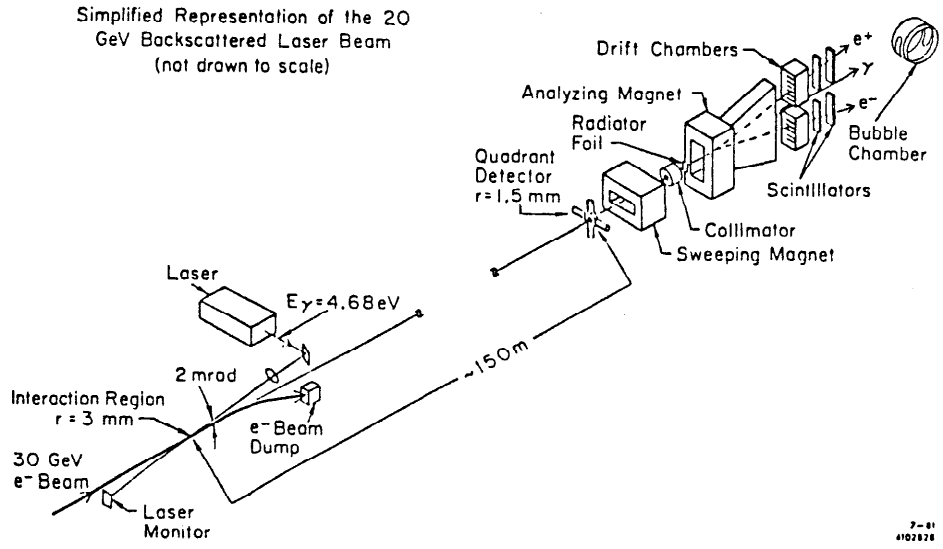

Figure 2.2: The 20 GeV backscattered photon beam.

of successive beam crossings of sufficiently high flux, can produce thermal disturbances in just the volume of hydrogen where charm decays occur thus distorting the image. In practice it was found that 30–35 γ/pulse was the tolerable upper limit to the photon flux.

2.2 THE BUBBLE CHAMBER

The bubble chamber used in these experiments was the SLAC 1-m chamber. Commissioned in 1967, BC75 was the last experiment for the chamber. The chamber was filled with liquid hydrogen that served as both proton target and charged particle detector. The chamber was a cylindrical in shape with a 1 m diameter and 43 cm deep, the beam was directed along a diameter through the middle of the chamber. Parallel to the axis of the chamber was a magnetic field of 26 kG and later 18 kG. The expansion piston formed the back wall of the chamber and was covered with Scotchlite, a retro-reflective material, for the bright field photography. A quartz glass window provided the opposite wall of the chamber through which the photographs were taken.

The operating conditions were optimized for the study of charm particles. In order to see short decays, a high bubble density is needed. Slow bubble growth is also required so that there is time to make a trigger for the flash lamps while the bubbles are still sufficiently small. Both conditions are met by running the chamber "hot", T = 29K instead of the more usual 26K, and by increasing the expansion ratio. This was demonstrated previous to BC72/73 at CERN with the hydrogen bubble chamber LEBC [13] and guided by their experience we found that with T = 29K and a bubble growth time of 200μs we obtained 55μm diameter bubbles with a linear density of 60 bubbles/cm. Assuming $\tau_D = 7 \times 10^{-13}$ sec and D momentum of 8 GeV (typical for $D\bar{D}$ pair production at $E_\gamma = 20$ GeV)

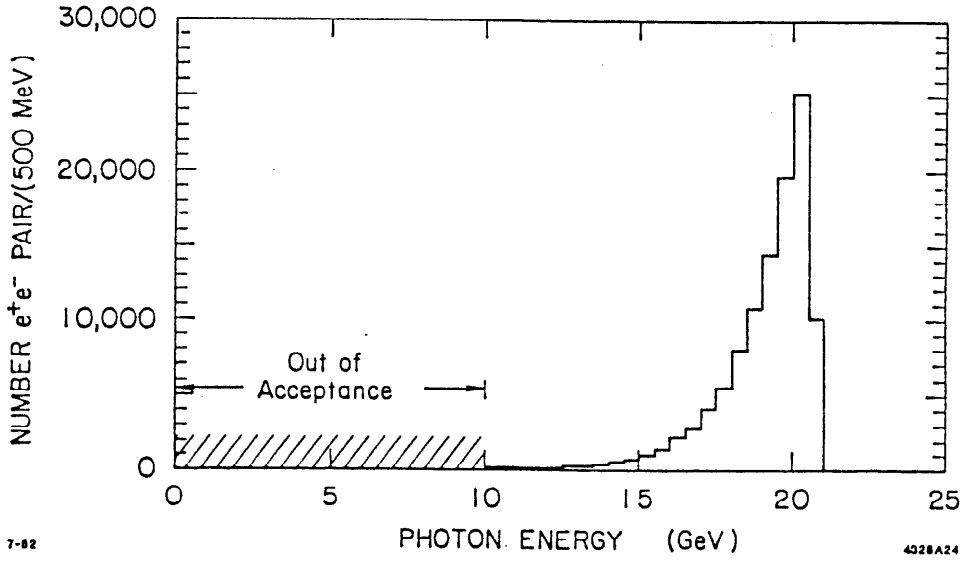

Figure 2.3: The photon beam energy spectrum.

then the mean D decay length expected for this experiment is about 1000 μm. Therefore the above operating conditions produce bubble size and density suitable for charm studies at the SHF provided the BC is equipped with a camera capable of resolving 55μm bubbles and can be triggered in $\lesssim$ 200μs. The camera and trigger are discussed later in this chapter. The bubble chamber expansion rate was 10–12 Hz; while 15 Hz was attained, the operation was not stable enough for sustained running and in practice 12 Hz was the upper limit.

2.3 High Resolution Optics Camera

The BC was equipped with two camera systems, a low resolution stereo triplet of cameras and a High Resolution Optics (HRO) camera. The low resolution cameras had 125 mm lenses operated at *f22* to get a depth of field covering the entire chamber volume with a resolution of about 300 μm and the 3-view stereo configuration provided 3-dimensional track reconstruction and kinematic analysis for charged tracks throughout the chamber. The HRO camera had much better resolution but substantially worse depth of field and was used solely to photograph the region near the production vertex of events to search for charm decays. This section is concerned primarily with the HRO camera, but first a description of the overall system. Figure 2.4 shows the layout with the BC window separated by 169 cm from the vacuum tank viewports through which photographs were taken. Figure 2.5 shows the positioning of the viewports as seen along the BC axis and indicates the relative positions of the cameras. In photographing an event, the bubbles are illuminated twice by the flash lamps. The first flash is 175μs after the beam spill by the HRO camera and the second flash is 3 ms later when the bubbles have grown to 400μm for the low resolution cameras. The durations of the flashes were 50μs and 300μs respectively. The coexistence of the two camera

systems caused several problems for the HRO images, the remedies are described below.

Table 2.1

Experiment	Lenses	Rayleigh Criterion Resolution	Depth of Field	Demagnification
BC72/73	One 360mm at *f11*	45μm	$\pm$6mm	5.5
BC75	Two 610mm at *f11*	30μm	$\pm$2mm	2.7

The parameters for choosing the optics for the HRO cameras in addition to the desired bubble resolution were (1) large enough depth of field so that tracks from events originating throughout the 3mm diameter beam travel sufficiently far before going out of focus, and (2) restricting the demagnification from space to film so that bubbles have images no smaller than $\sim$ 8μm on film while at the same time keeping the overall HRO frame size compatible with available scanning tables. The BC72/73 HRO camera was substantially upgraded for BC75, details of the optics for both cameras are summarized in Table 2.1. For BC72/73, a single lens HRO camera was installed which photographed the central 80% of the 1m beam path. Bubbles recorded on the HRO film were $\sim$ 55μm in diameter. The camera location, as shown in Figure 2.5, aligned the optical axis along the BC axis. In this position specular reflections off the window and Scotchlite surfaces from the HRO flash and low resolution View 2 camera flash resulted in flares on the HRO film which obscured $\sim$ 15% of the fiducial volume right along the beam. The low resolution camera flashes had two other detrimental effects for the HRO images: (1) they produced specular reflections (effectively dark field photography) off the 400μm bubbles which severely distorted the HRO bright field images, and

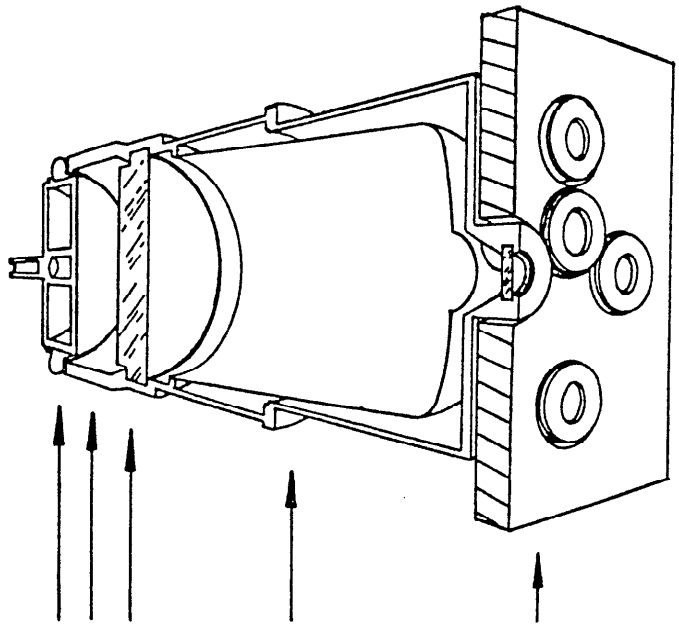

Figure 2.4: Vertical section along the bubble chamber cylindrical axis, shown in perspective. The arrows indicate, from left to right: the drive shaft and piston; the liquid hydrogen volume; the optical glass window; the snout of the vacuum tank; the camera positioning plate, penetrated by the viewport window mounts.

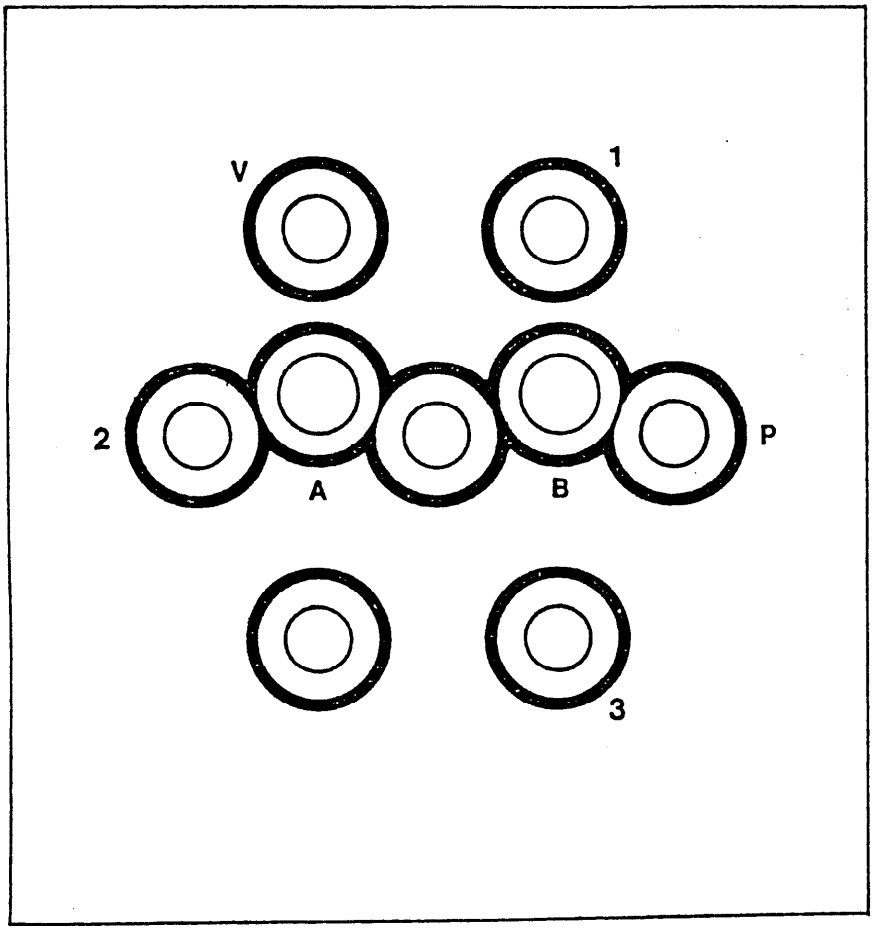

Figure 2.5: Layout of the bubble chamber vacuum tank view port window mounts. Numbers 1, 2 and 3 correspond to the low resolution cameras, while V and P were used by operators to monitor hydrogen conditions visually and photographically during running. The central view port was used by the BC72/73 HRO camera, the ports marked A and B were for the two lens BC75 HRO camera.

(2) they increased the general light level so that the average density on the HRO film was raised thus reducing contrast. The remedy for the low resolution camera flash problem was the installation of a mechanical shutter which was open for the HRO flash but closed in the 2.5 ms before the low resolution camera flash [14]. The BC75 HRO camera [15] cured the HRO flash problem by placing the lenses parallel to the window 6.7 cm above the BC axis, see Figure 2.5, so that the HRO flash was directed off the film.

Experience with BC72/73 film revealed that the most desirable improvements for the upgrade of the HRO camera were getting better resolution so that smaller bubbles could be photographed, and lower demagnification in order to increase the bubble image size relative to the film grain. The price to pay for these improvements is in reduced depth of field. It was decided that a depth of field of $\pm$2mm was sufficient for the charm studies and this turned out to be true. With these considerations in mind, the BC75 HRO camera consisted of a two lens system, each lens viewing roughly half the fiducial volume with a small overlap of the views at the center of the chamber. The longer focal length lenses allowed the BC75 HRO camera to resolve bubbles of $\sim$ 45μm in diameter. Using two lenses reduced the demagnification by a factor of 2 which resulted in film that was considerably easier to analyze.

2.4 Downstream Detectors

The function of the downstream detector system was twofold: (1) online it provided the trigger, and (2) offline it aided in charged particle momentum reconstruction, particle identification, and neutral particle detection. The trigger will be covered in the next section. This section will briefly describe each of the downstream detectors and their role in the analysis.

Proportional Wire Chambers Immediately downstream of the BC were 4 stations of Proportional Wire Chambers (PWCs) of which only the first 3 were used for BC73/75. For charged tracks in the PWCs' acceptance, which was determined by the BC exit window, the PWCs' tracking information was combined with the BC measurements to improve the momentum resolution. The resolution of these "hybridized" tracks is given by

$$\frac{\sigma_p}{p} = \left[(0.008)^2 + (0.00085\ p)^2\right]^{1/2}$$

for p in GeV.

Online, the PWCs also provided information for the trigger as described later in this chapter.

Cherenkov Counters Following the PWCs were two atmospheric pressure gas Cherenkov counters [16], the upstream counter was denoted by C1 and the downstream counter by C2. Each counter consisted of 12 cells arranged in two vertical stacks of 6 cells each, divided in the middle by blinds which contained the beam and e^+e^- conversion pairs. The threshold momenta for the particles of interest are given in Table 2.2 separately for BC72/73 and BC75. In BC75 the gas was changed in both counters to Freon 114 in an effort to get a lower π threshold thus extending the momentum range for π/K separation, an important feature for charm studies as discussed next.

The Cherenkov counters purpose was to help get a handle on the identity of the charm decays, and therefore the charm production mechanism, through charged particle identification. Although the acceptance of the counters is limited, it is not necessary to identify all decay products to determine which the species of charm particle. For example, even if a given neutral D decay has undetected neutral

decay products and thus can not be fully reconstructed, knowing the sign of the K or e from the decay distinguishes a D^0 from a $\bar{D}^0$.

Table 2.2

Threshold Momentum (GeV)

	BC72/73		BC75
Particle	C1 (Freon 12)	C2 (Nitrogen)	C1 + C2 (Freon 114)
e	0.01	0.02	0.01
μ	2.3	4.3	2.0
π	3.0	5.7	2.6
K	10.6	20.2	9.3
p	20.2	38.3	17.7

Lead Glass Wall After the Cherenkov counters was the Lead Glass Wall (LGW) shown in Figure 2.6 [17]. The LGW consisted of a filter hodoscope, a 1.13 radiation length lead passive converter, a lead glass active converter, and finally an array of 152 lead glass back blocks. The wall was divided in half vertically by an adjustable gap which contained the beam and e^+e^- conversion pairs.

The 24 cell filter hodoscope detected and flagged photons which converted upstream of the LGW, primarily in the BC exit window, to distinguish them from unconverted photons. The active converter was made up of 26 lead glass blocks on both sides of the detector and provided information on longitudinal development of showers. The finger hodoscope consisted of 46 vertical and 204 horizontal 2.5 cm wide fingers of scintillator and determined the shower position with a resolution of 7–8 mm. The back blocks were a lead glass absorber of 10.5 radiation lengths at wide angles and 21 radiation lengths in the central region

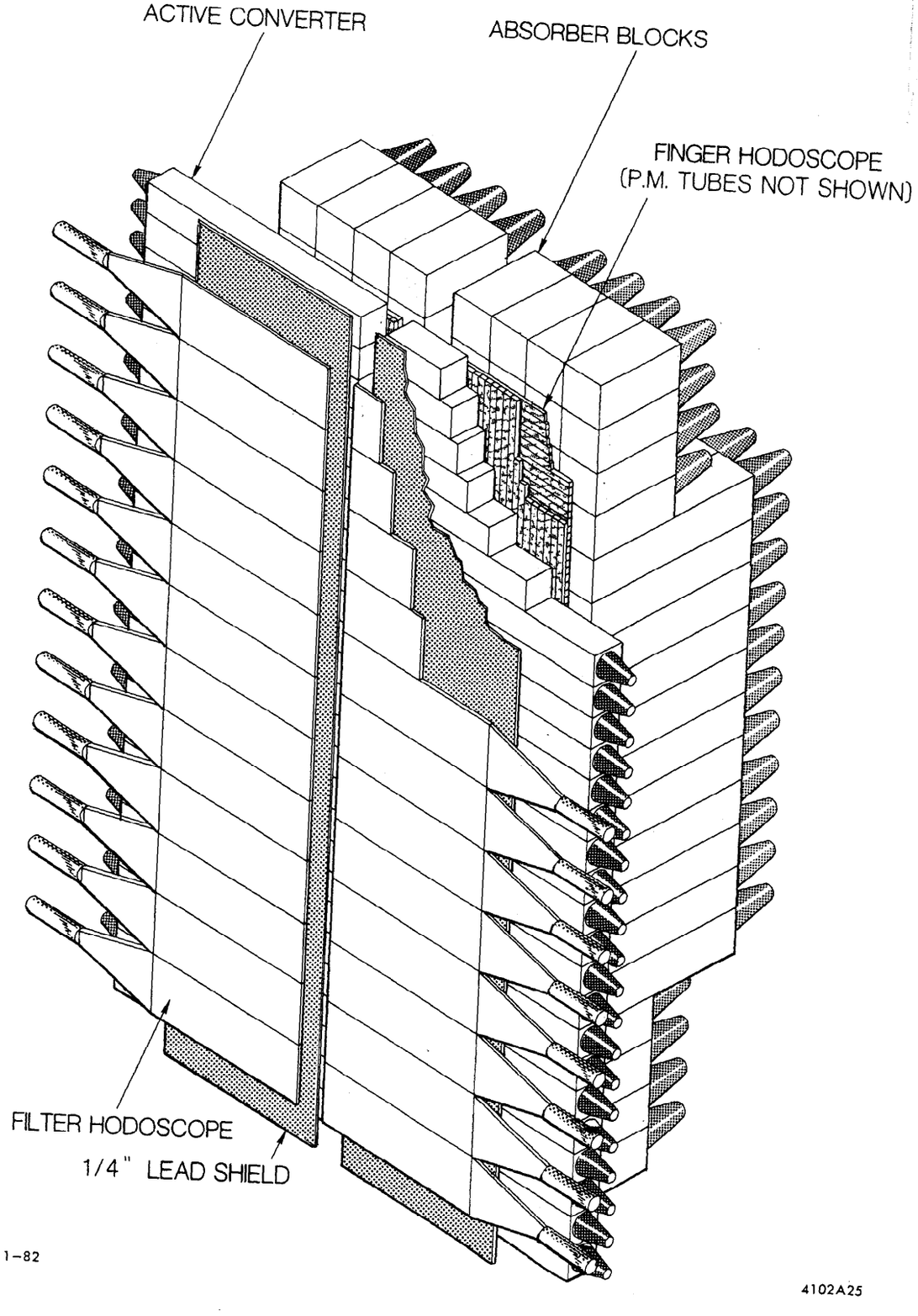

Figure 2.6: The Lead Glass Wall.

near the beam. For electron induced showers, the energy resolution of the wall was found to be

$$\frac{\sigma_E}{E} = \left(0.84 + \frac{4.8}{\sqrt{E}}\right)\%$$

for E in GeV.

The LGW had two contributions to the charm analysis: (1) particle identification by separating $e^{\pm}$'s from $\pi^{\pm}$'s, and (2) π^0 detection by measuring the decay γ's. On the first point, a set of cuts were developed on longitudinal and lateral shower development as well as total energy deposited in the LGW which test beam data demonstrated gave 10^{-4} pion rejection with 50% electron survival, see Ref. [17] for details. Such electron identification is useful for tagging semi-leptonic D decays. On the second point, since a substantial fraction of D decay modes have π^0's, in order to reconstruct these modes it is necessary to have some facility for detecting π^0's. The two γ mass plot from the LGW is shown in Figure 2.7 and the π^0 peak is clearly evident, the mass resolution at the π^0 mass is about 10 MeV.

Online, the LGW was also involved in the trigger decision as discussed in the next section.

2.5 TRIGGER

The camera trigger was composed of two separate triggers which were OR-ed together. One part of the trigger was supplied by the PWCs. Hits from the PWCs were combined online to reconstruct straight tracks in the non-bend plane. If a track intersected the BC fiducial volume a camera trigger was sent. For BC72/73 the track reconstruction was performed by a software algorithm in a 168/E processor [18] with the trigger decision available in about 115 μs. In order

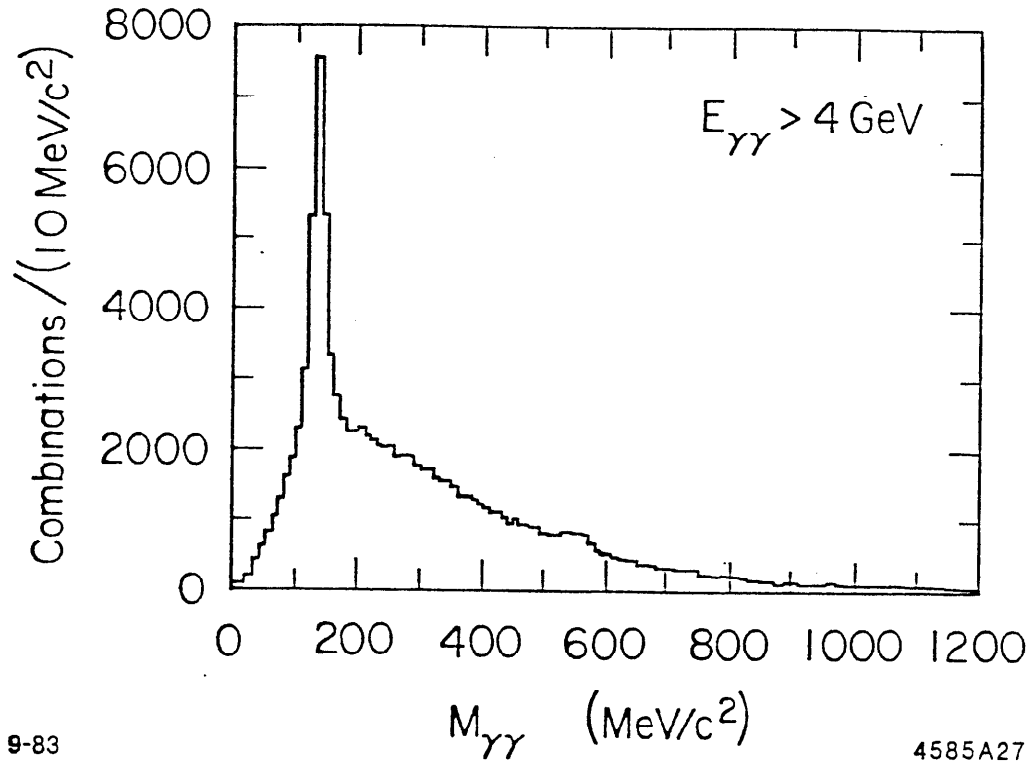

Figure 2.7: Two gamma invariant mass plot for photons in the LGW.

to photograph smaller bubbles in BC75, a dedicated hardware line processor [19] was installed, reducing the trigger decision time to about 90 μs.

The second part of the trigger came when sufficient energy was deposited in the LGW [17]. The dynode signals from the LGW photomultipliers were summed for each half of the active converter and back blocks by fast analog adders and then discriminated. A trigger was generated if 800 MeV was found in the active converter or 2.0 GeV in the back blocks. The LGW trigger was available within 1 μs.

The trigger was designed to provide an unbiased trigger on the entire 115μb γp hadronic cross section. To this end, the PWC and LGW triggers complimented each other so that the overall trigger was roughly independent of event charged multiplicity. The PWC trigger had higher efficiency for high multiplicity events while the LGW trigger had higher efficiency for events with lower multiplicity and therefore more neutral energy. There was considerable overlap of the two triggers, for charm events 84% had PWC triggers and 70% had LGW triggers. For all events, the combined trigger efficiency was about 90%, while for charm events alone the trigger efficiency was about 86%. The trigger efficiency was determined by taking every 50^{th} frame untriggered while still recording the PWC and LGW trigger decisions.

Chapter 3: Data

3.1 Data Taking History

The SHF ran for about four months per year for four years. BC72/73 first took data in the summer of 1980 and finished in spring 1982. BC75 consisted of two runs in 1983. Some details of the two experiments are given in Table 3.1.

Table 3.1

	BC72/73	BC75	Combined
Number of Chamber Expansions			1.5×10^8
Number of Pictures	2,408,000	1,225,000	3,633,000
Hadronic Events in Fiducial Volume	378,000	310,000	688,000
Events Containing Charm	65	71	136

3.2 Event Selection

Scanning Procedure The film was scanned for charm according to the following procedure. First the low resolution 70mm film was searched for evidence of hadronic interactions. These multiprong interactions are easily found because the beam energy and flux were low so there are generally a small number of tracks in each picture and hadronic interactions are readily distinguishable from photon conversions. The scanning efficiency for hadronic interactions was found to be

$(99 \pm 1)\%$. Once a given hadronic interaction was found, the HRO film for that event was searched for evidence of decays near the production vertex. A decay candidate was defined as having either

(i) a clear decay vertex, or

(ii) a track which does not extrapolate back to the production vertex.

All of BC75 film was scanned out to 1.5 cm from the production vertex, approximately 50% of BC72/73 was scanned to 3 cm and 50% to 1 cm.

Cuts to Reject Non-Charm Decays A first level set of cuts were imposed on the candidates found by the above procedure. The purpose of these cuts was to reject non-charm decays, in particular photon conversions and strange particle decays. The cuts were the following:

(i) require decays have ≥ 2 charged tracks,

(ii) reject 2-prong decays if consistent with photon conversions or neutral strange particle decays (specifically: $M_{e^+e^-} < 50$ MeV, $M_{\pi^+\pi^-} < 550$ MeV, $M_{p\pi^-} < 1130$ MeV or mass within 5σ of γ, K^0, Λ masses),

(iii) reject 3-prong decays consistent with charged strange particle decays:

$$K^{\pm} \rightarrow \pi^{\pm}\pi^{+}\pi^{-}$$

$$\Sigma^{+} \rightarrow p\pi^{0}(\pi^{0} \rightarrow e^{+}e^{-}\gamma)$$

or with a neutral strange particle decay superimposed on a track from the production vertex.

Scrutinizing After these cuts, 136 events containing 161 multiprong decays remain. These events were then carefully "scrutinized". This procedure involved making high magnification (at least 20× space) photographic prints from which quantities used in the lifetime analysis were measured. A fine point scribe was

employed to make a small hole in the center of each bubble along the tracks from the event seen on the photograph. The tracks were then reconstructed by drawing lines passing through the holes on the back of the photo. Curvature templates were used to account for tracks bending in the magnetic field. In this way the production vertex and decay vertices were resolved and decay lengths and impact distances measured directly (with a ruler!) in the film plane. An impact distance for a track is defined as the minimum distance by which the backward projection of the track misses the production vertex. For a given decay, the largest impact distance was called d_{max} and the second largest d_2, see figure 3.1.

3.3 Final Charm Decay Sample

Standard Cuts

A last set of cuts was applied to the remaining events to ensure the decays passing cuts were found with high and uniform efficiency. These "standard cuts" were:

(i) $d_{max} > 110\mu m$ (2-3 track widths). Impact distances passing this cut are easily seen on the scan table even when the decay vertex is obscured by overlapping tracks. Thus this cut ensures the scanning efficiency is high and independent of overall event topology.

(ii) $d_2 > 40\mu m$. Impact distances passing this cut are easily measured at the scrutinizing stage and ensure the decay is a multiprong.

(iii) Projected decay length $\ell > \ell_0 = 600\mu m$. This cut was used to reduce the number of topologically ambiguous decays in the sample by separating the decay from the region where the density of tracks from the production vertex was highest.

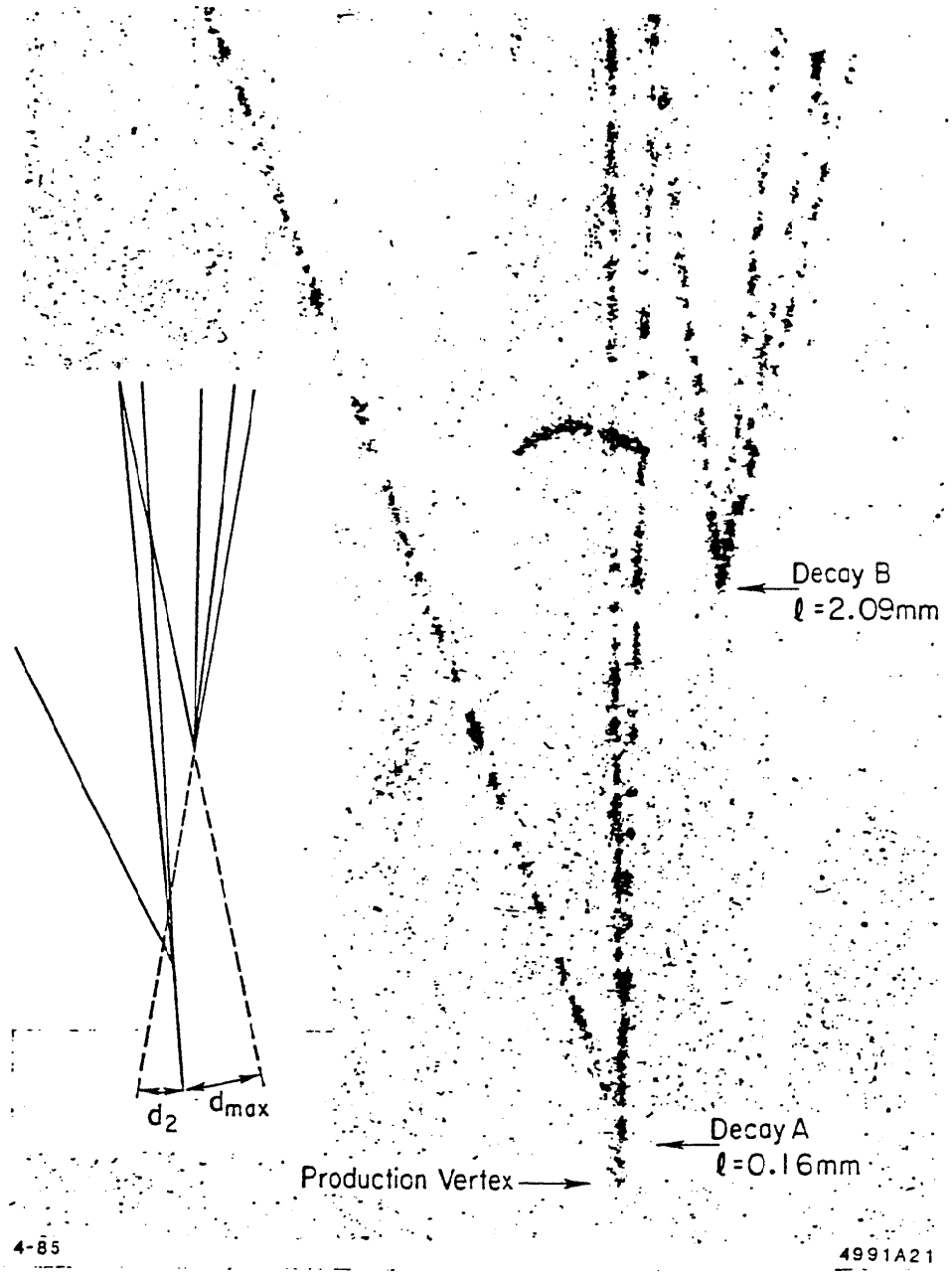

Figure 3.1: Photograph of an event taken by the HRO camera which contains two decays. The quantities d_{max} and d_2 for Decay B are shown in the inset.

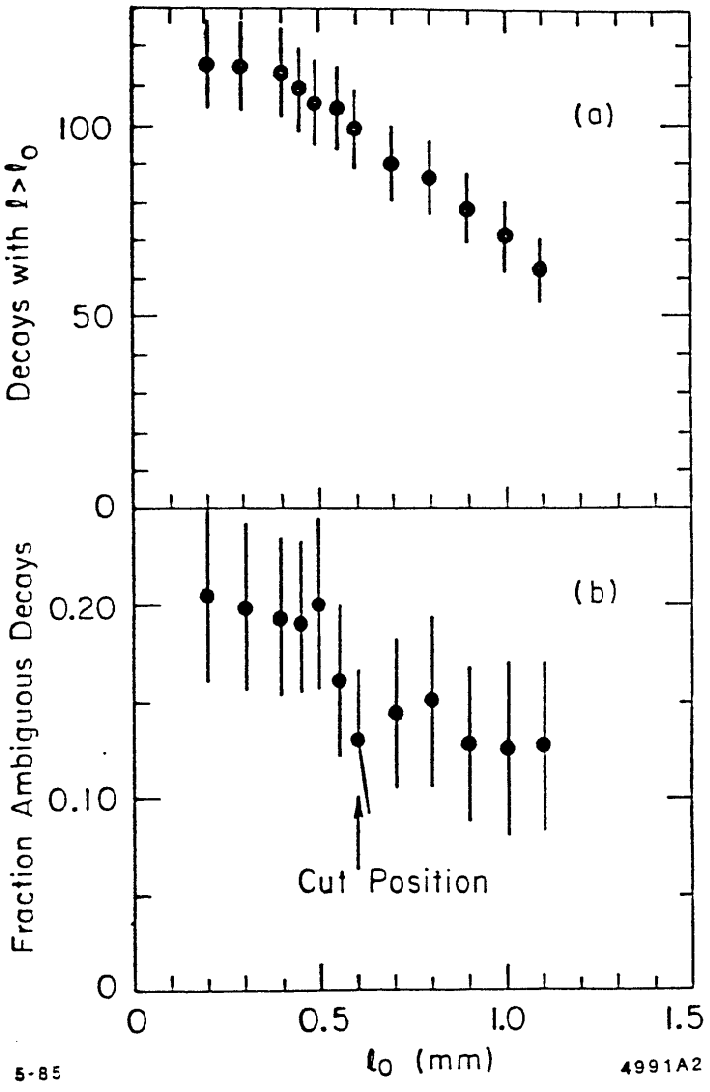

Figure 3.2: (a) Number of decays and (b) fraction of ambiguous decays passing all standard cuts as a function of length cut ℓ_0.

Figure 3.2 illustrates why the ℓ_0 cut was placed at 600μm. It shows that while the number of decays passing the ℓ_0 cut decreases steadily with increasing ℓ_0, the fraction of ambiguous decays in the sample passing the cut drops sharply between 500 and 600 μm and then levels off. Thus a cut at 600 μm reduces the fraction of ambiguous decays while retaining as many decays as possible for the lifetime calculation.

Ambiguous Decays

At this point there were 13 decays which were topologically ambiguous. This sort of ambiguity arises in one of two ways: (1) when a track from the production vertex overlaps the decay vertex making a neutral decay charged/neutral ambiguous or (2) when a genuine charged decay has a track with an impact distance consistent (within measurement error) with zero therefore simulating the first type of ambiguity.

The simplest and most common ambiguity is a 2-prong/3-prong ambiguity. This is illustrated in Figure 3.3 which shows a hypothetical event where $\gamma p \rightarrow$ 3 charged tracks and there are two multiprong decays that are, in principle, 2-3-prong ambiguous. The first criterion employed in resolving ambiguities is demanding decays be only neutral or singly charged. This requirement resolves the upper decay in Figure 3.3 as a negative 3-prong. The lower decay can not be unraveled on charge arguments alone. It could be either a positive 3-prong decay or a 2-prong decay with a positive track from the production vertex overlapping and additional criteria are needed to sort out the topology.

The following are the additional criteria used in resolving the 13 ambiguous decays:

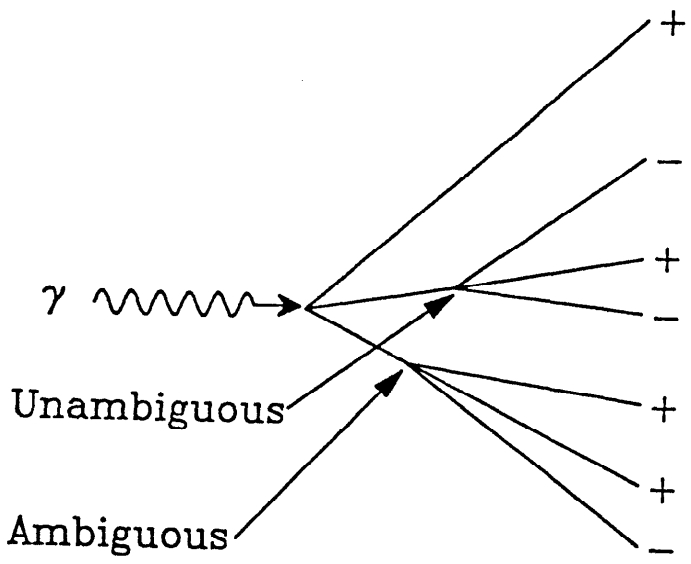

Figure 3.3: A hypothetical event with two decays which are 2-3-prong ambiguous. The charges of the particles are indicated on the right.

(i) An interpretation was rejected if the effective mass was larger than 2σ above the D mass. Five of the 13 decays had only one interpretation satisfying this condition and were resolved in this way. Note that no unambiguous charged or neutral decay failed this cut.

(ii) If a decay had one, and only one, interpretation consistent with being a Cabibbo favored D decay with no undetected neutrals (see section 3.6 for a detailed description of the "fully reconstructed" decay requirements) then that interpretation was taken. This criterion resolved three more decays.

(iii) An additional three decays were resolved as neutral D's because they had one interpretation consistent with being the product of $D^{*\pm} \rightarrow D^0\pi^{\pm}$ where the mass difference between the $D^0\pi$ system and the D^0 mass was less than 160 MeV/c^2. The background giving such a mass difference is small [20].

Only two decays remain unresolved. Both are charged/neutral ambiguous between 2- and 3-prong interpretations where one 3-prong is positive and the other negative. Their projected decay lengths were 1.32 and 1.95 mm and are typical for both charged and neutral D decays in this experiment, neither extraordinarily long or short.

Summary of Charm Decays

Figure 3.4 is a plot of ℓ *vs.* d_{max} for all 161 multiprong decays. Decays with $d_2 \leq 40\mu$m and the region excluded by cuts are indicated. Note that the cuts have been conservatively placed well into a smoothly varying distribution with many decays below the cuts.

After the standard cuts were applied, 100 decays from 94 events remain. Of the 100 decays, 48 are charged, 50 are neutral and 2 charged/neutral ambiguous and are summarized in more detail in Table 3.2.

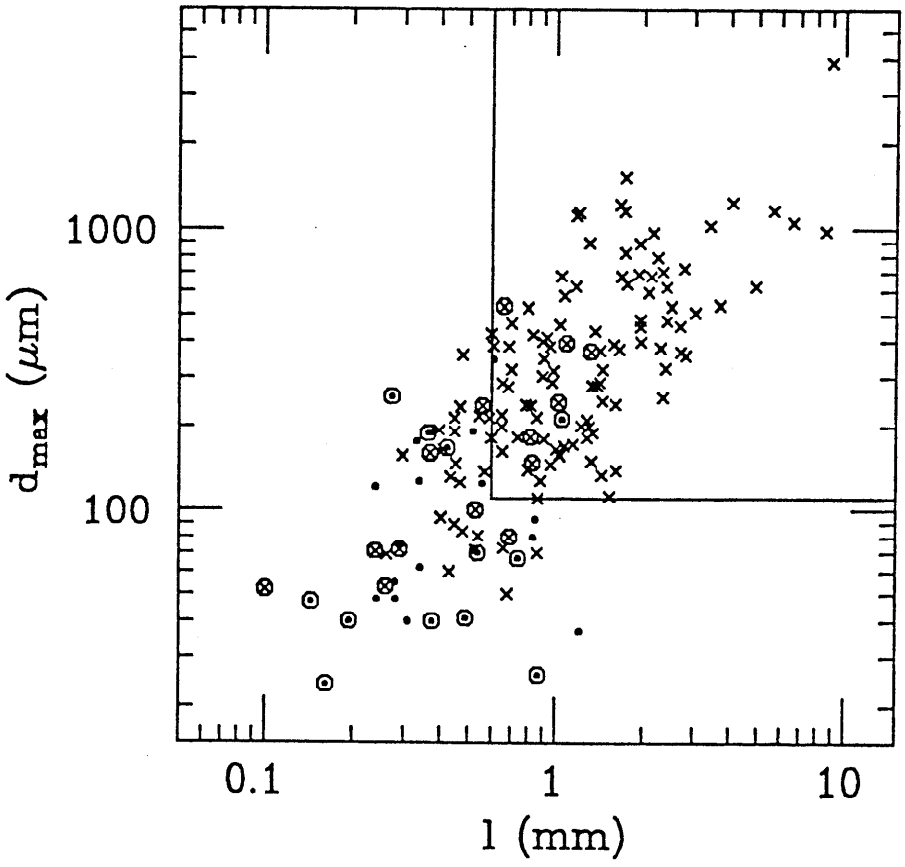

Figure 3.4: Scatterplot of d_{max} versus projected decay length ℓ for all multiprong decays. Decays with $d_2 > 40\mu$m are denoted by $\times$ and decays with $d_2 \leq 40\mu$m by $\bullet$. In addition, if a decay is the shorter decay in an event containing two visible multiprong decays then its symbol is surrounded by a circle.

Table 3.2					
		BC72/73	BC75	Combined	
Number of Events		50	44	94	
Number of Decays		53	47	100	
Positive Decays	3-prong	8	7	15	
	5-prong	0	0	0	48
Negative Decays	3-prong	16	15	31	
	5-prong	2	0	2	
Neutral Decays	2-prong	13	8	21	
	4-prong	13	16	29	50
Charged/Neutral Ambiguous		1	1	2	

3.4 CHARM SCANNING EFFICIENCY

The charm scanning efficiency is found by doing multiple scans. The efficiency is then calculated by a maximum likelihood method using the log likelihood function

$$\mathcal{L} = \left\{\sum_{i=1}^{n} N_i\right\} \log \epsilon + \left\{\sum_{i=1}^{n} (N_T - N_i)\right\} \log(1-\epsilon) - N_T \log\left[1-(1-\epsilon)^n\right]$$

where N_T is the total number of events found from all scans, N_i is the number of events found on scan i and n is the number of scans performed. The single scan efficiency ϵ is found by maximizing $\mathcal{L}$. Note that ϵ is assumed to be the same

for all scans. The combined charm scanning efficiency for all scans is found to be $(97^{+2}_{-4})\%$ for decays passing all cuts.

Figure 3.5 shows the scanning efficiency as a function of projected decay length for the charm decays and also for K^0 and Λ decays. Note that only decays passing the d_{max} and d_2 cuts are included. The figure demonstrates the efficiency is high and uniform for decays with lengths near and above the cuts.

A unique feature of this experiment is that the charm scanning efficiency can be independently checked. This is done by studying the relatively large sample of neutral strange particles, K^0's and Λ's, which decay in the chamber. These V^0's are visually quite similar to 2-prong D^0 decays and thus the efficiency for finding the V^0's in the charm scan region will provide a check on the charm scan efficiency.

The advantage we have is that the V^0 cross sections and momentum distributions have been measured in BC72/73 for V^0's found in the entire chamber volume where the scanning efficiency is high, uniform and well understood. Therefore this information can be used to predict, in a model independent way, the number of V^0's expected in the charm scan region as well as their distributions in length and impact distances, as will be described below.

As seen in Figure 3.5(b), the scan efficiency for V^0's in the charm scan region is high and uniform and is very similar to the charm scanning efficiency, thus confirming the utility of employing V^0's to investigate the charm scanning efficiency. As mentioned above, this V^0 efficiency can be checked in two ways: (1) see if the number of V^0's observed is consistent with the number predicted by the measured cross sections and (2) see if the ℓ and d_{max} distributions, those most important from a scanning efficiency standpoint, agree with the expected distributions.

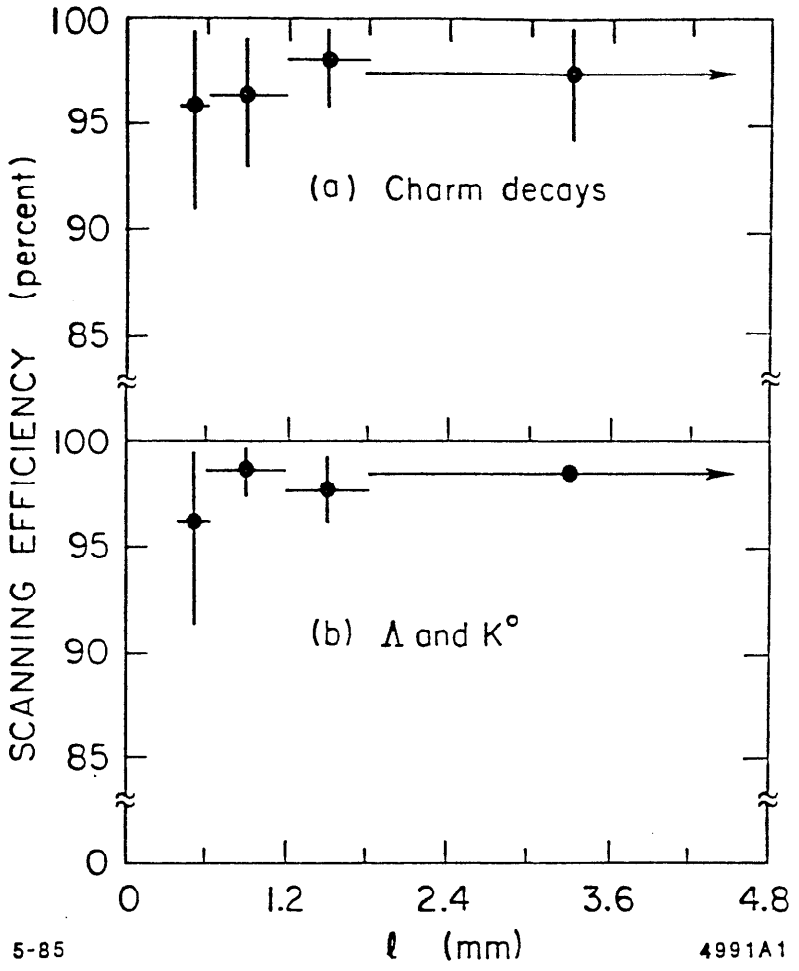

Figure 3.5: Scanning efficiency for (a) charm decays and (b) K^0 and Λ decays.

The first check is addressed in Table 3.3 which lists the cross sections for V^0's which decay in the charm scan region ($\ell < 1.5$ cm) and for V^0's found throughout the chamber from a published study of inclusive neutral strange particle photoproduction in BC72/73 [21]. The agreement is surprisingly good and we conclude we find the expected number of K^0's and Λ's, and therefore scanning losses are small for V^0's in the charm scan region.

Table 3.3

	$\sigma(\mu b)$	
	V^0 with $\ell < 1.5$ cm	All V^0
K^0	9.4 ± 0.9	9.45 ± 0.32
Λ	5.6 ± 0.6	5.60 ± 0.24

The second check is more sensitive to losses which could bias the lifetime measurement. As seen above, scanning losses, if any, are small for short V^0's. However if all losses occurred at, for example, short decay lengths then the resulting lifetime could be biased even by small losses. The efficiency for V^0's as a function of decay length is checked by plotting the ℓ distribution for the short V^0's as in Figure 3.6(a) where the V^0's are required to pass the d_{max} cut so that efficiencies at short lengths can be studied independently of d_{max}. The shape of the distribution is given by a model independent prediction made by taking the 4-vectors of real V^0's from the large sample found throughout the chamber and randomly assigning them decay lengths in the charm scan region. With the length and direction now fixed, the impact distances were then calculated and the decay was weighted by the inverse of the probability it would decay at its assigned decay

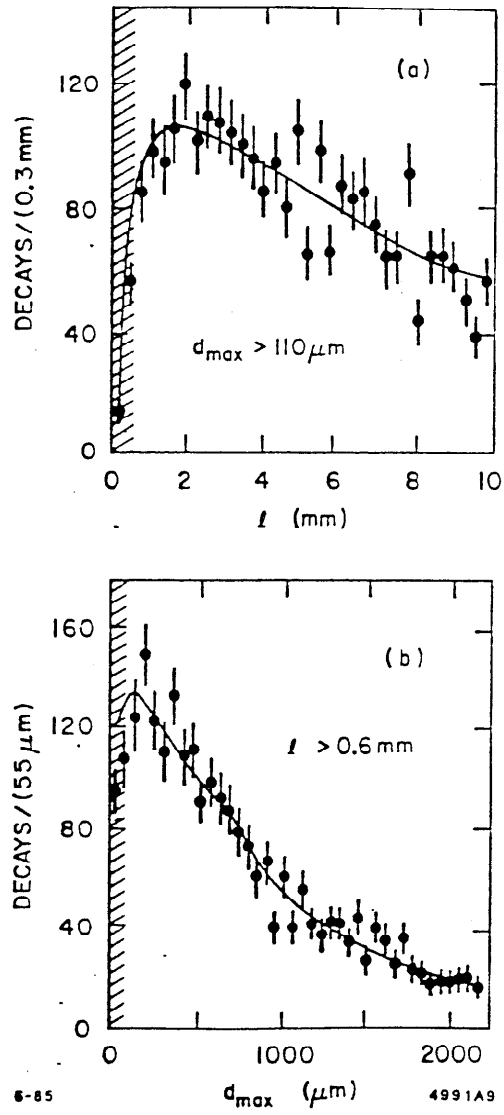

Figure 3.6: Distribution of K^0 and Λ decays as a function of (a) ℓ and (b) d_{max}. The shaded region is excluded by cuts. The curves are described in the text.

length. The 4-vectors were used as often as necessary to obtain smooth distributions. The resulting curve is normalized to the data above the ℓ cut. Figure 3.6(b) is the similar plot of d_{max} for V^0's passing the ℓ cut. The figures show very good agreement between the data and curve above the cuts and also that the data approach the curves even below the cuts indicating the efficiency is still high for small ℓ and d_{max}.

A final test of the V^0 scanning efficiency is to calculate the K^0 and Λ lifetimes using the V^0's found in the charm scan region (the same sample of V^0's used in the cross section calculation for Table 3.3). The results from a maximum likelihood determination of the lifetimes are given in Table 3.4 where the errors are statistical only. Also listed are the PDG [22] world average lifetimes and there is reasonable agreement between the values.

Table 3.4

	τ in units of 10^{-10} sec	
	V^0, $\ell < 1.5$ cm	PDG
K^0	$0.99^{+0.59}_{-0.28}$	0.8923 ± 0.0022
Λ	$1.53^{+1.13}_{-0.47}$	2.632 ± 0.020

The V^0 study confirms two points made earlier: (1) the cuts have been placed conservatively and not near some roll off of the scanning efficiency and (2) the multiple scan charm scanning efficiency calculation shows the efficiency is high and uniform. For the lifetime measurement, the fact that the efficiency is uniform is most important and has been demonstrated by Figure 3.5 where the efficiency is constant with decay length and checked in a model independent way using the

V^0's as in Figure 3.6. The conclusion is there is no significant scanning efficiency bias for the sample of decays passing cuts.

3.5 BACKGROUNDS

There are two main sources of possible background in the sample of 100 decays passing all cuts. The first possible source only affects the 2-prong sample and arises from decays of neutral strange particles. Two body decays of K^0's and Λ's can contribute when one (or both) of the decay particles either decays in flight or elastically scatters and the recoil proton is not observed. The momentum of the decay particle which kinks is then mismeasured resulting in an incorrect invariant mass for the 2-prong such that the decay passes cuts. The background from this source is estimated to be less than 0.4 events. A similar background for 2-prongs is from three body $\Lambda \rightarrow pe\nu$ decays, and is estimated to contribute less than 0.5 decays. The second type of potential background can contribute in principle to all decay topologies. This background results from secondary interactions of particles from the production vertex where the recoil proton has low momentum (< 60 MeV/c) and is not observed. On film, these secondary interactions will then look like decays. It is estimated that this background is negligible except for 2- and 3-prong simulated final states (with undetected neutrals) where the backgrounds are calculated to be 0.2 and 0.1, decays respectively.

Other sources of background such as two independent γp interactions close together or secondary interactions of tracks from the production vertex with deuterons present in the liquid hydrogen were found to be negligible. Therefore the results of these calculations is that the background is expected to be less than or about 1 event.

The background can be measured directly by considering the charm scan region beyond the zone occupied by the charm decays, as seen in Figure 3.4 this is beyond 10 mm. The point is, in going further from the production vertex, the number of charm decays drops rapidly while the number of background simulated decays persists and so the charm free portion of the charm scan region can be used to predict the number of background simulated decays in the region populated by charm decays. No charm candidates were found in the region beyond 10 mm which translates into an upper limit on the number of background events from all sources of less than 3.1 events (at 90% confidence level). The calculation takes into account that some sources of background are not constant with distance from the production vertex.

Finally, the sample of decays passing cuts was checked to determine if any decay was background. Each decay was carefully examined for kinks on outgoing decay tracks or for a proton stub which would indicate the decay was due to the backgrounds described above, and none were found. Also every decay was treated as if it was the product of a peripheral secondary interaction and the recoil proton momentum was calculated. Of the 48 charged decays, only two 3-prongs were consistent with having an unseen recoil proton, however, in each case there was another decay in the event, making the charm hypothesis very probable. In addition, each decay had a large transverse momentum imbalance (due to undetected neutral decay products) and therefore both are inconsistent with this background source. Of the 50 neutral decays, only three 2-prongs could have had an unseen recoil proton, although one had a large transverse momentum imbalance. It should be emphasized that all 100 decays passing cuts are entirely consistent with being charm decays.

To summarize the background studies, we expect from calculation less than or about 1 background event in the combined BC73/75 experiment. A direct measurement of the background puts a limit of less than 3.1 background events (at 90% confidence level). However, this limit would presumably be smaller if we had scanned further from the production vertex (as indeed was the case for BC72/73 where the higher HRO demagnification allowed scanning out to 3 cm and resulted in a limit of less than 1 background event for the experiment at 90% confidence level [23]). The decays have been carefully checked and there are only a few decays for which the background hypothesis can not be entirely ruled out. In conclusion, all the decays passing cuts are believed to be genuine charm decays and if there is any background, it is certainly $\lesssim 3$ decays.

3.6 JUST WHAT ARE THESE DECAYS ANYWAY?

Having obtained 100 clean multiprong decays, the question is what flavor charm particles are they? This section will endeavor to show that there is direct evidence for charged and neutral D mesons in the sample of decays passing cuts but no direct evidence for $F^{\pm}$ or Λ_c^+ decays.

Evidence for D Mesons Direct evidence for D mesons in the sample of decays passing cuts can be demonstrated by reconstructing exclusive D decays with no undetected neutrals. The following cuts were applied:

(1) Only Cabibbo favored non-leptonic modes with decay particle assignment consistent with available particle identification were tried. Specifically, all charged modes of the type $D \rightarrow K(n\pi)$ where $n = 1, 2, \ldots$ and also modes with one reconstructed π^0 or K_s^0 were included.

(2) The direction of the reconstructed 3-momentum vector for the decaying particle was required to match within 3σ with that measured in the film plane on the HRO blow-up photograph. The typical measurement error on this direction was $\sigma = 20$ milliradians.

(3) The error on the effective mass of the decaying particle was required to be less than 30 MeV/c^2.

Figure 3.7 shows the distributions of mass combinations passing these cuts. A signal at the $D^{\pm}$ mass of $m_{D^{\pm}} = 1869$ MeV/c^2 stands out clearly for the charged decays. The signal at $m_{D^0} = 1865$ MeV/c^2 is less clear for the neutral decays because there are 112 mass combinations for the 36 neutral decays while there are only 40 mass combinations for the 32 charged decays. A smaller combinatorial background exists for the charged decays because tracks with the same charge as the decaying particle were not tried as K's, thus for 3-prongs there is only one combination when no π^0 or K_s^0 has been reconstructed. For neutral decays, on the other hand, any charged decay particle can in principle be the K, as an extreme example a 4-prong decay can have up to 10 mass combinations if both a π^0 and K_s^0 are reconstructed in the event. Note that all decays having mass combinations above the D mass have a mass combination consistent with m_D when particle assignments are changed.

Decays were defined to be "fully reconstructed" if they satisfied the cuts (1)–(3) above and in addition had an effective mass within 3.5σ of the D mass. Fifteen charged and 16 neutral decays passed all cuts. Of these so-called "constrained" decays, 12 had identified kaons, 10 $K^{\pm}$ were identified by the Cherenkov counters and 2 K_s^0 were found which decayed in the chamber. The observed number of

fully reconstructed D decays is consistent with the total number of D's produced in this experiment [20] and the known branching ratios [22].

Search for $F^{\pm}$ Mesons A similar search was made for $F^{\pm}$ mesons in all pion modes and in $F^{\pm} \rightarrow K^{+}K^{-}\pi^{\pm}$ modes, again only when consistent with available particle identification. The effective mass combinations also satisfying cuts (2) and (3) are plotted in Figure 3.8. The enhancement seen near 2040 MeV/c^2 is due to the reflection of the fully reconstructed $D^{\pm}$ decays where a π has been assigned a K mass. Once the constrained $D^{\pm}$ decays are removed, leaving the shaded region in Figure 3.8, the enhancement disappears. Several experiments [24] have reported observing the F in the mode $F^{\pm} \rightarrow \phi\pi^{\pm}$ with an F mass of $m_F = 1971$ MeV/c^2 [22]. In a further effort to see the F by using the $\phi\pi$ mode, a plot has made for all two particle mass combinations in the charm events, again only if consistent with particle identification, and there was no signal in the vicinity of the ϕ. Therefore, no direct evidence for $F^{\pm}$ mesons has been observed in the events with decays passing cuts.

Search for Λ_c^+ Baryons No fully reconstructed Λ_c^+ decays were found in the sample of 15 positive decays passing cuts, and no Λ's or $\Sigma^{\pm}$'s were found in the events containing these positive decays. This is not surprising since the Λ_c^+ contamination of the positive sample is expected to be quite small, as will be shown in Chapter 4 and Appendix C. All mass combinations consistent with Cabibbo favored Λ_c^+ decays were examined both at the positive decay vertices and at the production vertices. These showed no signal above the combinatorial background at the Λ_c^+ mass of 2282 MeV/c^2 [22]. Although production mechanism studies have shown that $(71 \pm 11 \pm 6)\%$ [20] of the total charm production is $\Lambda_c^+ \bar{D}$

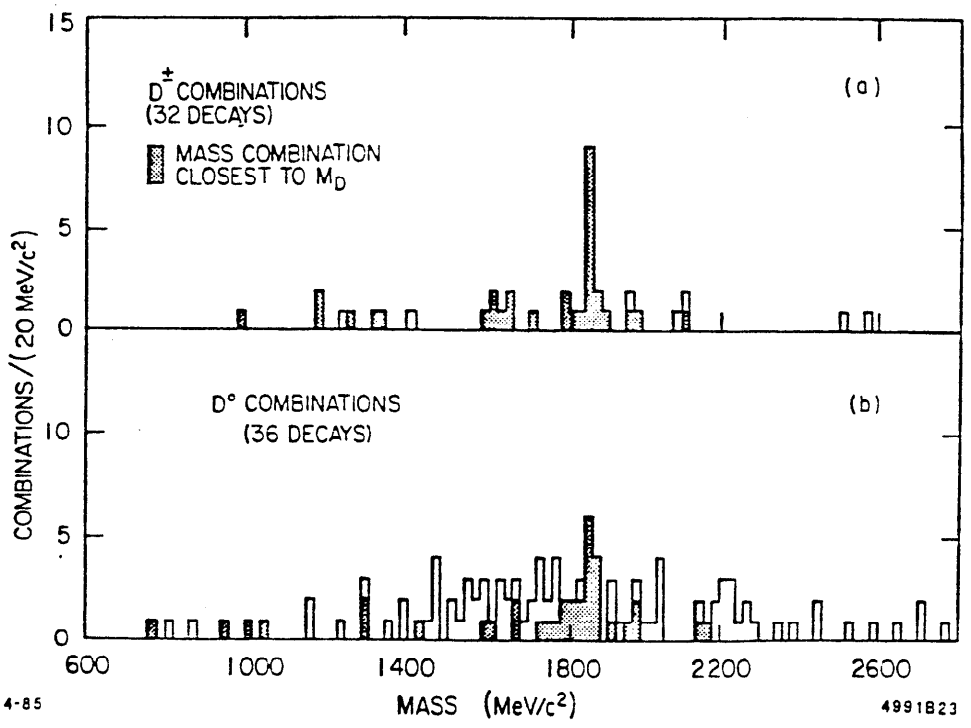

Figure 3.7: Distributions of effective mass combinations for (a) charged decays and (b) neutral decays. All decays pointing to the production vertex within 3σ including those containing one reconstructed π^0 or K_s^0 are plotted. Consistency with particle identification was imposed and the error on the effective mass was required to be less than 30 MeV/c^2. The shaded entries are the mass combination closest to the D mass for each decay.

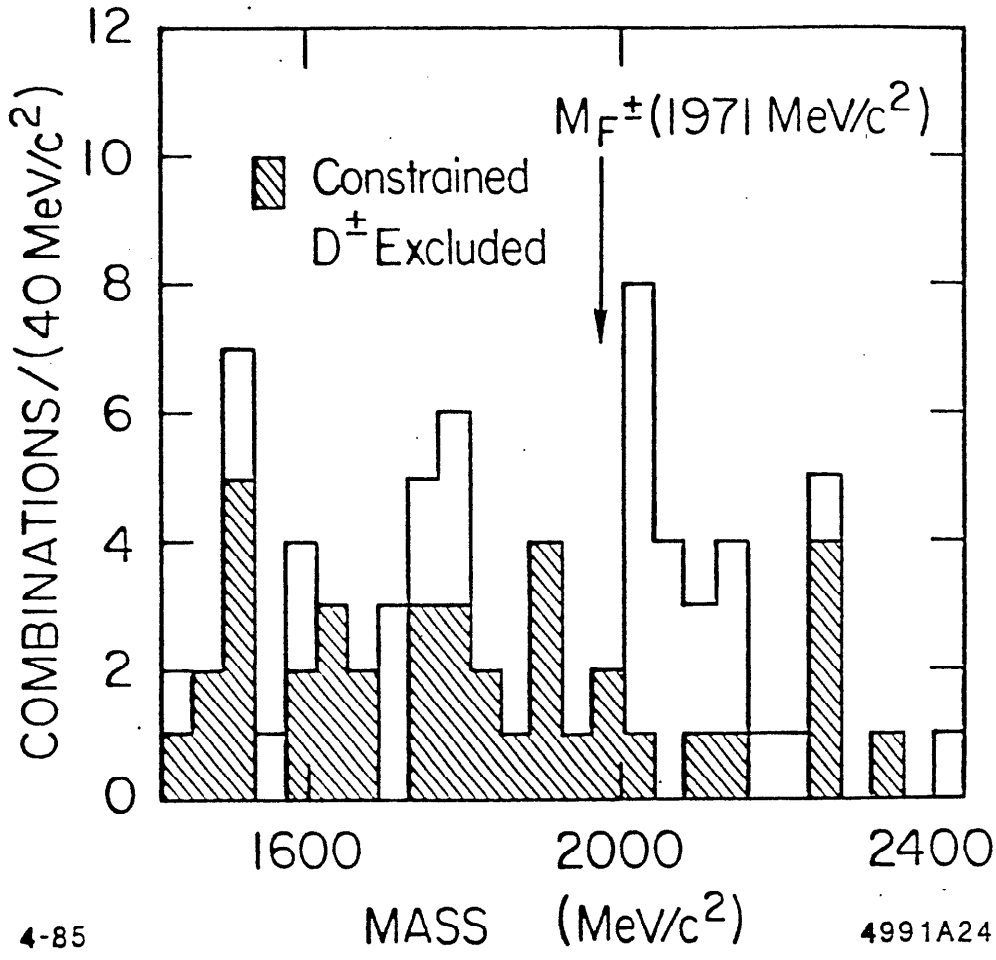

Figure 3.8: Distribution of effective mass combinations for the charged decays interpreted as $F^{\pm}$ mesons. Decays are required to point to the production vertex within 3σ, have decay particle assignments consistent with particle identification and the error on the effective mass less than 30 MeV/c^2. The hatch region shows those combinations remaining after the fully reconstructed $D^{\pm}$ decays are removed. The enhancement at 2040 MeV/c^2 is the reflection of the constrained $D^{\pm}$'s.

associated production, the cuts have excluded the Λ_c^+'s from the sample of decays passing cuts.

To summarize, there is direct evidence for charged and neutral D meson decays in the 100 decays passing cuts, while there is no direct evidence for $F^\pm$ or Λ_c^+ decays in the same sample. All of the 100 decays are compatible with being D decays, although for some unconstrained charged decays the $F^\pm$ or Λ_c^+ hypothesis can not be ruled out. The number of fully reconstructed D's is consistent with known D branching ratios. The conclusion is that it is most likely the decays passing cuts are D mesons and therefore all decays passing cuts will be treated as D's in the lifetime calculation. The effect on the charged D lifetime from possible $F^\pm$ or Λ_c^+ contamination of the charged D sample will be considered in the next chapter.

Chapter 4: Lifetime Calculation

4.1 INTRODUCTION

This chapter will describe the lifetime calculation performed using the sample of D mesons found in Chapter 3. The calculation employs a novel method for estimating the momentum of unconstrained decays so that they may be included in the lifetime determination. This method will be discussed at length. Before doing so, I will present the motivation for resorting to a non-standard method.

4.2 GENERAL APPROACH

The proper flight time for a given D decay is

$$t = \frac{\ell\, m_D}{c\, p_D}$$

where m_D and p_D are the mass and momentum of the D. For an experiment containing N decays, the lifetime τ is simply the average of the proper flight times

$$\tau = \frac{1}{N}\sum_{i=1}^{N} t_i.$$

This expression holds only if all decays have the same detection efficiency. However in this experiment, there are losses of decays with short lengths due to scanning inefficiencies. We can correct for the losses by using only the decays passing standard cuts which were chosen to assure a high and uniform scanning efficiency.

This requires replacing ℓ in the lifetime formula with an effective length ℓ_{eff} defined as

$$\ell_{eff} = \ell - \ell_{min}$$

where ℓ_{min} is the first point along the D flight path where the decay passes all cuts and is defined by

$$\ell_{min} = \max\left[\left(\frac{110\mu\text{m}}{d_{max}}\right)\ell, \left(\frac{40\mu\text{m}}{d_2}\right)\ell, \ell_0 = 600\mu\text{m}\right].$$

Since the distribution of flight times is exponential, ℓ can be replaced with ℓ_{eff} because the point at which a decay passes cuts does not depend on the decay point. Using ℓ_{eff} is equivalent to merely redefining the instant at which $t = 0$. The distribution of ℓ_{eff} for the 48 charged and 50 neutral decays passing cuts is shown in Figure 4.1.

The lifetime is now given by

$$\tau = \frac{1}{N}\sum_{i=1}^{N}\frac{\ell_{eff_i}\, m_D}{c\; p_{Di}}.$$

Thus all one needs to measure the lifetime is the ℓ_{eff} and momentum for a set of D decays. The usual procedure is to take only a subset of the data containing the constrained D's where ℓ_{eff} and p_D are known. As shown in Chapter 3, if we restricted ourselves to using only constrained decays, we would have just 15 charged and 16 neutral decays with which to calculate the lifetimes, roughly 1/3 our total sample of decays passing cuts. With 15 decays, the lifetime measurement is totally statistics limited. Since we have 100 decays which are perfectly good from an efficiency point of view, it is highly desirable to find a way in which to incorporate all the decays into the lifetime calculation. In order to do this, we must estimate the single quantity we do not measure for every decay – the

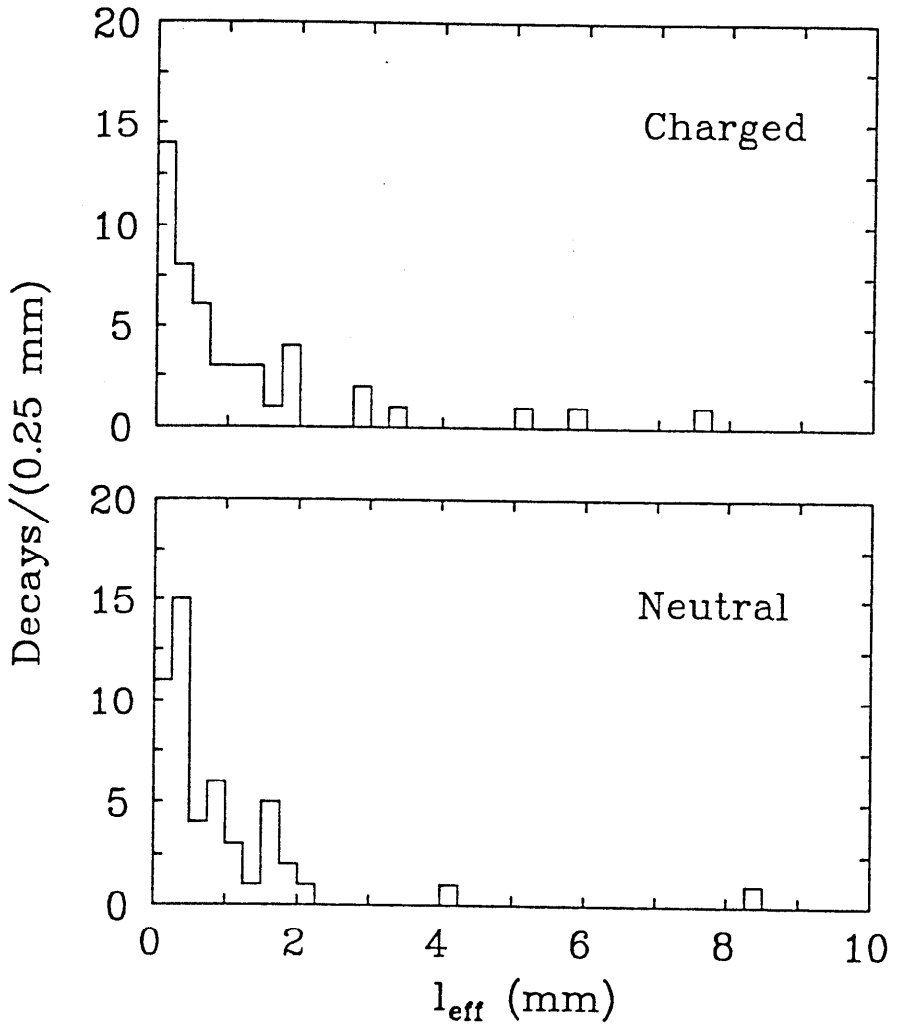

Figure 4.1: ℓ_{eff} distributions for the charged and neutral decays passing cuts.

momentum. This has been done using a new method which does not depend on any particular production model [25]. This experiment is unique in this respect.

4.3 LIFETIME ESTIMATE

For each decay the quantity $(\frac{1}{p_D})$ in the flight time is estimated by

$$\left(\frac{1}{p_D}\right)^{est} = \frac{\alpha\, m^{\pi}_{vis}}{m_D} \cdot \frac{1}{p_{vis}}$$

where p_{vis} is the magnitude of the vector sum of the momentum from charged particles emerging from the decay, m^{π}_{vis} is the corresponding mass where all the charged particles are assumed to be π's, and α is a constant determined by Monte Carlo. The subscript "vis" stands for visible, the method uses information from the charged tracks which are "visible" and thus well measured in the bubble chamber. The constant $\alpha = (1.10 \pm 0.02)$ is determined mainly by the D decay properties in the Monte Carlo. It differs from 1 largely because the true visible mass m_{vis} is replaced by m^{π}_{vis}, the replacement necessary because of our incomplete particle identification. The uncertainty in α reflects the uncertainty in the D branching ratios in the Monte Carlo. Note that the method requires only a single constant because, as will be demonstrated below, α is insensitive to the D production mechanism, variations in the standard cuts, and the D multiprong branching ratios.

The momentum estimate can be derived from the Lorentz transformation of the D meson from the D rest frame to the laboratory frame, and this is presented in Appendix A. A more intuitive derivation will be given here. Rewrite the flight time as

$$t = \frac{\ell}{c} \cdot \frac{m_D}{p_D} = \frac{\ell}{c} \cdot \frac{1}{\gamma\beta}$$

where γ and β are the usual Lorentz transformation parameters for a boost from the D rest frame and the lab. Now consider $\vec{p}^{\,*}_{vis}$, the visible momentum vector in the D rest frame. Since the D is a spin 0 particle, for a set of D decays $\langle \vec{p}^{\,*}_{vis} \rangle = 0$ and on average, $\vec{p}^{\,*}_{vis}$ will receive the same boost from the rest frame to the lab as the D itself. Therefore, for a set of D's with lab momentum p_D

$$\frac{1}{\gamma\beta} = \frac{m_D}{p_D} = \left\langle \frac{m_{vis}}{p_{vis}} \right\rangle .$$

The method takes the point of view that it is not necessary to estimate each individual p_D precisely but to be correct on the average, which is accomplished by replacing (m_D/p_D) by $(\alpha\, m^{\pi}_{vis}/p_{vis}) \approx (m_{vis}/p_{vis})$. This is sufficient for measuring the lifetime because the lifetime is the average of the flight times. The estimated lifetime is given by

$$\begin{aligned} \tau^{est} &= \frac{1}{N}\sum_{i=1}^{N} t_i^{est} = \frac{1}{N}\sum_{i=1}^{N} \frac{\ell_{eff_i}\, m_D}{c} \left(\frac{1}{p_D}\right)^{est}_{i} \\ &= \frac{1}{N}\sum_{i=1}^{N} \frac{\alpha}{c} \left(\frac{\ell_{eff}\, m^{\pi}_{vis}}{p_{vis}}\right)_i \end{aligned}$$

4.4 CHECKS ON METHOD

This section will investigate how well the method of estimating the lifetime works, calculate the statistical error on the lifetime and the ratio of lifetimes, and estimate the systematic errors both in the method and in the measurement.

How Well Does It Work? The quality of the lifetime estimate has been checked by generating a large number of Monte Carlo experiments which have the same number of decays in each experiment as seen in the real experiment, *i.e.* 50 neutral decays and 48 charged decays. The lifetime τ_{exp} found in each experiment is

calculated using the true momentum, so that $\tau_{exp} = \langle t \rangle$, and using the momentum estimate, so that $\tau_{exp} = \langle t^{est} \rangle$. Next, plot the quantity

$$S(N) = \frac{(\tau_{exp} - \tau)}{\sigma_\tau}$$

where τ is the true input lifetime, $\sigma_\tau = \tau/\sqrt{N}$, and N is the number of decays. For a large number of experiments and an unbiased lifetime estimator, $S(N)$ will be distributed normally with mean = 0 and $\sigma_S = 1$. Figures 4.2 and 4.3 show $S(N)$ for the charged and neutral lifetimes respectively. Note that the distributions of the estimated lifetimes are very similar to the distributions obtained using the true momentum. In fact, the width of the distributions are only 6% wider for the charged and 7% wider for the neutrals when the momentum estimate is used instead of the true momentum. Thus the precision of the lifetime estimate is quite good, the slightly wider distribution of lifetime is more than made up for by the increase in statistics by a factor of 3 resulting from using all the decays in the calculation.

The statistical error on the estimated lifetime has been calculated by plotting $\tau_\pm^{est}$ and τ_0^{est} for the Monte Carlo experiments described above and finding the $\pm 1\sigma$ points in the distributions. It is found that the formula

$$\sigma_t^{est} = \frac{t^{est}}{\sqrt{N \mp 1}}$$

works well in describing the statistical error and, in this experiment, the statistical error is nearly symmetric and basically gaussian. This is illustrated by Figure 4.4 which shows the distributions of $\tau_\pm^{est}$ and τ_0^{est} along with the expected curves for a gaussian distribution of τ^{est}. The distributions have only a slightly larger tail on the high τ^{est} side.

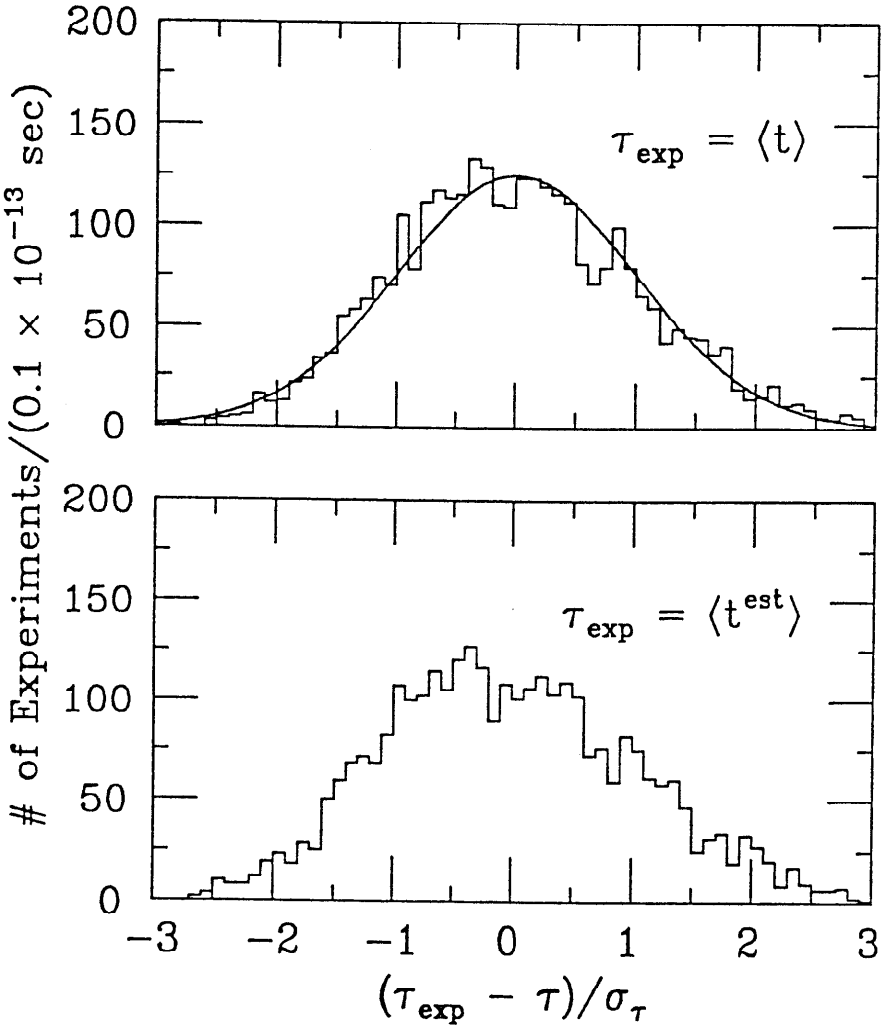

Figure 4.2: Distribution of $S(48)$ for charged lifetimes from 48 decay Monte Carlo experiments. The top plot uses the true momentum to calculate τ_{exp} while the bottom plot uses the momentum estimate. The curve in the top plot is the expected normal distribution for S.

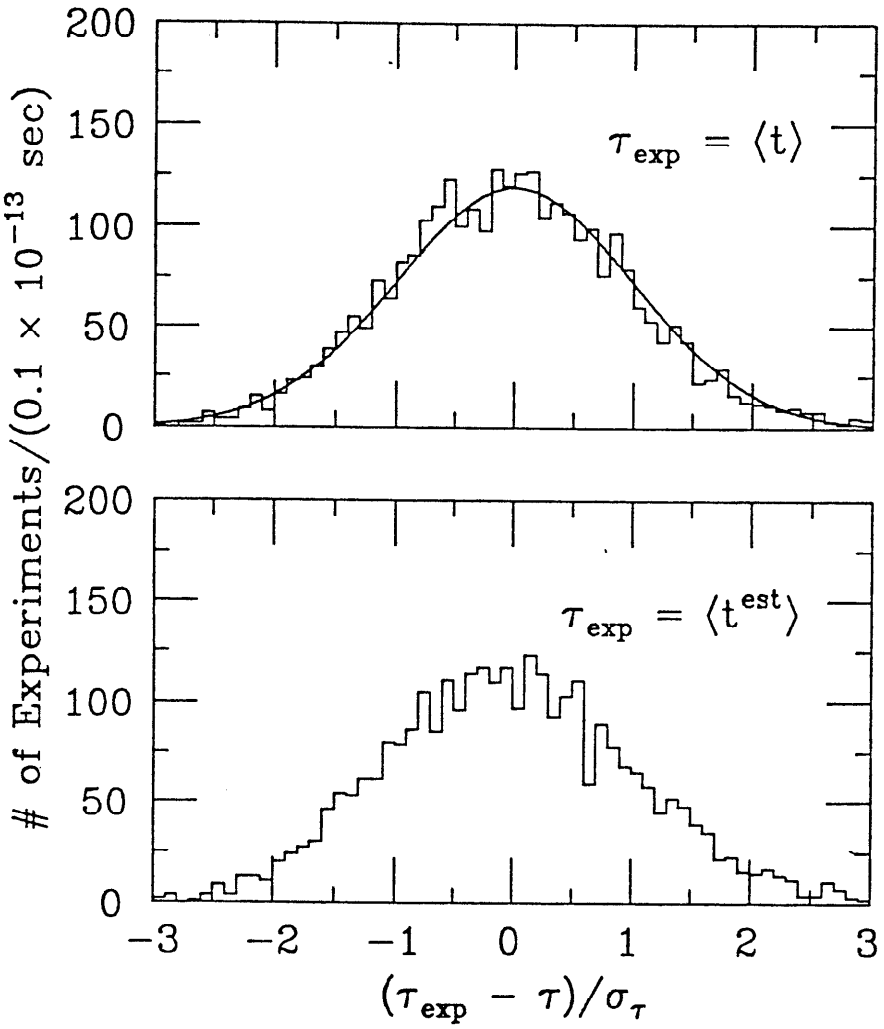

Figure 4.3: Distribution of $S(50)$ for neutral lifetimes from 50 decay Monte Carlo experiments. The top plot uses the true momentum to calculate τ_{exp} while the bottom plot uses the momentum estimate. The curve in the top plot is the expected normal distribution for S.

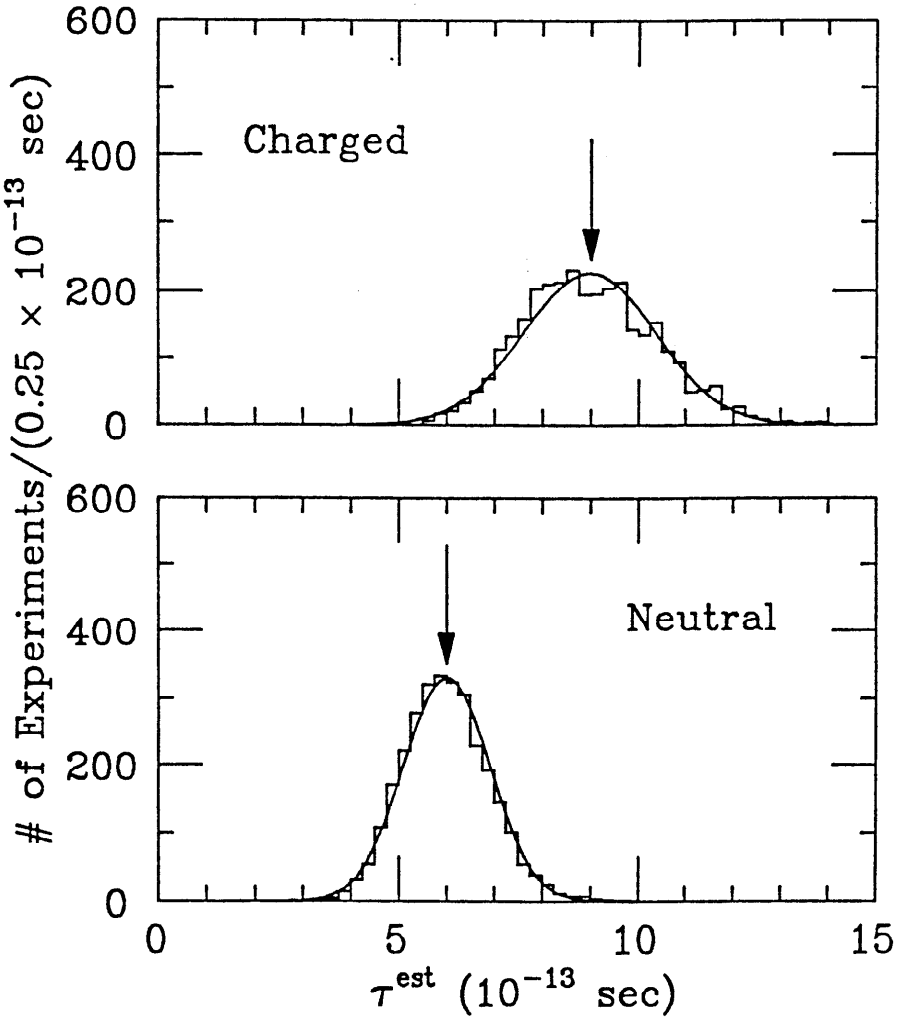

Figure 4.4: Distributions of $\tau_{\pm}^{est}$ and τ_0^{est} from a large number of Monte Carlo experiments. The curves are gaussians normalized to the number of experiments.

Sensitivity to Production Model For this experiment, it is very important that any lifetime estimate be independent of production model; specifically, independent of the momentum spectrum of the D's. The reason being that the production mechanism of D's in γp interactions at 20 GeV is not known *a priori*. BC73/75 has measured D production to result from $(71 \pm 11 \pm 6)\%$ $\Lambda_c^+ \bar{D}$ production with the remainder being $D\bar{D}$ pair production, while $F^{\pm}$ production is found to be negligible [20]. The kinematics of the two contributing production mechanisms are quite different and result in disparate D momentum distributions. Therefore it is desirable for the constant α to be independent of the production model in the Monte Carlo. Because the momentum estimate is based on a Lorentz transformation, it is manifestly D momentum distribution invariant up to small effects which are introduced by the approximations in the method. An example of an approximation being momentum dependent is m_{vis}^{π}, which is not Lorentz invariant and as $p_D \to \infty$, $m_{vis}^{\pi}/m_{vis} \to 1$.

Figure 4.5 shows the momentum dependence of the method. A set of Monte Carlo D's was generated at fixed $p_D = 2, 4, 6 \ldots 18$ GeV and the estimated lifetime $\tau^{est} = \left\langle t^{est} \right\rangle$ for each p_D was plotted. The figure demonstrates that, over the range of momenta possible for D's in this experiment, the lifetime estimate is independent of the D momentum distribution and therefore production model. Any p_D dependence due to approximations in the method is small. The systematic error due to production model uncertainties is estimated to be $\pm(0.05 \times 10^{-13}\text{sec})$.

Sensitivity to D Branching Ratios Although the lifetime estimate does not depend on the production model in the Monte Carlo, through the constant α it does depend on the Monte Carlo D decay model. In principle, the two features of the model with the largest impact on α are the D multiprong branching ratios

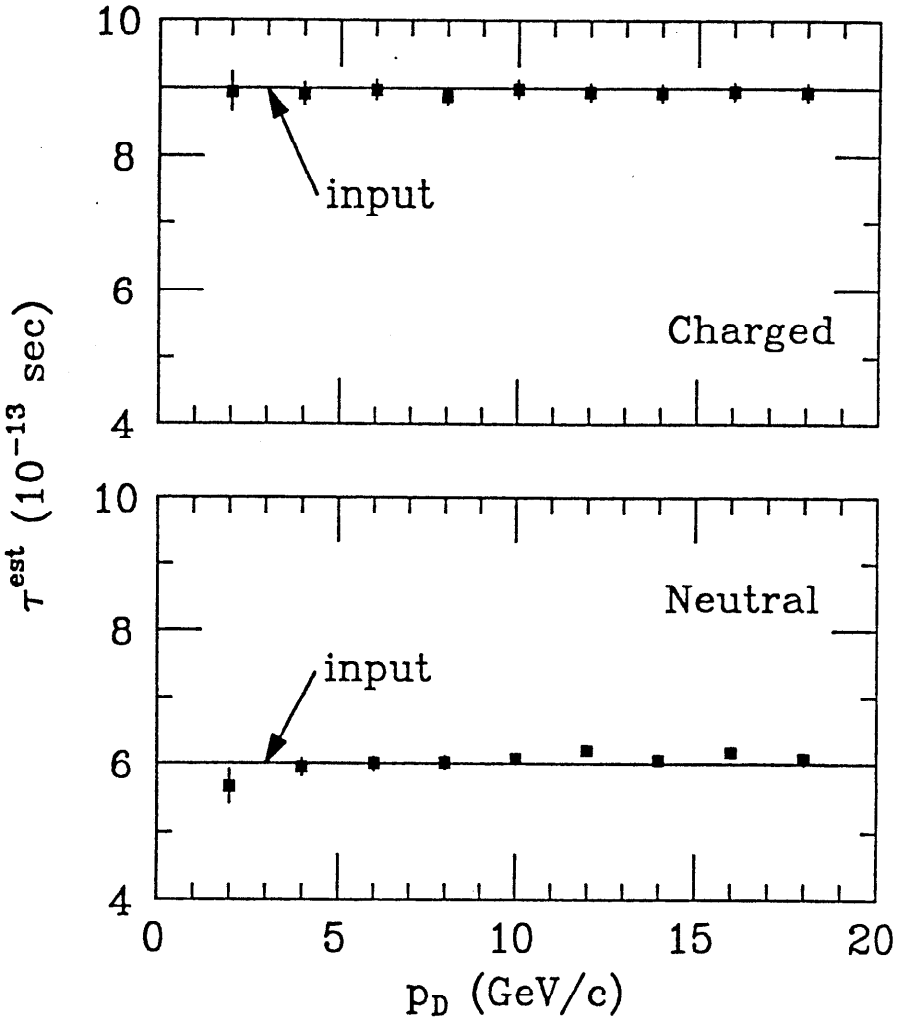

Figure 4.5: Monte Carlo study of the momentum dependence of the lifetime estimate.

and how often a D decays into a charged K rather than a neutral K. This section will deal with both features in turn.

In order to see the multiprong branching ratio dependence of the method, Figure 4.6 shows the lifetime estimate from the Monte Carlo as a function of D decay charged multiplicity. The method is independent of charged multiplicity for the following reason: D's which pass cuts decay for the most part into 2-, 3- or 4-prongs only. Although the value of α has a small multiplicity dependence (it becomes larger with multiplicity), the average of the 2- and 4-prong α's is nearly equal to the 3-prong value provided there are roughly equal numbers of 2- and 4-prongs decays passing cuts, which is the case in the Monte Carlo and in the data. In principle, a different α for each multiplicity could be used, but it is unnecessary and in this analysis α will be taken to be multiprong branching ratio independent.

The second possible systematic is due to how often D's in the Monte Carlo decay to charged K's rather than neutral K's. It is clear that if D's always decayed to K^0's then $m^{\pi}_{vis} = m_{vis}$, except for semi-leptonic modes, and $\alpha \simeq 1$. On the other hand, when D's decay to $K^{\pm}$'s, $m^{\pi}_{vis} < m_{vis}$ and $\alpha > 1$. The exact value of α we end up with is a weighted average of the different α's which result from the $D \to K^- X$, $D \to \bar{K} X$ and $D \to e^+ X$ decay modes and thus α depends on the D branching ratios in the Monte Carlo. The systematic error on α due to the specific D branching ratios in the our Monte Carlo will now be estimated. The effect of the semi-leptonic modes is small compared to the $K^{\pm}/K^0$ ratio and will be neglected. For both charged and neutral decays (a consequence of the decay multiplicity independence discussed above) the Monte Carlo finds that $\alpha = 1.00$ for $D \to K^0 X$ and $\alpha = 1.18$ for $D \to K^- X$. The typical experimental error on these inclusive branching ratios is about 10% in each case which implies an

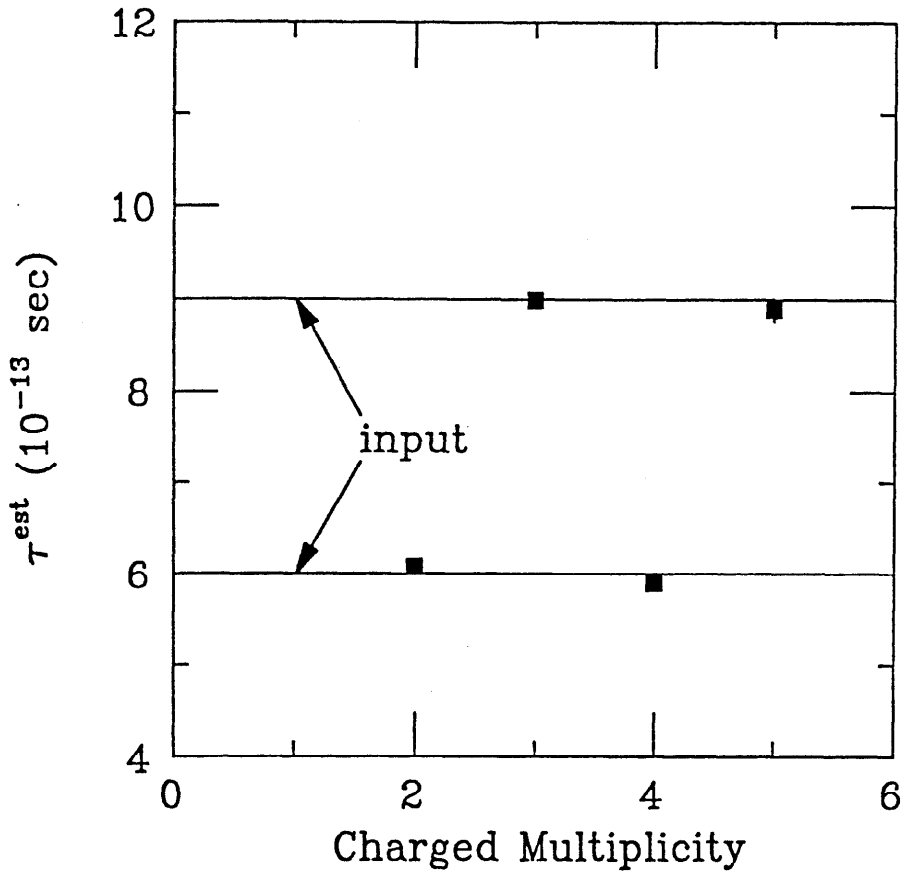

Figure 4.6: Monte Carlo study of the charged multiplicity dependence of lifetime estimate.

systematic error on α of ± 0.02 and therefore an error on the estimated lifetime of $\pm(0.02) \cdot \tau^{est}$.

Sensitivity to Lifetime It would obviously be disastrous for the constant α to depend on the particular $\tau_{D^\pm}$ and τ_{D^0} input to the Monte Carlo because the lifetime estimate would then depend on what the lifetime actually is. Figure 4.7 plots the charged and neutral lifetime estimates $\tau_\pm^{est}$ and τ_0^{est} for a single value of $\alpha = 1.10$ over a wide range of input lifetimes τ_{input}. The figure shows that the lifetime estimates track τ_{input} and therefore α does not depend of the specific τ_{input} used to calculate it.

Variations in Cuts The momentum estimate relies on the fact that in the D rest frame $\langle \vec{p}^{\,*}_{vis} \rangle = 0$. This will hold unless the cuts imposed on the decays exclude orientations of $\vec{p}^{\,*}_{vis}$ such that $\langle \vec{p}^{\,*}_{vis} \rangle \neq 0$. In order to investigate the effect of the cuts on the method, the charged and neutral lifetime estimates were calculated for Monte Carlo decays with different sets of cuts. The cuts on ℓ, d_{max} and d_2 were varied simultaneously by multiplying the standard cuts by a factor F. For a given F then, the cuts are $\ell > F \cdot 600\mu$m, $d_{max} > F \cdot 110\mu$m and $d_2 > F \cdot 40\mu$m. As an example, $F = 1$ yields the standard cuts. Figure 4.8 plots $\tau_\pm^{est}$ and τ_0^{est} as a function of F. The figure shows that τ_0^{est} is quite insensitive to even large variations in the cuts while $\tau_\pm^{est}$ tend to rise for $F > 1$. However, in the interval about $F = 1$ consistent with measurement errors on ℓ, d_{max} and d_2, $\tau_\pm^{est}$ is stable enough that no correction need be applied.

Another cut which could present a problem is requiring $m^{\pi}_{vis} > 550$ MeV/c^2 to remove strange particle contamination. Figure 4.9 plots $\tau_\pm^{est}$ and τ_0^{est} as a

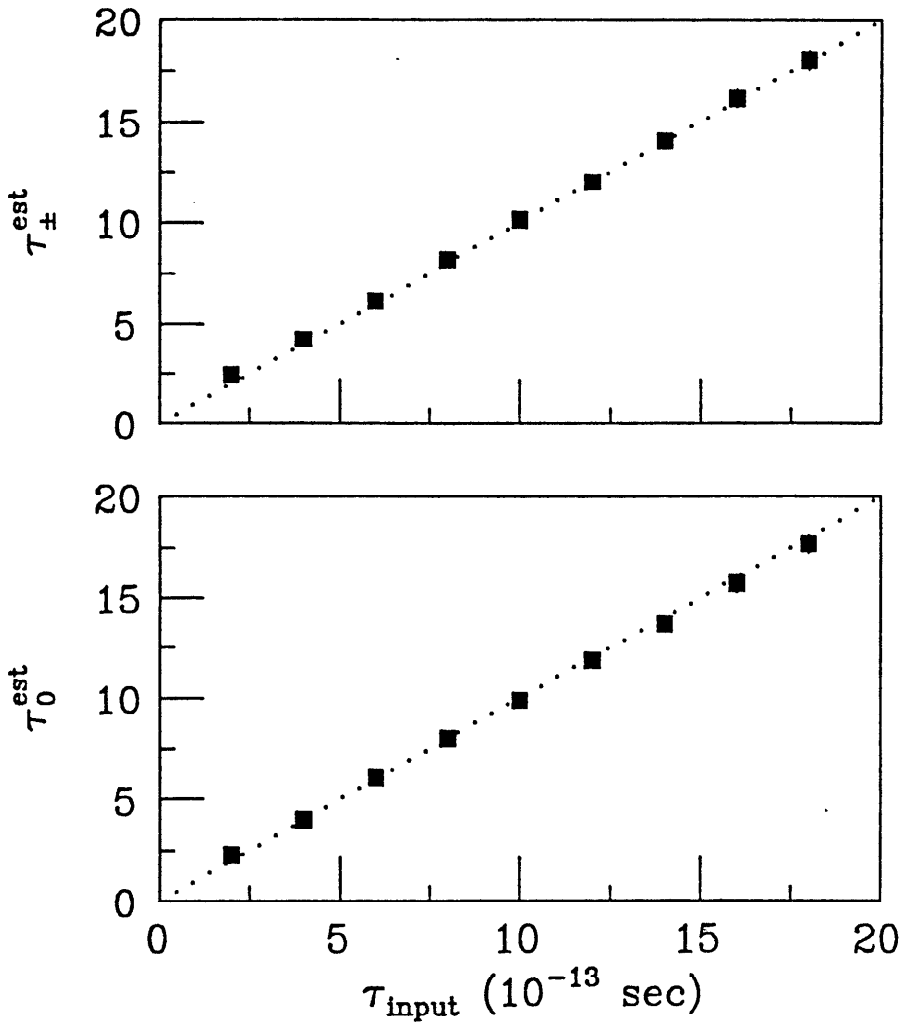

Figure 4.7: The lifetime estimates for the charged decays (top) and neutral decays (bottom) as a function of the lifetime input to the Monte Carlo. The dotted lines indicate equality between input and estimate.

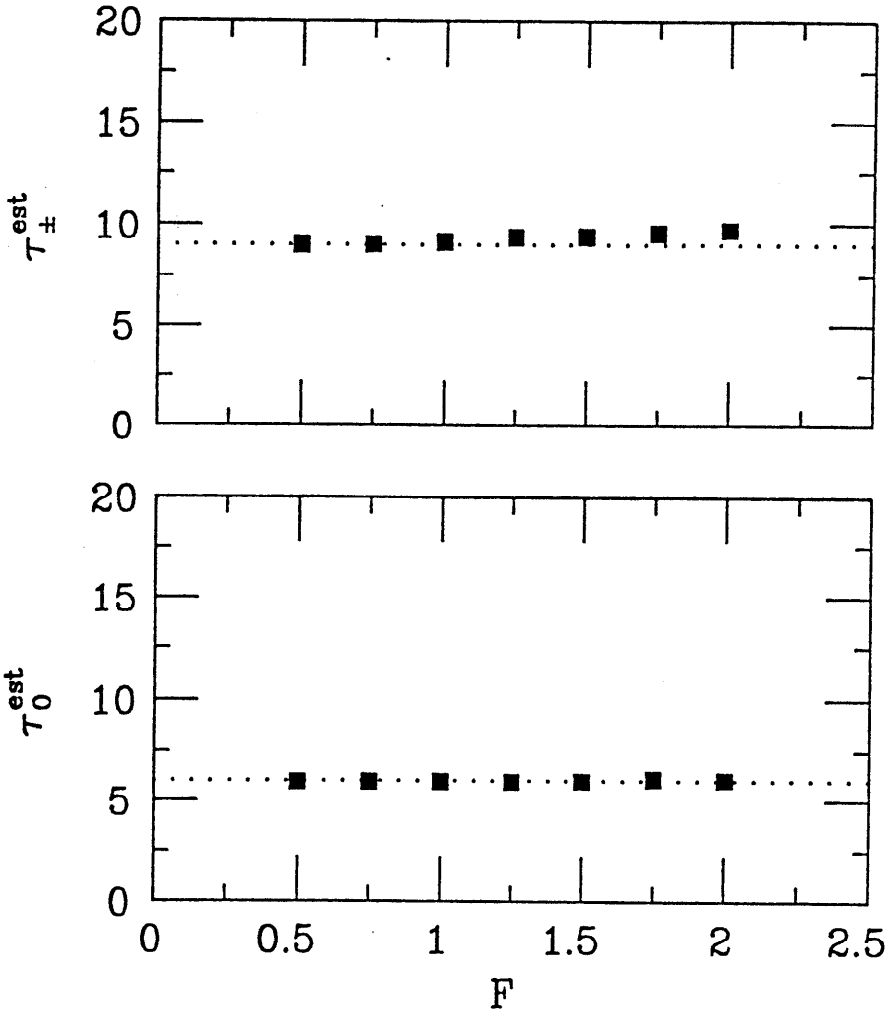

Figure 4.8: Monte Carlo study of the lifetime estimates (in units of 10^{-13} sec) as a function of the factor F defined in the text.

function of the m^{π}_{vis} cut for Monte Carlo decays and it is evident that $\tau^{est}_{\pm}$ and τ^{est}_{0} are insensitive to the m^{π}_{vis} cut.

The conclusion is then that reasonable variations in the cuts do not affect the lifetime estimate.

4.5 Weighting the Decays

Each t^{est} is weighted by the uncertainty in the estimate of $(\frac{1}{p_D})$. Weighting is necessary because the uncertainty in $\left(\frac{1}{p_D}\right)^{est}$ varies significantly as a function of m^{π}_{vis}. The reason for this behavior is clear: when m^{π}_{vis} approaches m_D, p_{vis} approaches the true momentum p_D and the spread in the estimate of $(\frac{1}{p_D})$ is small. Conversely, as m^{π}_{vis} nears the 550 MeV/c^2 cut there is more undetected momentum and the uncertainty in $\left(\frac{1}{p_D}\right)^{est}$ becomes larger. Therefore decays with the most missing momentum will be weighted least, and fully reconstructed decays will receive the largest weights. Note that the weights in this scheme are independent of flight time.

The weight for a given decay is

$$w = \frac{1}{1 + 2\sigma_y^2}$$

where

$$y \equiv p_D \left(\frac{1}{p_D}\right)^{est}.$$

The derivation of this weight formula is presented in Appendix B. The quantity σ_y is calculated by Monte Carlo for bins of m^{π}_{vis} and then fitted to a 3^{rd} order polynomial in m^{π}_{vis}. The resulting weight function is shown in Figure 4.10 where w is seen to be about 1 for $m^{\pi}_{vis} \approx m_D$ and falls to about 0.58 at the m^{π}_{vis} cut of 550 MeV/c^2. Also shown are the 48 charged and 50 neutral decays and it is evident that most decays receive large weights.

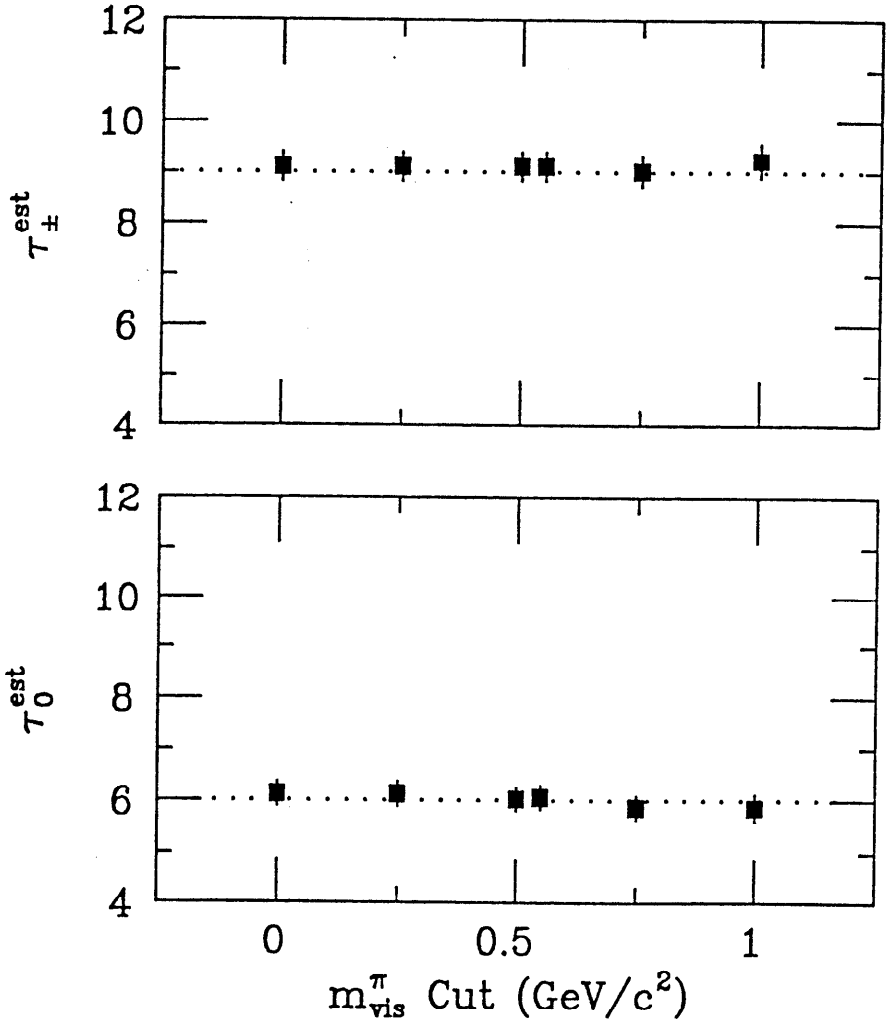

Figure 4.9: Monte Carlo study of the lifetime estimates (in units of 10^{-13} sec) as a function of the m_{vis}^{π} cut.

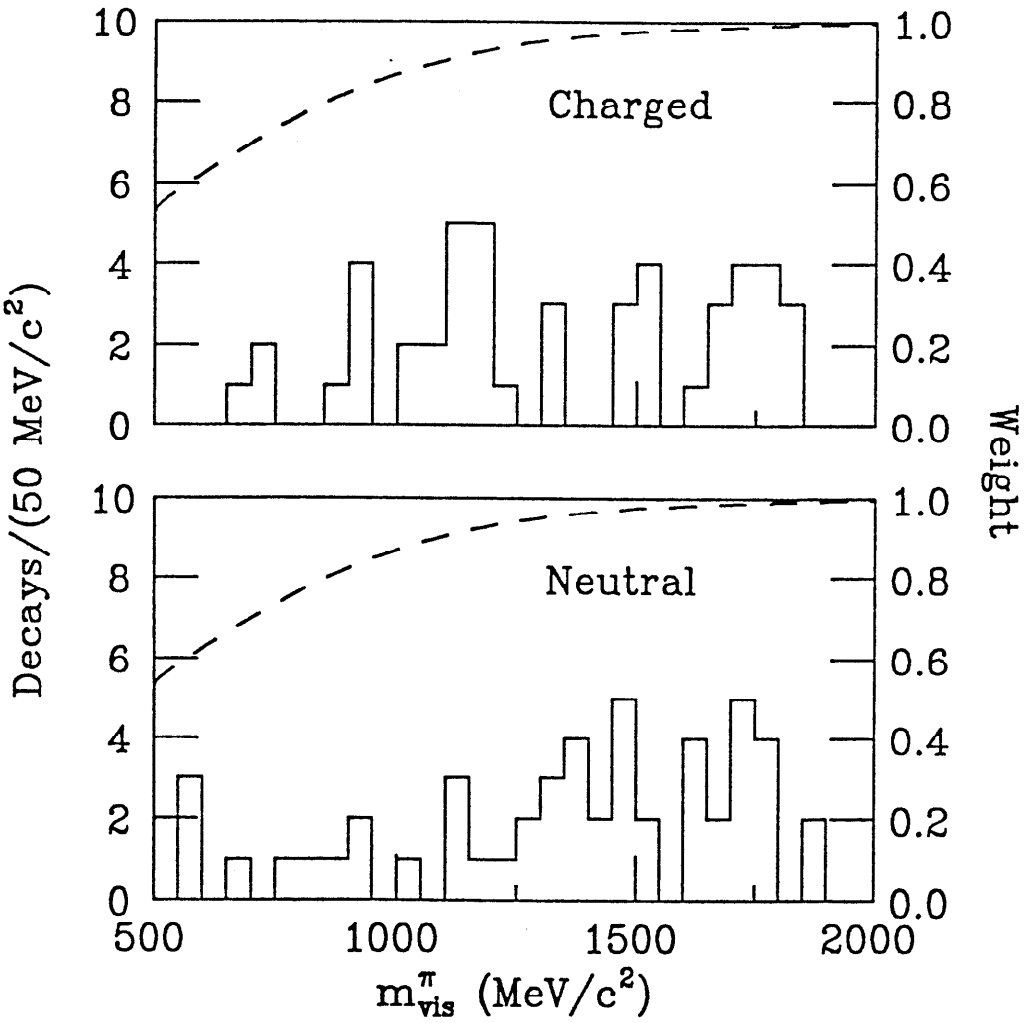

Figure 4.10: Flight time weights, charged and neutral decays as a function of m^{π}_{vis}. The weight function is plotted as the dashed line.

The lifetime estimate is now given by the weighted average of the estimated flight times

$$\tau^{est} = \frac{\sum_{i=1}^{N} w_i \, t_i^{est}}{\sum_{i=1}^{N} w_i}.$$

It turns out that the weighting is not a big effect because (1) the average weight for both the charged and neutral samples is $< w >= 0.92$ and (2) setting all the weights to 1 increases the charged lifetime estimate by only 4% and leaves the neutral estimate unchanged.

The statistical error on τ^{est} is now given by

$$\sigma_{\tau^{est}} = \frac{\tau^{est}}{\sqrt{\left(\sum_{i=1}^{N} w_i\right) \mp 1}}.$$

4.6 CORRECTING FOR AMBIGUOUS DECAYS

The lifetime estimates must be corrected for the two charged/neutral ambiguous decays remaining in the sample of decays passing all cuts. This correction is necessary because otherwise a bias could be introduced by the ambiguous decays if, for example, they all occurred at small ℓ_{eff}. The potential bias is not serious here for two reasons: (1) there are only two ambiguous decays out of 100 and (2) both have typical flight time estimates for all hypotheses that are not dissimilar from the uncorrected mean lifetimes for the unambiguous decays. Therefore the correction is expected to be small and in fact that is the case as will be seen below.

The procedure for making this correction is to recalculate $\tau_{\pm}^{est}$ and τ_0^{est} for each of the $2^2 = 4$ possible ways of assigning the two ambiguous decays to the charged and neutral samples, then take the average of the four values of $\tau_{\pm}^{est}$ and

τ_0^{est} as the corrected lifetimes. The result is to increase the neutral estimate by 0.1×10^{-13} sec and leave the charged estimate unchanged.

4.7 Measurement Error Systematics

The errors on the measurement of decay lengths and impact distances are important because the errors influence which decays pass the cuts for the lifetime calculation. The systematic error due to this source has been estimated by taking all the decays and smearing the decay lengths and impact distances by the measurement errors (typically about 50 μm for lengths and 15 μm for impact distances), recalculating $\tau_\pm^{est}$ and τ_0^{est}, then repeating this procedure a large number of times. The results are shown in Figure 4.11. Note that the means of the distributions are shifted toward higher τ^{est} than the $\tau_\pm^{est}$ and τ_0^{est} found using the unsmeared sample. The reason for this is that ambiguous decays were not used in the analysis and there are quite a few below the cuts. Thus there are, on the average, too few decays below the cuts which pass the cuts when smeared. This is not too serious because it is the width of the distributions that are used for the systematic error. The systematic due to measurement error is found to be $\pm(0.28 \times 10^{-13})$ sec for the charged decays and $\pm(0.20 \times 10^{-13})$ sec for the neutral decays.

4.8 Correcting for Λ_c^+ and $F^\pm$ Contamination

In the last chapter, it was demonstrated that there is not a substantial signal for either $F^\pm$ or Λ_c^+ in the sample of decays passing standard cuts. From production mechanism studies, it has been determined [20] that the fraction of total charm production due to associated production of $\bar{D}\Lambda_c^+ X$ is $\sigma_{D\Lambda_c^+ X}/\sigma_{charm} = (71 \pm 11 \pm 6)\%$. Therefore even though the Λ_c^+ lifetime is fairly short (about a

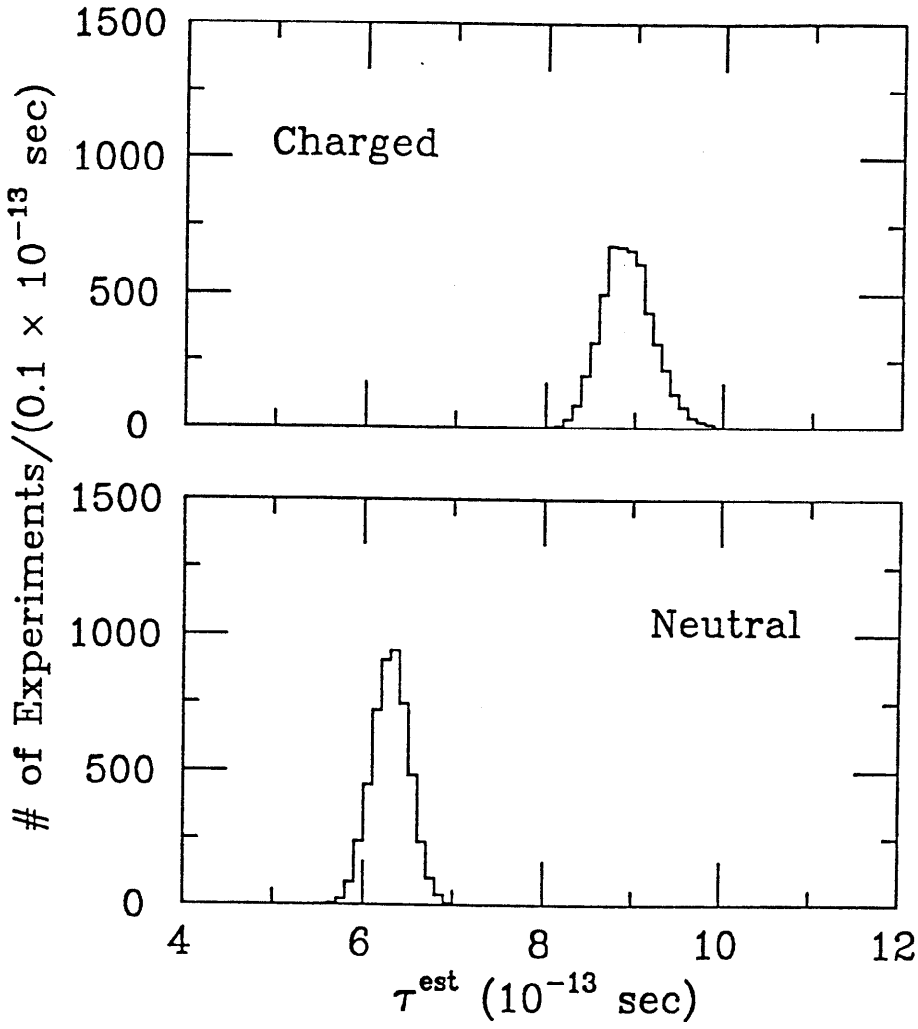

Figure 4.11: Distributions of τ^{est} where the decay lengths have been smeared by the measurement errors.

factor of 4 smaller than the charged D lifetime) there is the possibility that Λ_c^+ decays could pass cuts and thus bias the $D^\pm$ lifetime calculated from the charged decays.

While Λ_c^+ contamination obviously only applies to the positive decay sample, $F^\pm$ contamination can affect the entire charged sample. Unfortunately little is known about the F meson, the lifetime is probably comparable to that of the Λ_c^+ but the fraction of $F^\pm$ production in this experiment is not known. Thus the $F^\pm$ properties used below will merely be reasonable guesses.

The corrections which will be made come from a lengthy formula derived in Appendix C. This formula is very general and is included only for completeness, its complexity will be reduced considerably by the assumptions about $F^\pm$ and Λ_c^+ production in this experiment. The Λ_c^+ contribution will be considered first.

Λ_c^+ Contamination The assumptions made for this correction, in the notation of Appendix C, are listed in Table 4.1.

Table 4.1

$\tau_{\Lambda_c^+}$	$= 2.3 \times 10^{-13}$ sec
$f_{D\Lambda_c^+}$	$= 71\%$
$f_{F^+F^-} + f_{DF^+} + f_{DF^-}$	$= 0$
ϵ_D^{DD}	$= 21.4\%$
$\epsilon_{\Lambda_c^+}^{D\Lambda_c^+}$	$= 0.9\%$

Note that $F^\pm$ production is assumed to be zero. The Λ_c^+ lifetime comes from the PDG [22], $f_{D\Lambda_c^+}$ is measured in this experiment [20] and the efficiencies to pass standard cuts for D's and Λ_c^+'s , ϵ_D^{DD} and $\epsilon_{\Lambda_c^+}^{D\Lambda_c^+}$, are determined by Monte Carlo.

The Λ_c^+ lifetime and the efficiencies for D's and Λ_c^+'s are the same as before. The result is that the charged D lifetime is corrected to be $(2 \pm 2)\%$ larger than $\tau_{\pm}^{est}$.

It is clear that the corrections to $\tau_{\pm}^{est}$ for $F^{\pm}$ and Λ_c^+ production are small. Careful examination of the charged decay sample which passes cuts shows that all decays are compatible with being $D^{\pm}$'s and that there are no unique $F^{\pm}$ or Λ_c^+ decays. The conclusion is then that no correction to $\tau_{\pm}^{est}$ will be made for $F^{\pm}$ and Λ_c^+ production and any uncertainty will be put in the $D^{\pm}$ lifetime systematic error.

4.9 RESULTS

The number of decays and lifetime results for the charged, neutral, positive and negative D samples for various stages of the analysis are listed in Table 4.3. The sources of error for $\tau_{D^{\pm}}$ and τ_{D^0} are summarized in Table 4.4. The final results on D meson lifetimes from this experiment are

$$\tau_{D^{\pm}} = (8.6 \pm 1.3^{+0.8}_{-0.3}) \times 10^{-13} \text{ sec}$$

$$\tau_{D^0} = (6.1 \pm 0.9 \pm 0.3) \times 10^{-13} \text{ sec}$$

with a ratio of

$$R = \frac{\tau_{D^{\pm}}}{\tau_{D^0}} = 1.4 \pm 0.3^{+0.2}_{-0.1}$$

where the first error is statistical and the second systematic. The distributions of t^{est} for the charged and neutral decay samples are shown in Figure 4.12. The curves in the figure are exponentials calculated with the above final lifetimes and normalized to the number of decays in each plot.

Perhaps the most difficult factor to estimate is $\varepsilon^{D\Lambda_c^+}_{\Lambda_c^+}$ since it depends on the Λ_c^+ momentum distribution which is not measured and must be assumed in the Monte Carlo. In practice, the 4-momentum transfer squared of the primary γp interaction is tuned such that the Monte Carlo momentum distribution for all charged decays matches the observed spectrum. In this way, the value of $\varepsilon^{D\Lambda_c^+}_{\Lambda_c^+} = 0.9\%$ is obtained. Plugging in the numbers, the correction for Λ_c^+ contamination makes the charged D lifetime $(4 \pm 4)\%$ larger than $\tau_{\pm}^{est}$.

$F^{\pm}$ Contamination The problem with trying to correct for possible $F^{\pm}$ contamination is that the amount of $F^{\pm}$ production and the production mechanism are unknown. The assumptions are that F production is as large as 10% of the total charm cross section and that F^+F^- pair production occurs at roughly the same rate as $D\bar{D}$ pair production,*i.e.* about 1/3 of the time, and the remaining 2/3 being $F^+\bar{D}X$ associated production. The parameters used are listed in Table 4.2.

Table 4.2

$\tau_{F^\pm}$	$= 1.9 \times 10^{-13}$ sec
$f_{F^+F^-} + f_{DF^+} + f_{DF^-}$	$= 10\%$
$f_{F^+F^-}$	$= 3.3\%$
f_{DF^+}	$= 6.7\%$
f_{DF^-}	$= 0\%$
f_{DD}	$= 29\%$
$f_{D\Lambda_c^+}$	$= 61\%$
$\varepsilon_F^{FF} = \varepsilon_F^{DF}$	$= 2.3\%$

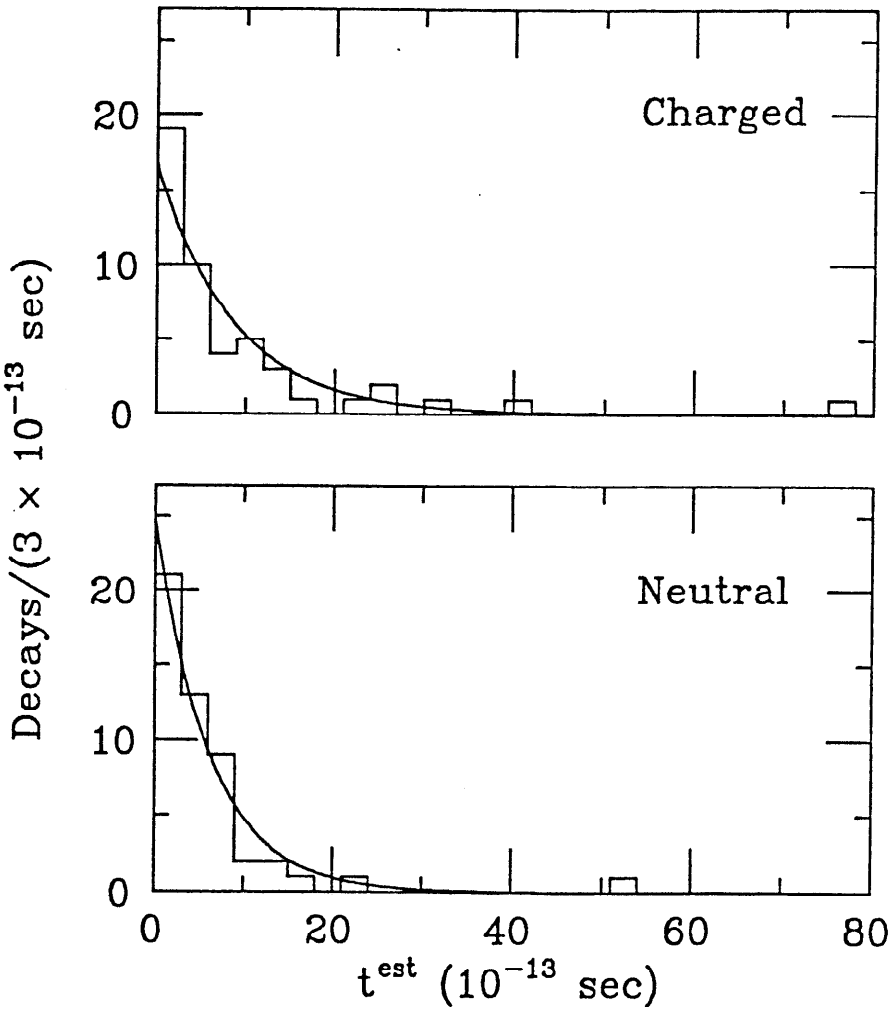

Figure 4.12: t^{est} distributions for the charged and neutral decays. Superimposed are exponential curves for the final lifetime results normalized to the data.

Table 4.3

τ^{est} in units of 10^{-13} sec

	Unweighted		Weighted		Weighted with Ambiguous Decay Correction	
Sample	τ^{est}	N	τ^{est}	$\sum w_i$	τ^{est}	$\sum w_i$
Charged	8.9	48	8.6	44.3	8.6	45.3
Neutral	6.0	50	6.0	46.2	6.1	47.1
Positive	9.4	15	9.2	13.4	9.0	13.8
Negative	8.7	33	8.3	31.0	8.4	31.4

Table 4.4

Sources of Lifetime Errors
(in units of 10^{-13} sec)

	$D^{\pm}$	D^0
Production Model	± 0.05	± 0.05
Decay Branching Fractions	± 0.17	± 0.12
Ambiguous Decays	± 0.09	± 0.13
Errors on ℓ, d_{max}, d_2	± 0.28	± 0.20
Λ_c^+ Contamination	$^{+0.69}_{-0.00}$	—
$F^{\pm}$ Contamination	$^{+0.34}_{-0.00}$	—
Statistical	± 1.3	± 0.9

Chapter 5: Discussion and Conclusions

5.1 Checks on Lifetime Results

A number of checks were made on the lifetime results to ensure the lifetimes calculated in Chapter 4 are reasonable and self consistent. The more important checks are described below.

Variations in Cuts The sensitivity of the lifetime results to the values of the standard cuts on ℓ, d_{max} and d_2 was investigated by simultaneously scaling these cuts by the factor F defined in Chapter 4, and then recalculating $\tau_{\pm}^{est}$ and τ_0^{est}. Recall that $F = 1$ yields the standard cuts. The results of this analysis are shown in Figure 5.1 for a wide range of F. The ambiguous decays were included by giving equal weight to every topological interpretation, then calculating $\tau_{\pm}^{est}$ and τ_0^{est} for each permutation and averaging. The lifetime results are seen to be quite stable under variations in the standard cuts.

Independent Lifetime Analysis The D meson lifetimes were calculated with a different and independent method which was used in our previous publication for BC72/73 data; details are found in [23]. Briefly the method consists of comparing, on an event by event basis, a set of parameters which describe each decay to those of Monte Carlo events passing the same cuts. The likelihood that the real and Monte Carlo decays have similar distributions in these parameters is then

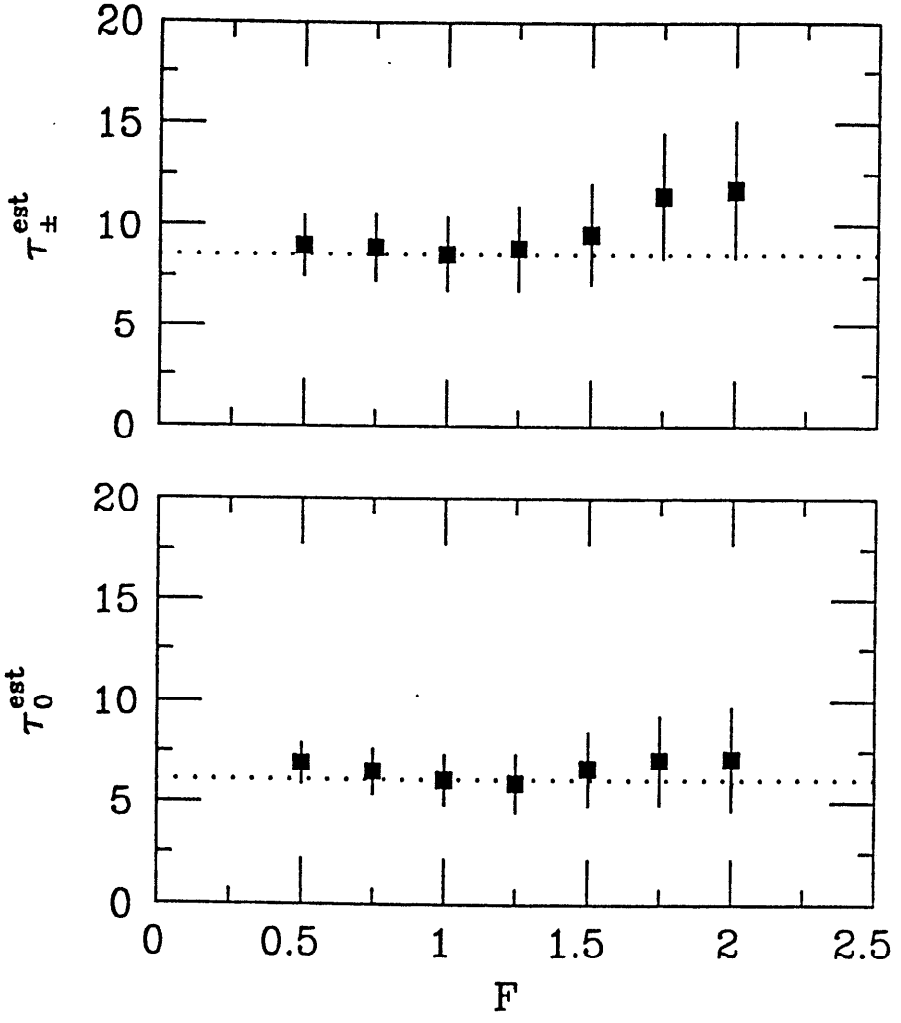

Figure 5.1: The lifetime estimates (in units of 10^{-13} sec) as a function of the factor F defined in Chapter 4. Ambiguous decays have been included by averaging all topological interpretations. The errors are statistical only.

maximized as a function of lifetime. Before correcting for ambiguous decays and associated production, the results of this method are $\tau_{D^\pm} = (7.9^{+1.3}_{-1.2}) \times 10^{-13}$ sec and $\tau_{D^0} = (6.0^{+0.9}_{-0.8}) \times 10^{-13}$ sec, where the errors are statistical only. Comparison with the results in Table 4.3 shows the two methods are totally consistent within the statistical uncertainty and thus provides confidence in the method of Chapter 4.

Constrained Decay Lifetimes The D lifetimes have been calculated using the sample of fully reconstructed D's found in Chapter 3. The results for the 15 charged and 16 neutral constrained decays are $\tau_{D^\pm} = (8.3^{+2.2}_{-2.1}) \times 10^{-13}$ sec and $\tau_{D^0} = (8.9^{+2.3}_{-2.2}) \times 10^{-13}$ sec, where the errors are statistical only. Again, the results are compatible with the lifetimes obtained from the total sample.

Multiprong Lifetimes The lifetimes, after weighting the decays and correcting for ambiguous decays, are listed in Table 5.1 as a function of charged multiplicity. The errors quoted in the table are statistical only.

Table 5.1

Multiprong Lifetimes
(in units of 10^{-13} sec)

# of prongs	$\sum w_i$	τ^{est}
3	43.3	8.7 ± 1.3
5	2.0	$4.8^{+4.8}_{-2.8}$
2	19.3	5.2 ± 1.2
4	27.8	$6.7^{+1.3}_{-1.2}$

There are two point to note: (1) the results are again fully compatible in each case with the total sample numbers and (2) the 2-prong lifetime is less than the 4-prong lifetime which indicates there is no residual strange particle contamination in the decays passing cuts.

5.2 LONGEST LIVED $\bar{D}^0$

In the sample of neutral decays there is a fully reconstructed decay of $\bar{D}^0 \to K^+\pi^+\pi^-\pi^-$ with a proper flight time of 55×10^{-13} sec. This decay is of interest for at least two reasons: (1) it is by far the longest lived neutral D recorded to date and as such has considerable influence on the D^0 lifetime obtained in this experiment as well as the interpretation of world average lifetimes discussed in the next section, and (2) there has been speculation [26] on the possibility of observing $D^0\bar{D}^0$ mixing analogous to $K^0\bar{K}^0$ mixing, in particular a $D_L D_S$ lifetime difference with this long lived $\bar{D}^0$ being an example of the D_L component. The rate for $D^0\bar{D}^0$ mixing is expected to be very small, on the order of $\lesssim 10^{-7}$, which corresponds to a $D_L - D_S$ lifetime difference of $\delta\tau \lesssim 10^{-3}\tau$ [27]. The Standard Model wisdom is then that the lifetime difference is too small to be measured directly. On the other hand, the best experimental limits on the mixing rate are only in the range of 4–8% [28], which implies $\delta\tau \lesssim 10^{-1}\tau$ and mixing at that level could presumably show up in our data. Therefore this section will also see how consistent the t^{est} distribution for the neutral decays is with being the product of a single exponential parent distribution.

Details of this decay are found in ref. [29]. The event is shown in Figure 5.2, where 9 mm downstream of the production vertex is the 4-prong decay of a $\bar{D}^0 \to K^+\pi^+\pi^-\pi^-$ where all the particles were identified either in the Cherenkov counters or by ionization in the chamber. The event is obviously very clean, the

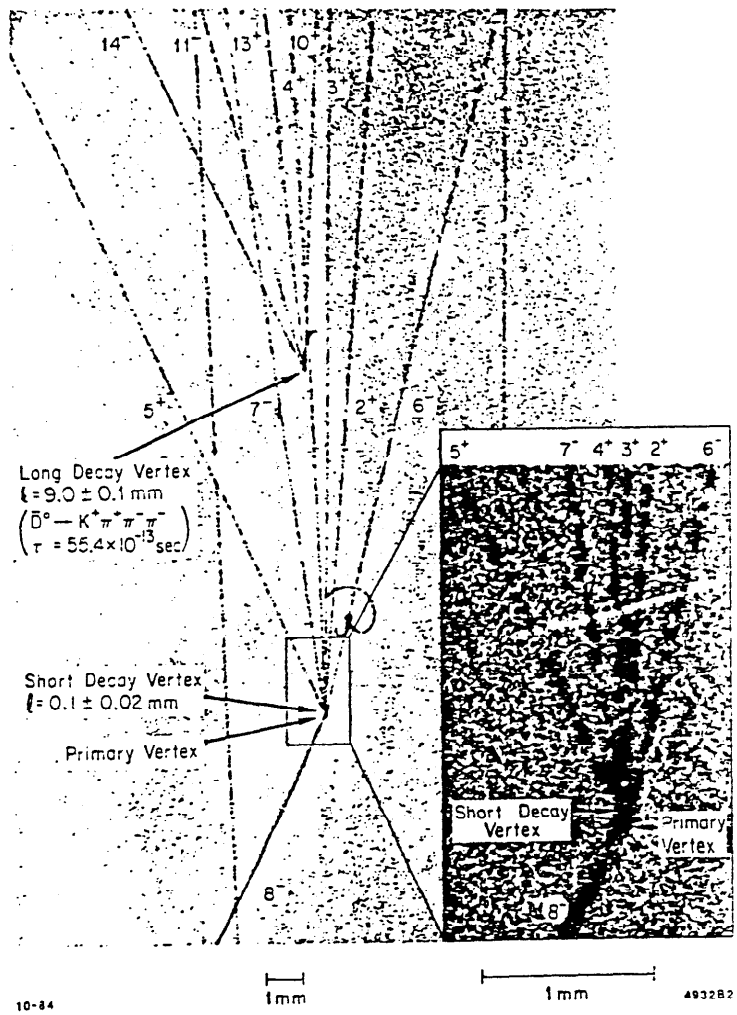

Figure 5.2: Photograph of the event taken by the HRO camera showing the long lived $\bar{D}^0$ as well as an additional decay near the production vertex.

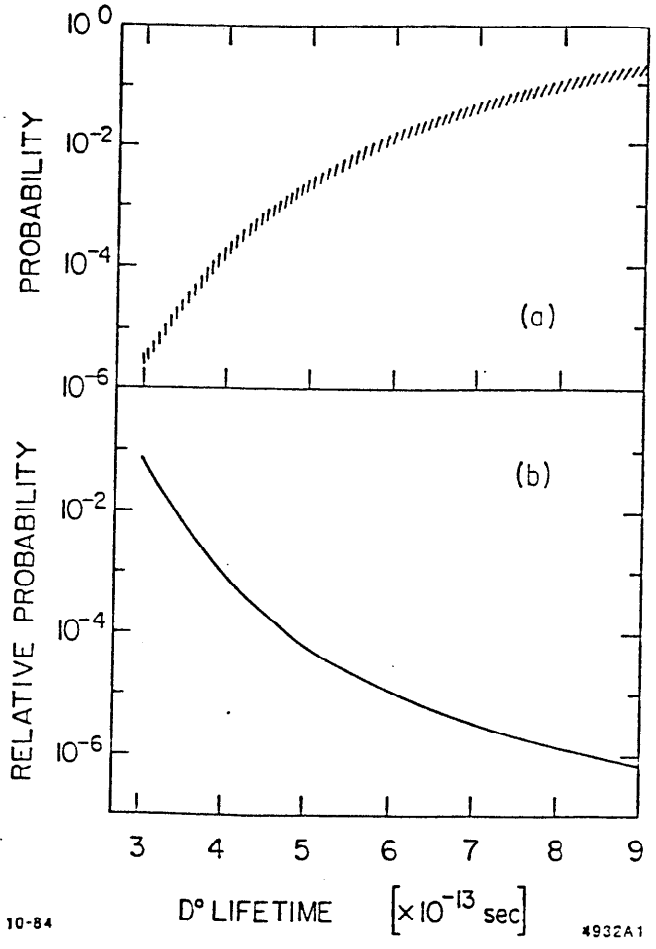

Figure 5.3: (a) Probability an experiment of the size of BC73/75 would observe a decay with proper flight time $> 55 \times 10^{-13}$ sec as a function of D^0 lifetime. The hatched band indicates the $\pm 1\sigma$ uncertainty in the total number of $\bar{D}^0$'s produced. (b) Upper limit to the relative probability that the event is due to background compared to the charm interpretation as a function of D^0 lifetime.

probability the decay is due to background has been estimated to be less than 2×10^{-8}, details of the background estimation are found in Appendix D. The probability of observing such a long lived decay in an experiment of this size is plotted as a function of τ_{D^0} in Figure 5.3 (a). Figure 5.3 (b) plots the relative probability that the decay is due to background compared to the probability of being the particular $\bar{D}^0$ that is seen, where the latter probability includes, for example, the branching fraction for $\bar{D}^0 \to K^+\pi^+\pi^-\pi^-$. The probability of observing this decay in this experiment is about 2% for $\tau_{D^0} = 6.1 \times 10^{-13}$ sec. The probability clearly decreases rapidly with decreasing τ_{D^0}, and is about 0.05% for the world average lifetime found in the following section. On the other hand, the relative probability remains small even for τ_{D^0} as short as 3×10^{-13} sec. Thus, although the neutral D^0 lifetime from BC73/75 is the longest observed to date, this single decay gives us confidence in the result.

The question of whether the neutral decay t^{est} distribution comes from a single exponential distribution has been explored via the Kolmogorov-Smirnov statistic [30]. The Kolmogorov-Smirnov statistic tests the shape of a distribution and is superior to the more common χ^2 test for small statistics. The test consists of comparing S_n, the normalized cumulative distribution of n decays, with the integrated probability density F as a function of lifetime t. In the case of an exponential decay distribution with lifetime τ, F is given by

$$\begin{aligned} F(t) &= \int_0^t \frac{e^{-t'/\tau}}{\tau} dt' \\ &= \left(1 - e^{-t/\tau}\right). \end{aligned}$$

These distributions are plotted in Figure 5.4 for the 50 neutral decays. The next step is to find $D(n)$, the maximum deviation between $S_n(t)$ and $F(t)$. The Kolmogorov-Smirnov statistic then provides a probability of seeing a smaller $D(n)$

for a given n and D, but is independent of the actual distributions involved. Thus the test gives the probability of seeing better agreement between the theory and the data. This probability as a function of $D(50)$ is shown in Figure 5.5. For the 50 decays, $D(50) = 0.092$ which translates into a probability of roughly 40% of seeing a smaller D. The conclusion is then that the neutral t^{est} distribution is quite compatible with a single exponential distribution indicating the long lived $\bar{D}^0$ is very consistent with the rest of the distribution of neutral decays and that $D^0\bar{D}^0$ mixing is certainly not required to explain the data.

5.3 Lifetimes From Around the World

This section will compare the results of BC73/75 with D meson lifetimes and ratios of lifetimes found by other experiments. The lifetimes are measured directly, that is by measuring decay lengths or impact distances of D decays. The measurement techniques fall into two categories: (1) visual detectors and (2) electronic detectors. The visual detectors include emulsions and high resolution bubble chambers. The electronic detectors are either high precision drift chambers or solid state devices such as silicon strip detectors or CCD's. Table 5.2 lists the experiments with D lifetime results according to measurement technique. A word of warning: the systematics of these various devices are inherently very different, a fact which is not taken into account when averages of the world data are made and therefore the errors quoted on these averages are perhaps optimistically small.

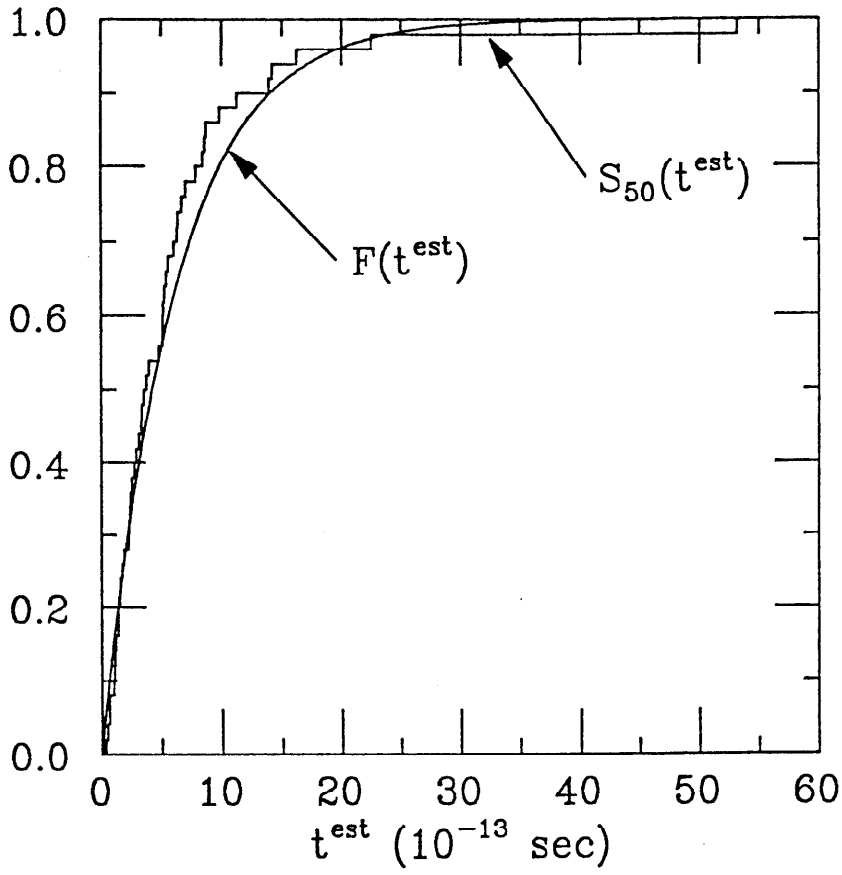

Figure 5.4: Normalized cumulative distribution $S_{50}(t^{est})$ of the 50 neutral decays as a function of t^{est} along with the integrated probability density $F(t^{est})$ computed for $\tau_{D^0} = 6.1 \times 10^{-13}$sec.

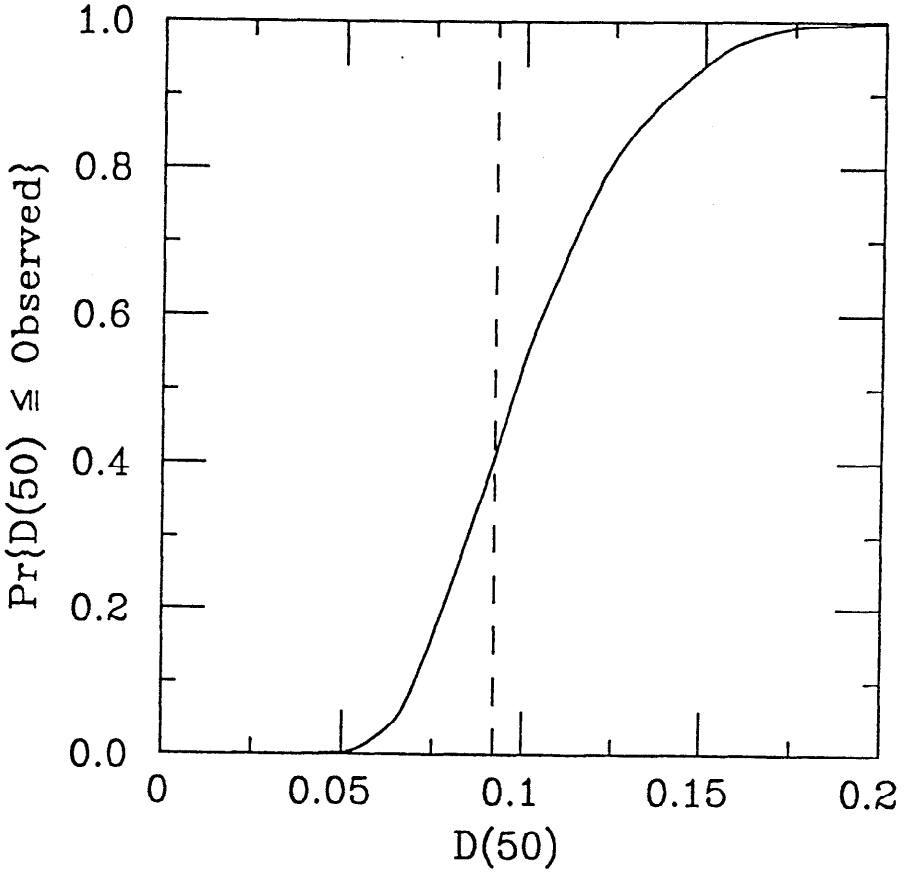

Figure 5.5: Probability of seeing a larger maximum deviation $D(n)$ between S_n and F for $n = 50$ decays as a function of D. The dashed line shows $D(50) = 0.092$ found for the neutral decays.

Table 5.2		
Technique	Device	Experiment (See Ref. [31] for details)
Visual	Emulsion	WA58, E531
	Bubble Chamber	NA16, NA18, NA27, BC73/75
Electronic	Drift Chamber	MARK II, HRS, TASSO, DELCO, CLEO
	Solid State	NA1, NA11

In contrast to the lifetimes, the ratio of lifetimes, $R = \tau_{D^\pm}/\tau_{D^0}$, can be measured directly or indirectly. The direct measurement simply involves taking the ratio of the individually measured D lifetimes. The indirect method measures the ratio of semi-leptonic branching ratios. This ratio was shown in Chapter 1 to be equivalent to the ratio of D lifetimes. The indirect method is important because it has the potential of statistically far out-stripping the direct measurements. This is because an experiment such as the MARK III at SPEAR [10] can sit on the ψ'' resonance and in a reasonable period of running produce thousands of clean $D\bar{D}$ events with which to extract R. On the other hand, as this dissertation demonstrates, it is a long and difficult task to obtain even 100 clean decays by direct measurement. For the time being, however, the two methods are competitive.

Figure 5.6 shows a compilation of data on the $D^\pm$ lifetime. The world average [31] of $\tau_{D^\pm} = (8.54 \pm 0.75) \times 10^{-13}$ sec is also indicated. The result of this experiment agrees well with this average and there seems to be general agreement among the experiments on the $D^\pm$ lifetime.

Figure 5.7 plots the τ_{D^0} data along with the world average [31] of $\tau_{D^0} = (4.35 \pm 0.32) \times 10^{-13}$ sec. The BC73/75 result is 1.5σ higher that this average.

Figure 5.8 presents the data on the ratio of charged to neutral D lifetimes. Using only direct lifetime measurements, the world average [31] is $R = (1.96 \pm 0.22)$. The BC73/75 result is about 1σ lower than this average. The best indirect measurement comes from the MARK III experiment and agrees well with the world average.

The value of $\tau_{D^\pm}$ found by BC73/75 is compatible with the world average. The D^0 lifetime from this analysis is somewhat longer than the world average but the τ_{D^0} situation is more unsettled. Figure 5.9 shows that historically the world average D^0 lifetime has tended to increase with time so that the disagreement of this experiment and the world average is probably not serious. The various checks on the D^0 lifetime result and the long lived $\bar{D}^0$ described in this chapter demonstrate our result for τ_{D^0} is solid. In any case, it is safe to say the definitive D meson lifetime experiment is yet to be done.

5.4 CONCLUSIONS

Based on 48 charged, 50 neutral and 2 topologically ambiguous decays, the D meson lifetimes are found to be

$$\tau_{D^\pm} = (8.6 \pm 1.3^{+0.8}_{-0.3}) \times 10^{-13} \text{ sec}$$

$$\tau_{D^0} = (6.1 \pm 0.9 \pm 0.3) \times 10^{-13} \text{ sec}$$

with a ratio of

$$R = \frac{\tau_{D^\pm}}{\tau_{D^0}} = 1.4 \pm 0.3^{+0.2}_{-0.1}.$$

The magnitude of these lifetimes agrees well with the naïve spectator model prediction obtained in Chapter 1 by scaling up the μ lifetime. This implies the spectator model approach plays a dominant role.

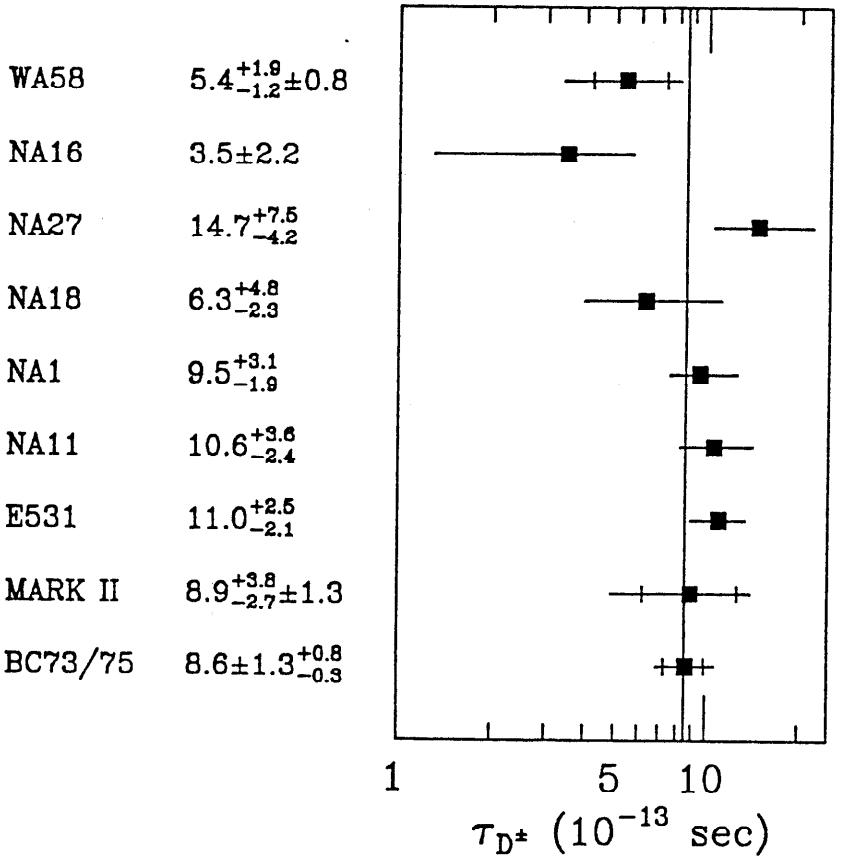

Figure 5.6: Data on the $D^\pm$ lifetime. The current world average is indicated by the vertical line.

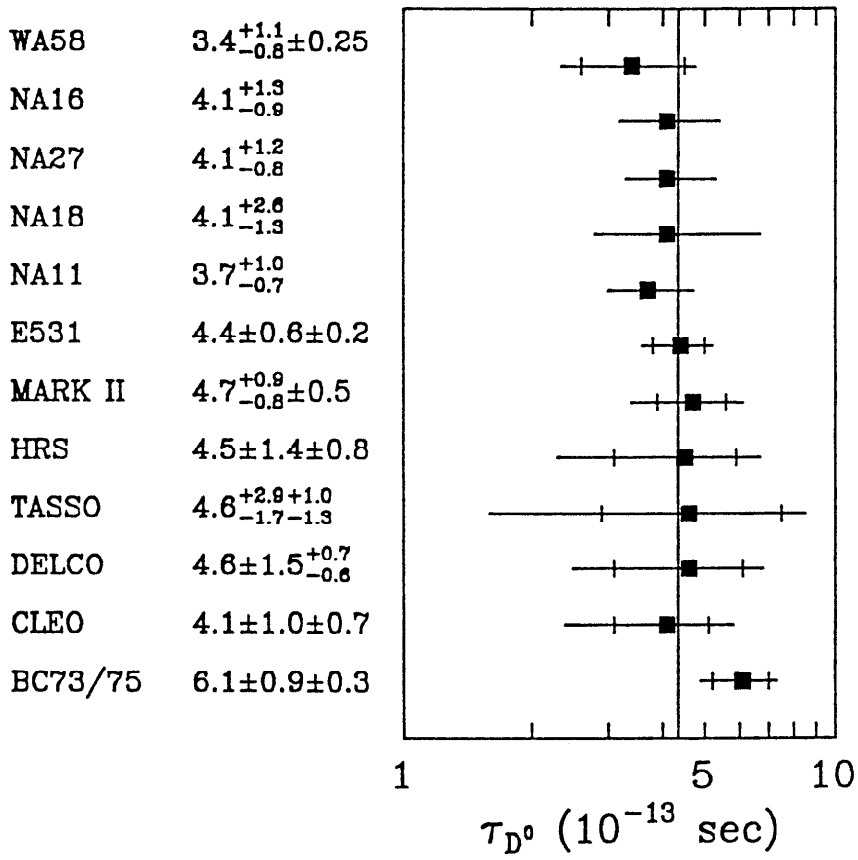

Figure 5.7: Data on the D^0 lifetime. The current world average is indicated by the vertical line.

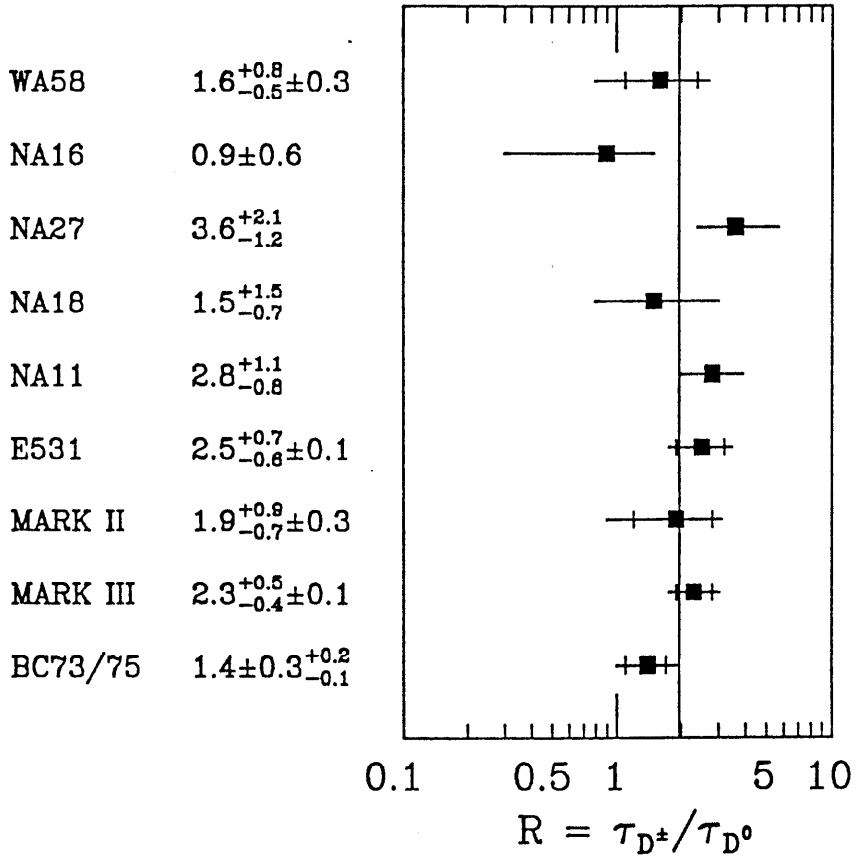

Figure 5.8: Data on the ratio of charged to neutral D lifetimes. The current world average from direct lifetime measurements is indicated by the vertical line.

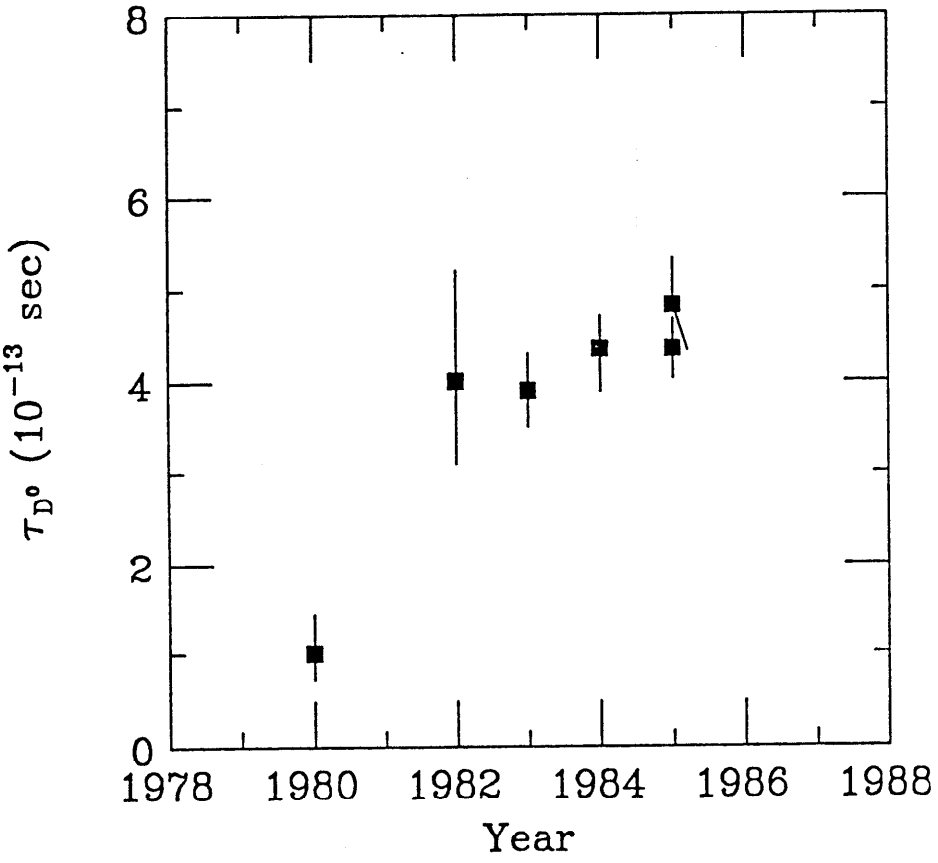

Figure 5.9: World average D^0 lifetime as a function of time. See Reference [32] for details.

The ratio of lifetimes has the ability to distinguish whether processes other that the spectator model contribute to the D decay rate. The measurement here of $R = 1.4 \pm 0.3^{+0.2}_{-0.1}$ can be interpreted in two ways discussed below.

The first interpretation notes that the value of R is consistent, within errors, with $R = 1$. We could assume then that R actually is 1 and that would imply the spectator model is totally dominant. The measurement does not, however, discriminate between the naïve spectator model and the QCD corrected version, but the D semi-leptonic branching ratios could provide that information.

The other approach is to take R as measured and determine the consequences. For $R \neq 1$, the naïve spectator model is not the whole story. The measurement of $1 \lesssim R \lesssim 2$ means other processes contribute at some level but do not dominate the decay rate. The most likely mechanisms are W-exchange and final state interactions enhancing the D^0 rate and Pauli Principle interference suppressing the $D^{\pm}$ rate. Recall from Chapter 1 that these processes are not rigorously calculable in the theory and therefore their relative contributions are not known. Thus any one mechanism or any combination of them could be responsible for $R = 1.4$. Each mechanism will now be discussed in turn.

Direct evidence for W-exchange has been detected by the ARGUS experiment at DESY [33]. They report observing the decay mode $D^0 \rightarrow \phi \bar{K}^0$ with a branching ratio of $(0.99 \pm 0.32 \pm 0.17)\%$. This decay proceeds mainly through W-exchange since in the spectator model it only contributes via an OZI forbidden process with a branching ratio of less than 10^{-5} [34]. W-exchange could therefore be the mechanism responsible for seeing $R = 1.4$.

It was argued in Chapter 1 that final state interactions (FSI) are expected to be important in D decay. At the same time it was noted that a theoretical treatment was difficult since most of the final states are highly inelastic. Nevertheless, the

example of the $K\pi$ final states of the D^0 shows that FSI can wipe out the pattern reflecting the basic decay dynamics and generate $R \neq 1$ within the spectator model. Although it is hard to be quantitative about the overall effect of FSI on the total decay rate, it seems reasonable that FSI alone could account for a D lifetime difference yielding $R = 1.4$.

Pauli Principle interference in charged D decays is another candidate for causing $R > 1$. Recent results from the MARK III experiment [10] suggest this interference has been observed. The evidence comes in part from the measurements of the Cabibbo suppressed modes $D^+ \to \pi^0\pi^+$ and $D^+ \to \bar{K}^0K^+$, where exact SU(3) symmetry predicts $\Gamma(D^+ \to \pi^0\pi^+) = \Gamma(D^+ \to \bar{K}^0K^+)$ and phase space considerations would lead to $\Gamma(D^+ \to \pi^0\pi^+) > \Gamma(D^+ \to \bar{K}^0K^+)$. The experimental results, normalized to the Cabibbo favored $D^+ \to \bar{K}^0\pi^+$ mode, are

$$\Gamma(D^+ \to \pi^0\pi^+)/\Gamma(D^+ \to \bar{K}^0\pi^+) < 0.21 \text{ at } 90\% \text{ CL}$$

$$\Gamma(D^+ \to \bar{K}^0K^+)/\Gamma(D^+ \to \bar{K}^0\pi^+) = 0.317 \pm 0.086 \pm 0.048.$$

Since Pauli Principle interference can occur for the $D^+ \to \bar{K}^0\pi^+$ and $D^+ \to \pi^0\pi^+$ modes but not for the $D^+ \to \bar{K}^0K^+$ mode, these results suggest interference plays a significant role in the $D^\pm$ rate. Thus Pauli Principle interference could account for our observed D lifetime difference.

Each of the mechanisms described above is capable of producing a lifetime difference compatible with our measurement of $R = 1.4 \pm 0.3^{+0.2}_{-0.1}$. Unfortunately, our data can not differentiate between the mechanisms. Nonetheless, this measurement of R can put constraints on the contribution to the decay rate of other processes relative to the Spectator Model. The D^0 decay rate can be written as

$$\Gamma_{D^0} = \Gamma_{SM} + \Gamma_{WE} + \Gamma_{FSI}$$

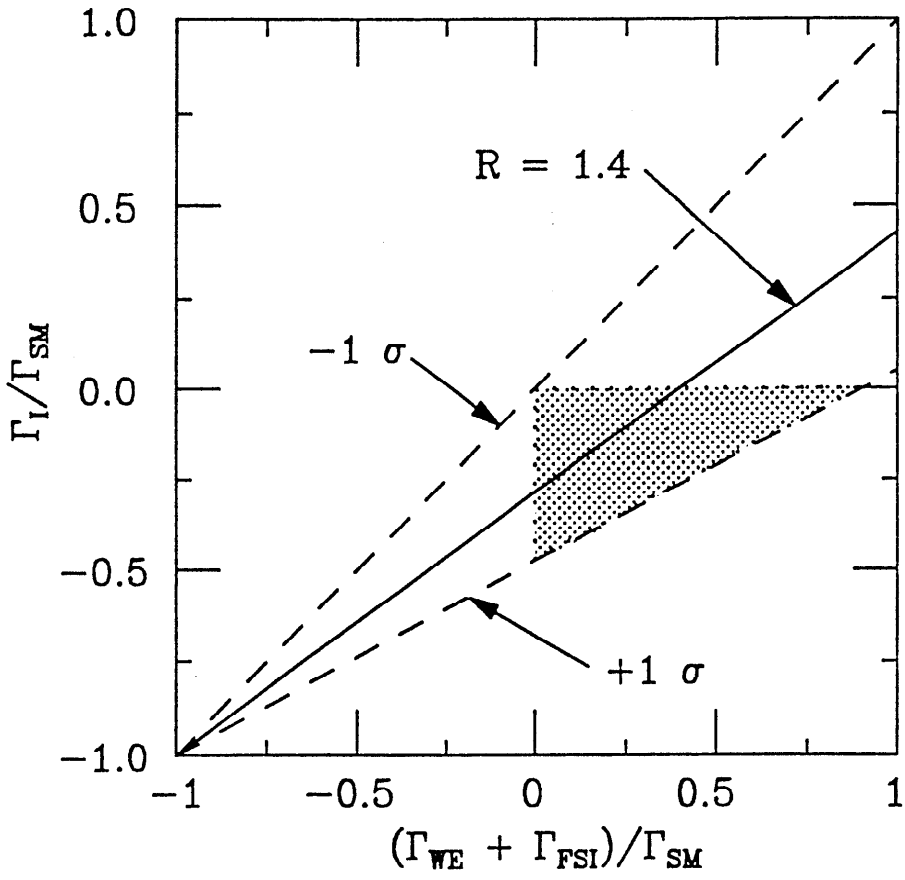

Figure 5.10: R and $R \pm 1\sigma$ as a function of the fraction of non-Spectator Model processes contributing to the D^0 rate and the $D^{\pm}$ rate. Γ_{SM} is the Spectator Model contribution to the total decay rate, Γ_{WE} results from W-exchange, Γ_{FSI} from final state interactions and Γ_I from Pauli Principle interference.

where Γ_{SM} is the Spectator Model piece, Γ_{WE} is the W-exchange contribution, and Γ_{FSI} comes from final state interactions. Similarly for the $D^{\pm}$ decay rate,

$$\Gamma_{D^{\pm}} = \Gamma_{SM} + \Gamma_I$$

where Γ_I is the contribution from Pauli Principle interference. Thus R can be expressed as

$$R = \frac{\Gamma_{D^0}}{\Gamma_{D^{\pm}}} = \frac{\Gamma_{SM} + \Gamma_{WE} + \Gamma_{FSI}}{\Gamma_{SM} + \Gamma_I} = \frac{1 + (\Gamma_{WE} + \Gamma_{FSI})/\Gamma_{SM}}{1 + \Gamma_I/\Gamma_{SM}}.$$

Figure 5.10 plots R and $R \pm 1\sigma$ as a function of $(\Gamma_{WE} + \Gamma_{FSI})/\Gamma_{SM}$ and Γ_I/Γ_{SM}, the fractions of non-Spectator Model processes contributing to the D^0 and $D^{\pm}$ rate, respectively. Making the reasonable assumption that Γ_{WE} and Γ_{FSI} only enhance Γ_{D^0} and Γ_I only suppresses $\Gamma_{D^{\pm}}$, then the allowed region in the figure is restricted to the shaded region. There are two limiting cases: (1) when there is no Pauli Principle interference suppressing $\Gamma_{D^{\pm}}$ and so $\Gamma_I = 0$ which implies $(\Gamma_{WE} + \Gamma_{FSI}) = (0.4^{+0.5}_{-0.4})\Gamma_{SM}$, and (2) when Pauli Principle interference accounts for the entire lifetime difference so that $(\Gamma_{WE} + \Gamma_{FSI}) = 0$ and $\Gamma_I = (-0.3^{+0.3}_{-0.2})\Gamma_{SM}$. If suppression of $\Gamma_{D^{\pm}}$ and the enhancement of Γ_{D^0} are roughly equal in magnitude then $(\Gamma_{WE} + \Gamma_{FSI}) \sim -\Gamma_I \sim (0.2^{+0.1}_{-0.2})\Gamma_{SM}$. Therefore the upshot of the measurement of $R = 1.4 \pm 0.3^{+0.2}_{-0.1}$ is that the Spectator Model rate is always the largest contribution to the total D decay rate, and for the reasonable assumption that the suppression of $\Gamma_{D^{\pm}}$ and enhancement of Γ_{D^0} are about the same size then these other processes are only $\sim 20\%$ of the Spectator Model piece.

In conclusion, the D meson lifetimes measurements of BC73/75 indicate the Spectator Model describes the main features of D lifetimes with only moderate modification and in fact this experiment is consistent at the 1σ level with total Spectator Model dominance. The world average value of $R = (1.96 \pm 0.22)$ implies

there are larger contributions from other mechanisms but the Spectator Model is still a dominant piece in the D decay rate. It should be noted that all experiments to date, including BC73/75, are statistics limited. It will be left to a future high statistics D lifetime experiment to determine precisely all of the contributions to the decay rate.

APPENDIX A

Derivation of the Momentum Estimate

The Lorentz transformation between the lab frame and the D rest frame (denoted by superscript *) is

$$E_{vis} \equiv \sqrt{{p_{vis}}^2 + m_{vis}^2} = \gamma(E^*_{vis} + \beta p^*_{vis} \cos\theta)$$

where vis stands for visible and refers to the charged tracks from the decay which are "visible" in the bubble chamber , and θ is the angle between $\vec{\beta}$ and $\vec{p}^*_{vis}$ in the rest frame decay plane. The boost parameters are

$$\gamma = \frac{E_D}{m_D} \ , \quad \gamma\beta = \frac{p_D}{m_D}$$

and so

$$E_{vis} = \frac{E_D}{m_D} E^*_{vis} + \frac{p_D}{m_D} p^*_{vis} \cos\theta .$$

Now take the point of view that the primary objective is to estimate p_D correctly *on the average* since the average of the flight times is the desired quantity. Given this, take the average of the above keeping p_D and m_{vis} fixed

$$\langle E_{vis} \rangle = \frac{E_D}{m_D} \langle E^*_{vis} \rangle + \frac{p_D}{m_D} \langle p^*_{vis} \cos\theta \rangle .$$

Since the D is a spin 0 particle and thus decays isotropically in its rest frame, $\langle p^*_{vis} \cos\theta \rangle = 0$. While this is certainly true, the cuts imposed on decays can in principle exclude certain configurations of $\vec{p}^*_{vis}$ which would lead to a non-zero average. The effect of the cuts is studied in Chapter 4. In general, for D decays $|\vec{p}^*_{vis}| \ll m_{vis}$ and so take $E^*_{vis} = a \cdot m_{vis}$ where $a \cong 1$. This leads to

$$\langle E_{vis} \rangle = \frac{E_D}{m_D} \, a \, m_{vis} .$$

Given that particle identification is generally incomplete, to avoid bias m_{vis} is approximated by $m_{vis} \cong b \cdot m_{vis}^{\pi}$ where m_{vis}^{π} is the visible mass taking all particles to be π's, and $b \cong 1$.

Defining $\alpha = a \cdot b$ then

$$E_D = \frac{m_D}{\alpha\, m_{vis}^{\pi}} \langle E_{vis} \rangle$$

which, to a good approximation, is equivalent to

$$p_D = \frac{m_D}{\alpha\, m_{vis}^{\pi}} \langle p_{vis} \rangle .$$

Therefore the momentum estimate is

$$p_{est} = \frac{m_D}{\alpha\, m_{vis}^{\pi}} p_{vis} .$$

APPENDIX B

Derivation of Flight Time Weights

The proper flight time estimate for a given decay can be written

$$t^{est} = \frac{\ell_{eff}\, m_D}{c}\left(\frac{1}{p_D}\right)^{est} = \frac{\ell_{eff}\, m_D}{c\, p_D} p_D \left(\frac{1}{p_D}\right)^{est}$$
$$= t \cdot y$$

where

$$y \equiv p_D \left(\frac{1}{p_D}\right)^{est}$$

and t is the true D effective flight time.

The variance of t^{est} is

$$\sigma^2_{test} = < t^{est2} > - < t^{est} >^2$$
$$= < (t \cdot y)^2 > - < t \cdot y >^2$$
$$= < t^2 >< y^2 > - < t >^2 < y >^2$$

The last step follows because t and y are independent variables. Since the distribution of t is exponential

$$< t >= \tau = \sigma_\tau$$

where τ is the true proper lifetime. On the average the momentum estimate is constructed to give the true momentum and so

$$< y >= 1.$$

The variance can now be manipulated

$$\sigma^2_{test} = < t^2 >< y^2 > -\tau^2 \cdot 1$$
$$= (\sigma^2_\tau + < t >^2)(\sigma^2_y + < y >^2) - \tau^2$$
$$= (\tau^2 + \tau^2)(\sigma^2_y + 1) - \tau^2$$
$$= \tau^2(1 + 2\sigma^2_y)$$

Therefore the standard deviation of t^{est} is simply

$$\sigma_{test} = \tau\sqrt{1 + 2\sigma_y^2}$$

Finally the weight for a given decay is defined as

$$w = \frac{\tau^2}{\sigma_{test}^2} = \frac{1}{1 + 2\sigma_y^2}.$$

This weight is equivalent to the more usual $1/\sigma^2$ weight because in any weighted average, the overall factor of τ^2 cancels out. Defining the weight as $(1 + 2\sigma_y^2)^{-1}$ merely removes an irrelevant scale factor and restricts the range of w to be

$$0 \leq w \leq 1.$$

APPENDIX C

Correction to Charged D Lifetime for $F^{\pm}$ and Λ_c^+ Production

If the production of D mesons proceeds through mechanisms other than $D\bar{D}$ pair production, then the D lifetimes must be corrected for the possible contribution of charm particles which enter the sample that are not D's although they are treated in the analysis as such. The correction derived here assumes that the only weakly decaying charm particles produced in this experiment are D's, $F^{\pm}$'s and Λ_c^+'s, with no contribution from, for example, the A^0 or A^+ charm baryons. Therefore the neutral D lifetime requires no correction for non-$D\bar{D}$ pair production while the charged D lifetime could be affected by $F^{\pm}$ or Λ_c^+ contamination of the charged decay sample. The modes considered, the production fraction of each mode and the relevant efficiencies are listed in Table C.1.

Table C.1

Mode	Fraction	Efficiencies
$D\bar{D}X$	$f_{D\bar{D}}$	$\varepsilon_D^{D\bar{D}}$
F^+F^-X	$f_{F^+F^-}$	$\varepsilon_F^{F\bar{F}}$
DF^-X	f_{DF^-}	$\varepsilon_D^{DF}, \varepsilon_F^{DF}$
$\bar{D}F^+X$	$f_{\bar{D}F^+}$	$\varepsilon_D^{\bar{D}F}, \varepsilon_F^{\bar{D}F}$
$\bar{D}\Lambda_c^+X$	$f_{\bar{D}\Lambda_c^+}$	$\varepsilon_D^{\bar{D}\Lambda_c^+}, \varepsilon_{\Lambda_c^+}^{\bar{D}\Lambda_c^+}$

The fractions are constrained by the requirement

$$f_{D\bar{D}} + f_{F^+F^-} + f_{DF^-} + f_{\bar{D}F^+} + f_{\bar{D}\Lambda_c^+} = 1.$$

The efficiency ε_A^{AB} is defined as the efficiency for particle A produced in mode ABX to pass all standard cuts. Note that for $D\bar{D}$ (F^+F^-) pair production it is assumed the D (F^+) has the same efficiency as the $\bar{D}$ (F^-). The efficiencies are calculated by Monte Carlo and are functions of the lifetimes, production mechanisms and decay models used as input.

Define also f_{D/D^+} ($f_{\bar{D}/D^-}$) to be the fraction of D's ($\bar{D}$'s) which are D^+'s (D^-'s), where it is assumed that f_{D/D^+} and $f_{\bar{D}/D^-}$ are independent of production mode.

Let N^{tot} be the total number of c quarks produced in the experiment. N^{tot} is clearly also the total number of $\bar{c}$ quarks produced. The number of $D^\pm$'s, $F^\pm$'s and Λ_c^+'s passing cuts can then be written as

$$
\begin{aligned}
N_{D^+} &= f_{D/D^+}(\varepsilon_D^{D\bar{D}} f_{D\bar{D}} + \varepsilon_D^{DF} f_{DF^-})N^{tot} \\
N_{D^-} &= f_{\bar{D}/D^-}(\varepsilon_D^{D\bar{D}} f_{D\bar{D}} + \varepsilon_D^{DF} f_{DF^+} + \varepsilon_D^{D\Lambda_c^+} f_{D\Lambda_c^+})N^{tot} \\
N_{F^+} &= (\varepsilon_F^{DF} f_{DF^+} + \varepsilon_F^{FF} f_{F^+F^-})N^{tot} \\
N_{F^-} &= (\varepsilon_F^{DF} f_{DF^-} + \varepsilon_F^{FF} f_{F^+F^-})N^{tot} \\
N_{\Lambda_c^+} &= \varepsilon_{\Lambda_c^+}^{D\Lambda_c^+} f_{D\Lambda_c^+} N^{tot}
\end{aligned}
$$

Define now the total number of positive and negative particles passing cuts

$$
\begin{aligned}
N^+ &= N_{D^+} + N_{F^+} + N_{\Lambda_c^+} \\
N^- &= N_{D^-} + N_{F^-}
\end{aligned}
$$

The average positive lifetime is

$$
\begin{aligned}
\tau^+ &= \frac{1}{N^+}\left[\sum_{i=1}^{N_{D^+}} t_i^{D^+} + \sum_{i=1}^{N_{F^+}} t_i^{F^+} + \sum_{i=1}^{N_{\Lambda_c^+}} t_i^{\Lambda_c^+}\right] \\
&= \frac{1}{N^+}\left[N_{D^+}\tau_{D^+} + N_{F^+}\xi_{F^\pm}\tau_{F^+} + N_{\Lambda_c^+}\xi_{\Lambda_c^+}\tau_{\Lambda_c^+}\right]
\end{aligned}
$$

where $\xi_{F^\pm} \equiv \alpha_{F^\pm}/\alpha$; α is the factor in the D lifetime estimate of Chapter 4 and $\alpha_{F^\pm}$ is the equivalent factor for an $F^\pm$ lifetime estimate, and $\xi_{\Lambda_c^+}$ is similarly

defined. The ξ factors account for the fact that all t_i are calculated assuming the particle which decays is a D.

Solving for τ_{D^+}

$$\begin{aligned}\tau_{D^+} &= \frac{1}{N_{D^+}}\left[N^+\tau^+ - N_{F^+}\tau_{F^+} - N_{\Lambda_c^+}\tau_{\Lambda_c^+}\right] \\ &= \tau^+ + \frac{N_{F^+}}{N_{D^+}}(\tau^+ - \xi_{F^\pm}\tau_{F^\pm}) + \frac{N_{\Lambda_c^+}}{N_{D^+}}(\tau^+ - \xi_{\Lambda_c^+}\tau_{\Lambda_c^+}).\end{aligned}$$

From this relation, define a weight W_{τ^+} for the positive lifetimes

$$\begin{aligned}W_{\tau^+} &= \frac{\tau_{D^+}}{\tau^+} \\ &= \left[1 + \frac{(\varepsilon_F^{\bar{D}F} f_{\bar{D}F^+} + \varepsilon_F^{FF} f_{F^+F^-})(\tau^+ - \xi_{F^\pm}\tau_{F^\pm}) + \varepsilon_{\Lambda_c^+}^{\bar{D}\Lambda_c^+} f_{\bar{D}\Lambda_c^+}(\tau^+ - \xi_{\Lambda_c^+}\tau_{\Lambda_c^+})}{\tau^+ f_{D/D^+}(\varepsilon_D^{D\bar{D}} f_{D\bar{D}} + \varepsilon_D^{DF} f_{DF^-})}\right].\end{aligned}$$

Following the above analysis, the D^- lifetime can be written

$$\begin{aligned}\tau_{D^-} &= \frac{1}{N_{D^-}}\left[N^-\tau^- - N_{F^-}\tau_{F^-}\right] \\ &= \tau^- + \frac{N_{F^-}}{N_{D^-}}(\tau^- - \xi_{F^\pm}\tau_{F^\pm}).\end{aligned}$$

From this relation define a weight W_{τ^-} for the negative lifetime

$$W_{\tau^-} = \frac{\tau_{D^-}}{\tau^-} = \left[1 + \frac{(\varepsilon_F^{DF} f_{DF^-} + \varepsilon_F^{FF} f_{F^+F^-})(\tau^- - \xi_{F^\pm}\tau_{F^\pm})}{\tau^- f_{D/D^-}(\varepsilon_D^{D\bar{D}} f_{D\bar{D}} + \varepsilon_D^{DF} f_{DF^+} + \varepsilon_D^{\bar{D}\Lambda_c^+} f_{\bar{D}\Lambda_c^+})}\right].$$

Weights for the number of decays are found in similar fashion and are given by

$$\begin{aligned}W_{N^+} &= \frac{N_{D^+}}{N^+} = \frac{1}{1 + \left(\frac{N_{F^+} + N_{\Lambda_c^+}}{N_{D^+}}\right)} \\ &= \left[1 + \frac{(\varepsilon_F^{\bar{D}F} f_{\bar{D}F^+} + \varepsilon_F^{FF} f_{F^+F^-} + \varepsilon_{\Lambda_c^+}^{\bar{D}\Lambda_c^+} f_{\bar{D}\Lambda_c^+})}{f_{D/D^+}(\varepsilon_D^{D\bar{D}} f_{D\bar{D}} + \varepsilon_D^{DF} f_{DF^-})}\right]^{-1}\end{aligned}$$

and

$$W_{N^-} = \frac{N_{D^-}}{N^-} = \frac{1}{1 + \frac{N_{F^-}}{N_{D^-}}}$$

$$= \left[1 + \frac{(\varepsilon_F^{DF} f_{DF^-} + \varepsilon_F^{FF} f_{F^+F^-})}{f_{D/D^-}(\varepsilon_D^{DD} f_{DD} + \varepsilon_D^{DF} f_{DF^+} + \varepsilon_D^{D\Lambda_c^+} f_{D\Lambda_c^+})} \right]^{-1}.$$

The charged D lifetime corrected for associated production is then

$$\tau_{D^\pm} = \frac{(W_{N^+}\, N^+\, W_{\tau^+}\, \tau^+ \;+\; W_{\tau^-}\, N^-\, W_{\tau^-}\, \tau^-)}{(W_{N^+}\, N^+ \;+\; W_{N^-}\, N^-)}.$$

In this expression, N^+, N^-, τ^+ and τ^- are directly measured while the weights are obtained from production mechanism studies of the data to get the production fractions, the PDG [22] for $\tau_{F^\pm}$ and $\tau_{\Lambda_c^+}$, and Monte Carlo calculation to determine the efficiencies.

APPENDIX D

Background Estimate for Longest Lived $\bar{D}^0$

Perhaps the most remarkable feature of the longest lived $\bar{D}^0$, aside from its proper flight time of 55×10^{-13} sec, is that it is so clean that the probability the decay was simulated by background is incredibly small. This appendix presents some details of the background estimate and follows closely the discussion found in References [29] and [20]. The event is shown in Figure 5.2 and relevant details are listed in Table D.1. There are two decays in the event, a topologically ambiguous short decay with $\ell = (0.10 \pm 0.02)$ mm and the long 4-prong decay (9.0 ± 0.1) mm downstream of the production vertex. The event is completely consistent with the production and decay of two charm particles. There are two categories of possible background: the decays are (1) actually strange particle decays, or (2) simulated by a secondary interaction of a neutral particle where the recoil proton is unobserved. Both backgrounds will be considered.

Both decays can be shown to be inconsistent with being strange particle decays. The minimum effective mass for the short decay comes from combining the two unambiguously assigned tracks, 5^+ and 8^-, yielding $m(e^+(5)\pi^-(8)) = (652 \pm 5)$ MeV/c^2, thus ruling out the strange particle interpretation. The strange particle interpretation for the long decay is $K^0_L \rightarrow \pi^+\pi^-\pi^0$ where the π^0 undergoes a Dalitz decay. This hypothesis is ruled out on several counts: (1) there is no e^+e^- mass combination less than 135 MeV/c^2, (2) particle 10^+ is not an e or a π, and (3) all $m(\pi^+\pi^-e^+e^-) \gg m_K$. Therefore there is no possible background from strange particle decays.

Table D.1					
Track No.	Charge	Momentum (MeV/c)	Particle ID	Identified By	Vertex Assignment
6	−	489 ± 6	$e/\mu/\pi$	Ionization	Production
3	+	4017 ± 48	—	—	Ambiguous:
4	+	382 ± 4	$e/\mu/\pi$	Ionization	Production
7	−	431 ± 4	$e/\mu/\pi$	Ionization	or
2	+	3030 ± 330	K/Σ	Decay	Short Decay
5	+	1072 ± 12	Not proton	Ionization	Short
8	−	65 ± 2	π	Range	Decay
10	+	5452 ± 56	K/p	Cherenkov	
11	−	599 ± 6	$e/\mu/\pi$	Ionization	Long
13	+	3694 ± 33	$e/\mu/\pi$	Cherenkov	Decay
14	−	466 ± 4	$e/\mu/\pi$	Ionization	
15	0	574 ± 53	γ	Lead Glass	Any

The only source of background left then is the secondary interaction of a neutral particle where the recoil proton stub is so short that it is not observed on the HRO film. Note that the interaction of any neutral particle with a proton is ruled out since the minimum proton recoil range is 1.3 cm which is easily seen. The only possibility remaining is a secondary interaction on a deuteron present in the liquid hydrogen. Given the fraction of deuterons in the hydrogen is about 1.5×10^{-4}, it is clear from the start that the background is small. The background calculation requires, for γd or $K^0 d$ interactions, the 4-prong system have a mass within 5σ of the $\bar{D}^0$ mass, and for a nd interactions, a mass within 5σ of the $p\pi^+\pi^-\pi^-$ mass of 2159 MeV/c^2 (the mass resulting from taking particle 10^+ to be

a proton instead of a K^+). The background estimate also includes the probability of seeing the short decay. The joint probability P that an experiment of the size of BC73/75, *i.e.* the same total number of charm events produced, would contain a background event simulating two charm particle decays was calculated. The four background sources considered and the value of P found for each are

(1) An ordinary γp hadronic interaction with a short decay (not of a charm particle) followed by a secondary interaction of a K^0 from the production vertex with a deuteron, $K^0 d \rightarrow K^+\pi^+\pi^-\pi^-(\pi^0)n(p_s)$, has $P < 6 \times 10^{-10}$.

(2) Production and short decay vertices as in (1) and a secondary interaction of a neutron with a deuteron, $nd \rightarrow p\pi^+\pi^-\pi^-(\pi^0)n(p_s)$, has $P < 2 \times 10^{-10}$.

(3) Two independent beam γ interactions, one giving the production and short decay vertices and the other giving the 4-prong vertex at 9 mm separation downstream has $P < 0.3 \times 10^{-10}$.

(4) Production of a charm anticharm pair at the production vertex with the short decay being the decay of one of the charm particles and the other charm decay not visible. The 4-prong results from a $K^0 d$ interaction as in (1) where the K^0 is a decay product of one of the charm decays. This source has $P < 1.7 \times 10^{-8}$.

It is interesting to note that the largest source of background is from a real charm event. The conclusion is that the probability is less than 1.7×10^{-8} that the event is due to background or, put another way, we would expect to see an event like this in less than 1 in 6×10^7 experiments of the size of BC73/75.

REFERENCES

1. For a comprehensive review see

   R. Rückl, *Weak Decays of Heavy Flavours*, CERN Preprint 83-1063.

2. J. Gasser and H. Leutwyler, Phys. Rep. **87C** (1982) 77.

3. S.L. Glashow, Nucl. Phys. **22** (1961) 579;

   A. Salam and J.C. Ward, Phys. Lett. **13** (1964) 168;

   S. Weinberg, Phys. Rev. Lett. **19** (1967) 1264;

   C. Quigg, *Gauge Theories of Strong, Weak and Electromagnetic Interactions* (Benjamin and Cummins, Reading, 1983).

4. M. Kobayashi and T. Maskawa, Prog. Theor. Phys. **49** (1973) 652.

5. M.K. Gaillard, B.W. Lee and J.L. Rosner, Rev. Mod. Phys. **47** (1975) 277;

   J. Ellis, M.K. Gaillard and D.V. Nanopoulos, Nucl. Phys. **B100** (1975) 313.

6. J.D. Bjorken and S.D. Drell, *Relativistic Quantum Mechanics* (McGraw Hill Book Company, New York, 1964).

7. N. Cabibbo and L. Maiani, Phys. Lett. **79B** (1978) 109.

8. M. Bander *et al.*, Phys Rev. Lett. **44** (1980) 7.

   H. Fritzsch and P. Minkowski, Phys. Lett. **90B** (1980) 455.

   Rückl, Ref. 1.

9. H. Lipkin, Phys. Rev. Lett. **11** (1980) 710;

   C. Sorensen, Phys. Rev. **D23** (1981) 2618;

   A.N. Kamal, SLAC-PUB-3443, 1984 (Submitted to Phy. Rev. D).

10. D. Hitlin, *Proceedings of the Twelfth SLAC Summer Institute on Particle Physics*, Stanford, 1984.

11. B. Guberina *et al.*, Phys. Lett. **89B** (1979) 111;
G. Altarelli and L. Maiani, Phys. Lett. **118B** (1982) 414;
H. Sawayanagi *et al.*, Phys. Rev. **D27** (1983) 2107.
12. J.C. Kent, Ph.D. Thesis, U.C. Berkeley, 1983, Report No. UCPPG-830520 (unpublished).
13. J.L. Benichou *et al.*, Nucl. Instrum. Methods **190** (1981) 487.
14. J.D. Ferrie, R.C. Field and D.A. Talaska, Nucl. Instrum. Methods **203** (1982) 223.
15. J.D. Ferrie and R.C. Field, Nucl. Instrum. Methods **221** (1984) 330.
16. A. Bevan *et al.*, Nucl. Instrum. Methods **203** (1982) 159.
17. J.E. Brau *et al.*, Nucl. Instrum. Methods **196** (1982) 403.
18. J.T. Carroll *et al.*, SLAC-PUB-2726, 1981 (unpublished);
P. Rankin, Ph.D. Thesis, Imperial College, London (1982) Report No. HEP-T-99 (unpublished).
19. D. Price *et al.*, IEEE Trans. Nucl. Sci. **NS-32** (1985).
20. K. Abe *et al.* (SHF Photon Collaboration), Phys. Rev. **D33** (1986) 1.
21. K. Abe *et al.* (SHF Photon Collaboration), Phys. Rev. **D29** (1984) 1877.
22. Particle Data Group, Rev. Mod. Phys. **56**, No. 2, Part III (1984).
23. K. Abe *et al.* (SHF Photon Collaboration), Phys. Rev. **D30** (1984) 1.
24. A. Chen *et al.*, Phys. Rev. Lett. **51** (1983) 634;
M. Althoff *et al.*, Phys. Lett. **136B** (1984) 130;
H. Albrecht *et al.*, Phys. Lett. **153B** (1985) 343.
25. B. Franek, Rutherford Appleton Laboratory Report RAL85-026, 1985 (unpublished).
26. K.D. Tolstov *et al.*, DESY L-Trans-299, 1985 (unpublished).
27. L.L. Chau, Phys. Rep. **95** (1983) 1.

28. A. Bodek *et al.*, Phys. Lett. **113B** (1982) 82.

H. Yamamoto *et al.*, Phys. Rev. Lett. **54** (1985) 522.

29. K. Abe *et al.* (SHF Photon Collaboration), SLAC-PUB-3493, 1984 (unpublished).

30. A.G. Frodesen, O. Skjeggestad and H. Tofte, *Probability and Statistics in Particle Physics*, Columbia University Press, 1979.

31. E.H. Thorndike, *International Symposium on Lepton and Photon Interactions at High Energies*, Kyoto 1985, except:

MARK II: L. Gladney, Ph.D. Thesis (unpublished);

NA11: R. Bailey *et al.*, Z. Phys. **C28** (1985) 357.

32. World average values of τ_{D^0} listed by year:

1980: S. Wocjicki, *High Energy Physics - 1980, XX International Conference*, Madison 1980,

Not really an average, but the results of the only experiment which had more than a few decays, namely the E531 experiment who found $\tau_{D^0} = (1.01^{+0.43}_{-0.27}) \times 10^{-13}$ sec;

1982: G. Kalmus, *21st International Conference on High Energy Physics*, Paris 1982,

excluded WA58 and found $\tau_{D^0} = (4.0^{+1.2}_{-0.9}) \times 10^{-13}$ sec;

1983: N.W. Reay, *International Symposium on Lepton and Photon Interactions at High Energies*, Cornell 1983,

found $\tau_{D^0} = (3.9 \pm 0.4) \times 10^{-13}$ sec;

1984: R. Klanner, *XXII International Conference on High Energy Physics*, Leipzig 1984,

excluded WA58 and found $\tau_{D^0} = (4.29^{+0.42}_{-0.40}) \times 10^{-13}$ sec;

1985: E.H. Thorndike, Ref. [30],

found $\tau_{D^0} = (4.35 \pm 0.32) \times 10^{-13}$ sec;

Bari 1985 conference,

found $\tau_{D^0} = (4.83 \pm 0.49) \times 10^{-13}$ sec.

33. H. Albrecht *et al.*, Phys. Lett. **158B** (1985) 525.

34. I.I.Y. Bigi and M. Fukugita, Phys. Lett. **91B** (1980) 121.